MINISTERUL EDUCAȚIEI ŞI CERCETĂRII

ANALELE UNIVERSITĂȚII "DUNĂREA DE JOS" DIN GALAȚI

Fascicula IX

FACULTATEA DE METALURGIE ŞI ŞTIINȚA MATERIALELOR

ANUL XXIV (XXIX), noiembrie 2006, nr.2

ISSN 1453-083X

MINISTRY OF EDUCATION AND RESEARCH

THE ANNALS OF "DUNAREA DE JOS" UNIVERSITY OF GALATI

Fascicle IX

FACULTY OF METALLURGY AND MATERIALS SCIENCE

YEAR XXIV (XXIX), November 2006, no.2

ISSN 1453-083X

EDITING MANAGEMENT

RESPONSIBLE EDITOR: **Prof. Dr. Eng. Emil CONSTANTIN**

ASSISTANT EDITORS: **Prof. Dr. Eng. Mircea BULANCEA**
Conf. Dr. Ec. Daniela ŞARPE
Conf. Dr. Anca GÂȚĂ
SECRETARY: **Assoc. Prof. Dr. Eng. Ion ALEXANDRU**

EDITING BOARD

Fascicle IX

METALLURGY AND MATERIALS SCIENCE

EDITOR IN CHIEF: **Prof. Dr. Chim. Olga Mitoşeriu**

SECRETARY: **Prof. Dr. Eng. Marian Bordei**

MEMBERS:

Acad. Prof. Dr. Hab. **Iurie Nicolaevich Shevcenko**–Director of the Termoplasticity Department, National Academy of Science of Ukraine
Acad. Prof. Dr. Hab. **Valeriu Kantser**–Coordinator of the Technical and Scientific Section of the Academy of Moldova Republic
Prof. Dr. **Rodrigo Martins**–President of the Department of Materials Science, Faculty of Science and Technology, NOVA University of Lisbon, Portugal
Prof.Dr.Hab. **Vasile Marina**–Director of Department, State Technical University of Moldova, Kishinau, Moldova Republic
Prof. Dr. Eng. **Elena Drugescu**
Prof. Dr. Eng. **Nicolae Cănănău**
Prof. Dr. Eng. **Anişoara Ciocan**
Prof. Dr. Eng. **Maria Vlad**
Prof. Dr. Eng. **Petre Stelian Niță**
Prof. Dr. Eng. **Alexandru Ivănescu**
Asoc.Prof. Dr. Eng. **Sanda Levcovici**

AFFILIATED WITH:

- ***ROMANIAN SOCIETY FOR METALLURGY***
- ***ROMANIAN SOCIETY FOR CHEMISTRY***
- ***ROMANIAN SOCIETY FOR BIOMATERIALS***
- ***ROMANIAN TECHNICAL FOUNDRY SOCIETY***
- ***THE MATERIALS INFORMATION SOCIETY (ASM INTERNATIONAL)***

TABLE OF CONTENT

1.Nelu Cazacu, Sorin Dobrovici, Adolf Bâclea, Victor Tănăsescu, Nelu Preda - Oxidizing Influence over Surface Structures and Properties for A3k Steel Nitrocarburized in Fluidized Bed..... 7
2.Ion Bostan, Valeriu Dulgheru - Some Aspects Regarding the Elaboration of Multiple Precessional Gear Theory and Modern Manufacturing Technology……. 12
3.Viorel Munteanu, Simona Sava - Mathematical Modelling of Steel Continuous Casting Hydrodynamics (1)…….. 17
4.Nicolae Cananau, Gheorghe Gurau, Petrica Alexandru, Gheorghe Corobete - Experimental Equation of Deformation Behaviour of a Concrete Steel..... 23
5.Viorica Muşat, Joao Canejo, Catalina Iticescu - On the Kinetics of Sol Gel Al:ZnO Thin Films Crystallization on Silicon Substrate..... 27
6.Stefan Dragomir, Georgeta Dragomir, Marian Bordei - Research about the Vibration Parameters for a Cold Rolling Mill Machine..... 31
7.V. Grechanyuk, I. Grechanyuk, N. Grechanyuk - Protective and Decorative Vacuum's Coatings on Wares of Artistic Castings..... 35
8.Adolf Bâclea, Sorin Dobrovici, Elena Drugescu, Nelu Cazacu, Nelu Preda - Surface Hardening of 40Cr10 Steel after Short Time Nitriding in Fluidized Bed…… 40
9.Mihai Gaita, Marian Bordei - The Influence of Polarization Tension of the Grading over Thin Layer Properties of TiN Deposed through PDV Method……..... 45
10.Florentina Potecasu, Octavian Potecasu, Elena Drugescu - Hardened Aluminum with Oxide Particles..... 49
11.Maria Vlad - Thermodynamic Assesment of The Cu - Ti System in Microalloyed Copper Base Alloys ……..... 53
12.Elisabeta Vasilescu, Marian Neacsu, Ana Doniga - Research Concerning the Influence of Heat Treatment on Physical and Mechanical Properties of Aluminium Based Alloys 58
13.Ana Doniga, Elisabeta Vasilescu - Study of the Inclusions from the Oriented Grains Silicon Steels and their Influence on the Texture……..... 63
14.Ioan Carcea, Florin Diaconescu, Cristian Diaconescu - Art Pieces Casting from Brass, Destined to Artificial Local Lightening, Used in Orthodox Cult…..... 69
15.Carmen Penelopi Papadatu - Tribological Behaviour of Nitrocarburized Superficial Layer after Thermo-Magnetic Treatments Applied to Steels, During Friction Process……. 73
16.Alexandru Olevschi - Some Issues Concerning Gear Wheels Fabrication by Sintering……. 79
17.Octavian Potecasu, Florentina Potecasu, Petrica Alexandru - Hardened Aluminum with Discontinuous Copper Threads..…….…… 83
18.Ovidiu Dima - Behavior of Welded Joints From Some Stainless Austenite Steel Types During Nitriding Process…… 86
19.Lucica Balint, Minodora Rîpă, Simion Ioan Balint, Petre Stelian Niţă, Gina Nastase - Air Quality Monitoring in Galaţi. Case Study ……. 89
20.Aurel Ciurea, Marian Bordei, Stefan Dragomir - Studies Regarding the Cooling of the Rolled Pieces with Atomizing Water…… 92

21.Gheorghe Gurau, Carmela Gurau, N. Andronache - Kinetic of Martensite Transformation in a Cu-13wt. %Al-4 wt.%Ni Shape Memory Alloy…….. 95
22.Sorin Dobrovici, Nelu Cazacu, Adolf Bâclea, Elena Drugescu, Nelu Preda - Behavior of 1%Cr Steels at Fluidized Bed Nitrocarburizing…… 98
23.Ovidiu Dima, Olga Mitoseriu - Behavior of Some Stainless Nitrided Austenite Steel Types to Corrosion and Abrasion……. 103
24.Adrian Vasiliu, Gina Năstase, Natalia Beglet, Vasile Mirea - The Decreasing of the Energetic Losses at a Coke Dry Cooling Plant……... 108
25.Petre Stelian Nita - Possibilities to Evaluate the Value of the Marangoni Effect and of the Marangoni Number in Refining Steel-Slag/Inclusion Systems……..... 112

OXIDIZING INFLUENCE OVER SURFACE STRUCTURES AND PROPERTIES FOR A3k STEEL NITROCARBURIZED IN FLUIDIZED BED

Nelu CAZACU[1], Sorin DOBROVICI[1], Adolf BÂCLEA[2], Victor TĂNĂSESCU[3], Nelu PREDA[4]
[1]Universitatea"Dunărea de Jos" din Galați,[2]SOCOMAR SRL, Sorento Italia,
[3]S.C.Nalba S.R.L.Galați, [4]Bristol International, Los Angeles, California, USA
email: cazacu.nelu@ugal.ro

ABSTRACT

Surface duplex thermochemical treatment (oxinitrocarburizing) has principal scope to obtaining superficial mechanical higher properties with increasing corrosion capacity. The paper is based by oxinitrocarburizing experiments made in laboratory conditions over steel samples (low carbon steels, A3k). Active media for treatments was obtaining by ammonia, methane and air. Effective treatment was made in endothermic atmosphere, methane and ammonia that produced smooth fluidization. In a second stage o postoxidation at different time was made. The results of duplex surface treatments were investigated by superficial hardness (HV_5) and by metallographic structure.

KEYWORDS: oxinitrocarburizing, fluidized bed

1. Introduction

Oxinitrocarburizing is a duplex thermochemical treatment that makes higher surface hardness, associated with good corrosion behavior and a superior surface aspect, thus the ulterior surface treatments is unnecessary. This technology is applied at the mechanical parts obtained by stamping, deep drawing, drilling and other. Examples of these parts are in automobile industry and these are made from wire and plate of steel with low carbon and high plastic cold deformation capability. An ulterior treatment by nitrocaburizing induces in first stage a substantial modification in surface structure and superior values of surface properties. Second stage is oxidizing at Fe_3O_4 and final impregnation of surface with emulsions that have a higher stability in time. Oxidizing at the high temperature steam conduced to increasing corrosion resistance by two mechanisms:

- bonding free atoms (Fe) at Fe_3O_4 (stabile combination)
- surface topology that have an irregular profile after intense oxidation (deep crevice) with high capacity of absorption for protection emulsion [2].

Table 1. *The chemical composition of the steel specimens used in experiments.*

C	Mn	Si	P	S	Al	Cr	Ni
max.0,11	max.0,45	max.0,5	max.0,035	max.0,04	0,02…0,10	max.0,08	max.0,1

2. Working methods

For experiments were used specimens from low carbon steel that having with good behavior at the cold plastic deformation.

A3k steel (STAS 9485-80) is non-alloyed steel with lower carbon content, for cold plastic deformation, in special for deep drawing, and ulterior protection painting.

Chemical composition is showed in Table 1. The specimens for experiments were cut by L profile (section 25mm x 25mm) with 25mm in length and ulterior grouped for fluidized bed charging.

The samples were arranged in fluidized bed furnace in central positions. An *air/gas=2,3* rapport

was maintained, that represents a condition for economical gas (CH_4) consumption. In the fluidized bed an endothermic atmosphere was produced and a rest of methane is present for nitrocarburising processes.

Samples surface were successive polished with 80, 150, 320, 400, 600, 800 abrasive paper, and ulterior cleaning with alcohol.

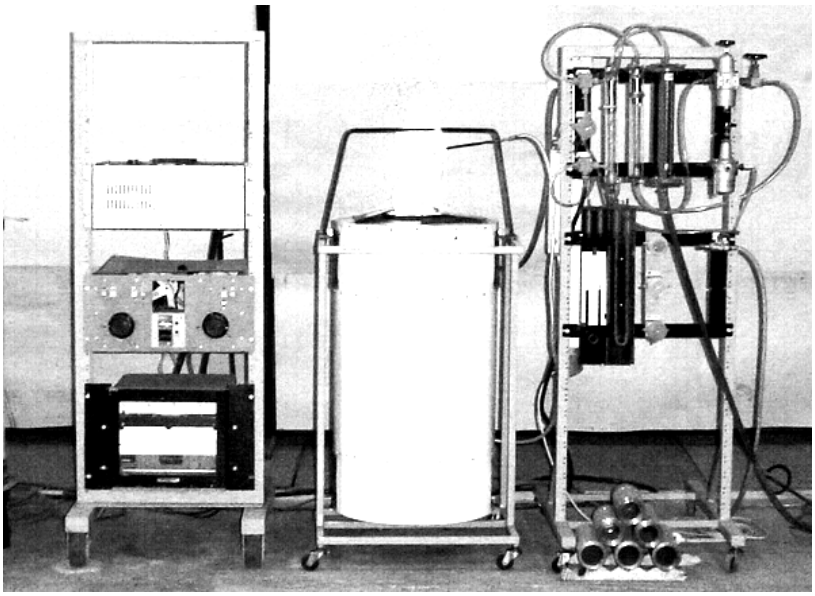

Fig. 1. *Laboratory fluidized bed plant for thermochemical treatments.*

Oxinitrocarburizing is a complex thermo-chemical treatment that is possible to realize on the same fluidized bed furnace. The classical technology offers three stages in furnaces with retort:

- nitrocarburising
- postoxidation in hot steam
- emulsion impregnation

At the nitrocarburizing process in fluidized bed following factors have important influences [4]:

- nitrocarburizing temperature (three valuees: 630°C, continuous cooling from 630 to 570°C, 570°C)
- nitrocarburizing time (1,5h; 2h; 2,5h)
- chemical activity of media (initial ammonia concentration or initial partial ammonia debit: aprox 23%)

Factors that have influence over post oxidation are:

- oxidation temperature (adopted 570°C, according to Figure 2)
- oxidation time (20,40 and 60min)
- oxidant gas concentation (hot steam, initial debit 1l/h)
- sample positions in furnace (central)

Thermochemical treatment media was realized in open furnace (Figure 1) that conduced to important decreasing of heating and cooling time and specimens were easy removal from furnace.

An open furnace has an important advantage: easy control processes because partial pressure of gasses is in direct correlation with initial debit participation.

Active nitrocarburizing media was obtaining by introduction in furnace a gas initial mixture from air, natural gases (>95% methane) and ammonia. Total initial debit was constant (500l/h air, 230 l/h methane, 520 l/h ammonia). In the furnace some initial gasses having thermal decomposing and some reactions:

- ammonia has a partial decomposition in mollecular nitrogen and hydrogen
- mathane has a partial decomposition in carbone and hydrogen
- methane has a interaction with the oxygen from air, thus the endothermic atmosphere is produced (air/gas=2,3 raport)

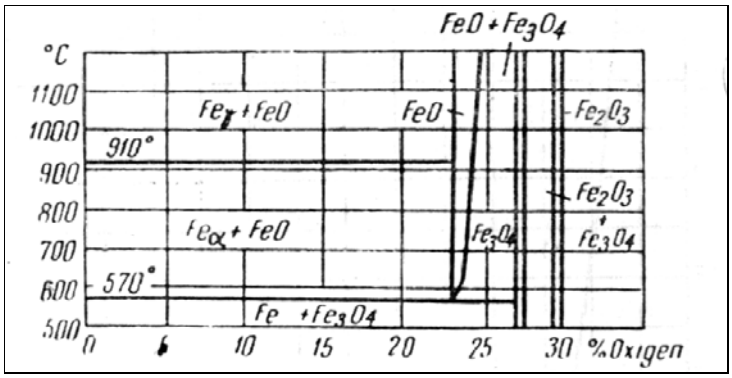

Fig. 2. *Fe-O equilibrium diagram, [3].*

Table 2. *Oxinitrocarburizing in fluidized bed regimes*

sample experiment	nitrocarburizing media	nitrocarburizing temperature	nitrocarburizing time	oxidizing media	oxidizing temperature	oxidizing time
U.M.	-	°C	h		°C	min
1	fluidized bed by solid granular (burned fire clay) and gas mixture (ammonia and nitrogen)	630	1,5	steam	570	20
2						40
3						60
4			2,0			20
5						40
6						60
7			2,5			20
8						40
9						60
10		630-570	1,5			20
11						40
12						60
13			2,0			20
14						40
15						60
16			2,5			20
17						40
18						60
19		570	1,5			20
20						40
21						60
22			2,0			20
23						40
24						60
25			2,5			20
26						40
27						60

The chemical composition of gas mixture that makes the fluidization and nitrocarburizing are hydrogen, nitrogen, carbon monoxide, ammonia (rest), methane (rest). Oxidizing is an ulterior operation that is made in concordance with Fe-O diagram (Figure 2), by water debit inlet (approx. 1l/h) to the base of bed.

After intense vaporization vapor continue up heating to regime temperature (570°C).

Water vapors make fluidization and will be realize favorable conditions for heat and mass transfer. Experimental matrix is presented in Table 3.

3. Results obtained

Results of oxinitrocarburizing in fluidized bed experiments were metallographic investigated for structure modifications (surface-core transition zone) and mechanical investigated (superficial hardness) for property modifications at surface.

Representative microstructures are presented in Figure 3…Figure 10. Nitrocarburizing time influence over surface hardness is showing in Figure 11 Postoxidation time influence over surface hardness is presented in Figure 12.

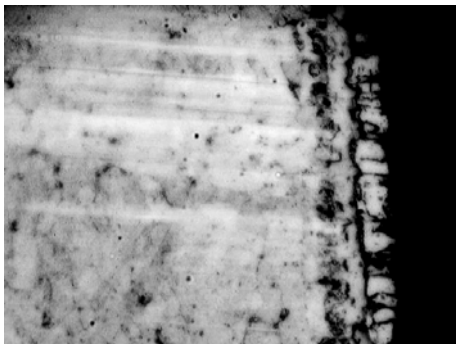

Fig. 3. *Microstructure of A3k sample 2 (350x).*

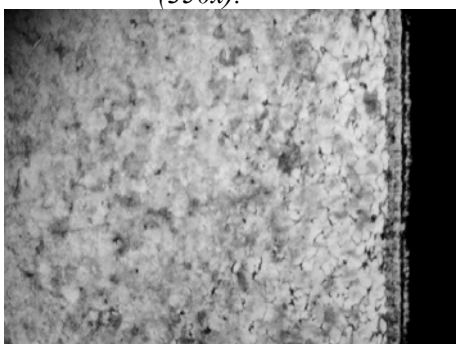

Fig. 4. *Microstructure of A3k sample 7 (170x)*

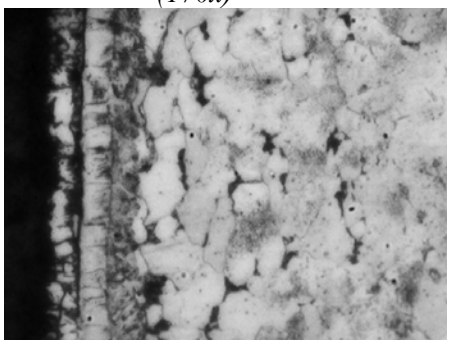

Fig. 5. *Microstructure of A3k sample 7 (350x)*

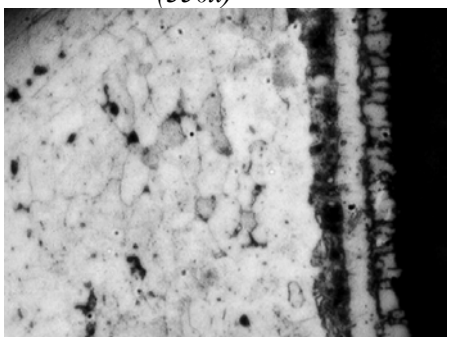

Fig. 6. *Microstructure of A3k sample 8 (350x)*

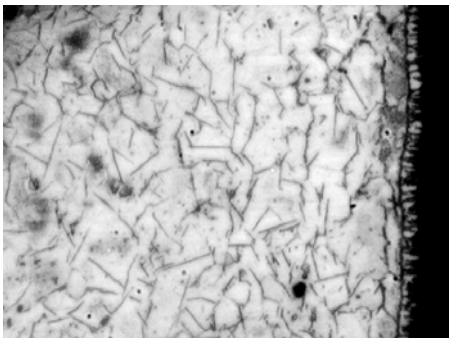

Fig. 7. *Microstructure of A3k sample 13 (350x)*

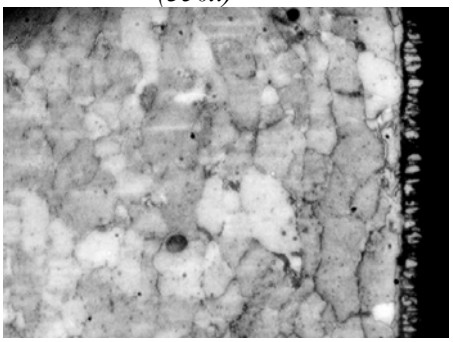

Fig. 8. *Microstructure of A3k sample 15 (170x)*

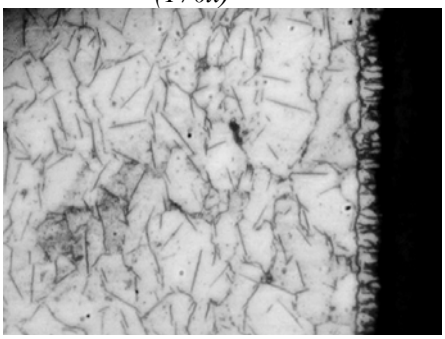

Fig. 9. *Microstructure of A3k sample 16 (350x)*

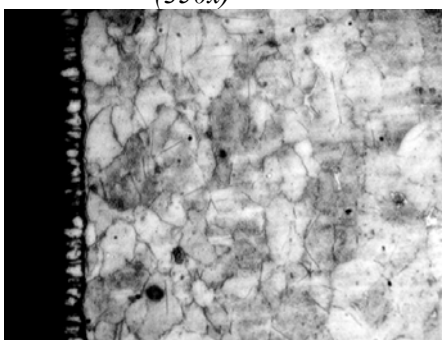

Fig. 10. *Microstructure of A3k sample 17 (350x)*

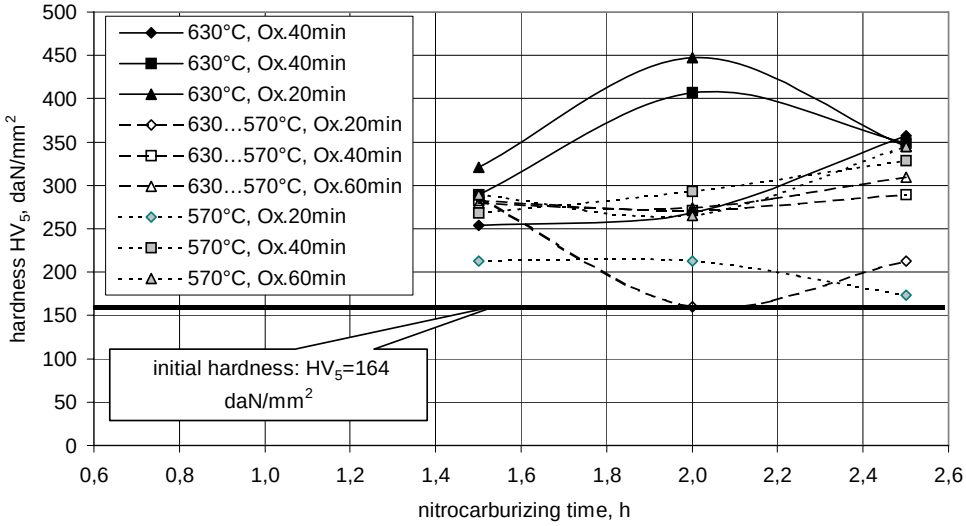

Fig. 11. *Influence of nitrocarburizing time over surface hardness.*

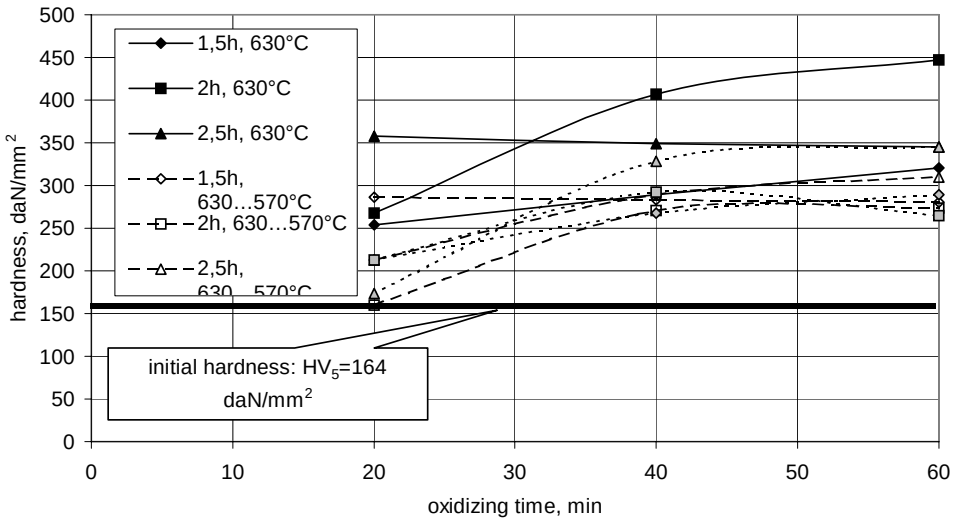

Fig. 12. *Influence of post oxidation time over surface hardness.*

4. Conclusions

For all oxinitrocarburizing in fluidized bed experiments, surface hardness having a normal increasing with treatment time.

Microstructures showing diffusion zone for all experiments and combination layer for long nitrocarburizing times. After oxidation deep crevices were formed in combinations layer (ε+γ') that having an important role for (emulsion accumulator) for increasing corrosion resistance,

For 40 and 60 min oxidizing time surface hardness decreasing because long oxidizing time produce nitrogen desorption, that affecting surface structure and superficial hardness.

Fluidized bed technology applications for oxinitrocarburizing treatment are useful for small series of parts with medium importance.

References

[1]. Nitrotec®, patented Surface Engineering Process for the treatment of steels and cast irons

[2]. Roland A, *Oxycad(R) NT en four a tapis. Nitrocarburation, oxydation, trempre*, Traitement thermique, no. 346, Avr 2003. p37

[3]. Popescu, N., Vitănescu,C., *Tehnologia tratamentelor termice*, Editura Tehnică, Bucureşti, 1974;

[4]. Cazacu N, Dobrovici S, Bâclea A, Tănăsescu V, *Oxinitrocarburarea otelurilor în strat fluidizat aplicată oțelurilor cu conținut scăzut de carbon/Fluidized Bed Oxinitrocarburizing Treatment For Low Carbon Steel*

THE ANNALS OF "DUNAREA DE JOS" UNIVERSITY OF GALATI
FASCICLE IX METALLURGY AND MATERIALS SCIENCE, ISSN 1453 – 083X. N^0. 2 – 2006

SOME ASPECTS REGARDING THE ELABORATION OF MULTIPLE PRECESSIONAL GEAR THEORY AND MODERN MANUFACTURING TECHNOLOGY

Ion Bostan, Valeriu Dulgheru
"Technical University of Moldavia" Kishinew, Moldova Republic
e-mail: dulgheru@mail.utm.md

ABSTRACT

The engineering complex study of the triad "gear-technology-transmission" has permitted to elaborate a new type of precessional transmissions with multicouple gear. In this paper, the authors present the mathematic model of the multicouple gear. A computer program for doing this it is also elaborated. It is shown a block-scheme of the algorithm of the program modules including the calculus modalities exposed in the paper.

KEYWORDS: multicouple gear, technology, precessional, transmission,

1. Introduction

The engineering complex study of the triad "gear-technology-transmission" has permitted to elaborate a new type of precessional transmissions with multicouple gear, which, from the technological point of, view can be manufactured via a new method of conical teeth with convex-concave profile processing.

The specific character of sphere-spatial (precessional motions of the precessional transmissions pinion makes impossible the utilisation of teeth classical involute profiles. This fact requires the elaboration of new profiles adequate to the sphere-spatial motion of pinion which would ensure high performances to the precessional transmission. Carrying out on the principle of the transfer function continuity and gear based on the principles of the transfer function continuity and gear multiplicity which aims to:

- the elaboration of the gear mathematics model with account of the peculiarities;
- the analytical description of teeth profiles by a system of parametric equations on spherical surface and normal teeth section for inner and plane gear;
- the determination by CAD of geometrical and cinematic parameters influence of the gear upon the teeth profiles shape and the justification of their rational limits of variation;
- the elaboration of the theoretical basis evaluation of teeth gear multiplicity in precessional transmissions;
- the definition of area of gear multiplicity existence by 100% teeth couples.

The production of non-standard teeth profiles requires a new manufacturing technology. In the complexity of problem "gear-synthesis-profile study-manufacturing " an important role plays the elaboration of efficient methods of teeth manufacturing which ensures a maximum productivity and reduced cost while satisfying the requirements related to the gear with precessional motion. To solve this problem the following has been done:

- we elaborated the mathematics model of teeth generation which shows the interaction of teeth in precessional gear;
- we investigated the kinematics of the mechanism of method realisation for teeth generating;
- we determined the trajectory of the tool motion and the wrapping of the generating surface family of it by using the computer;
- we elaborated and manufactured from metal milling and tooth grinding tools, inclusively their longitudinal modification.

Constructions peculiarities and high multiplicity of gear create favourable premises for the improvement of precessional transmissions kinematics accuracy. Within these activities we elaborated:

- theoretical basis for the identification of kinematics error generated by various primary error (frontal and radial knocking), on the basis of error independent action principle by fulfilling computer assisted mathematics experiment;
- compensation method for manufacturing and assembling errors;

- method of determination of probable limit error for precessional reducers with account of the stochastic character of manufacturing and assembling errors.

Special attention was paid to precessional reducer's experimental research. For this purpose two laboratories were set up: 1) for mechanical tests and; 2) working technology for gear wheels. The laboratories are equipped with stands for testing and with control and modern measuring devices.

Know-how in the elaboration of the multicouple precessional gear, manufacturing technology and control methods, and a range of precessional transmission diagrams belong to research team from the Technical University of Moldova. During the last 20 years the team patented about 127 inventions.

2. Analytical description of the teeth profiles

The engineering complex study of the triad "gear-technology-transmission" has permitted to elaborate a new type of precessional transmissions with multicouple gear, which, from the technological point of, view can be manufactured via a new method of conical teeth with convex-concave profile processing.

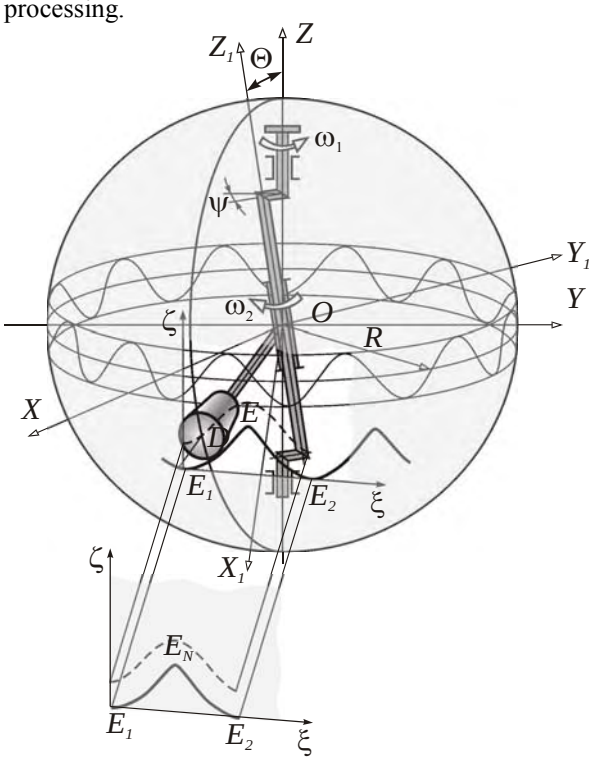

Fig. 1. *Profile teeth's determination*

In precessional transmission the gear wheel produces sphere-spatial motion round a fixed point.

As mentioned the literature, that the body, which produces spherical motion, has three degrees of freedom. As a rule, in theoretical mechanics, the position of the body, which produces precessional motion, is determined by Euler angles. In this case, the mobile system of co-ordinates $OX_1Y_1Z_1$ is bound rigidly with the gear wheel, as origins of the system of co-ordinates the immobile point O (centre of precession) being chosen (Figure 1). This system of co-ordinates produces jointly with the gear wheel spherical motion related to the immobile system of coordinates $OXYZ$. Analytical relationship between the co-ordinates of gear wheel points, shown in the mobile $OX_1Y_1Z_1$ and immobile $OXYZ$ system of co-ordinates, was obtained analysis of the two pinion positions - initial one, when the system of coordinates axis coincide, and final one, when the axis al removed (displaced).

By expressing vectors $\bar{i}_1', \bar{j}_1', \bar{k}_1'$ via basic vectors $\bar{i}_1'', \bar{j}_1'', \bar{k}_1''$ of the immobile system of coordinates $OXYZ$ we obtain:

$$\begin{aligned} &\bar{i}_1' = \bar{i}\cos\psi + \bar{j}\sin\psi, \\ &\bar{j}_1' = -\sin\psi + \bar{j}\cos\psi,\ \bar{k}_1' = \bar{k} \end{aligned} \tag{1}$$

The second rotation is produced at angle θ $(O \le \Theta \le \pi)$ round joint lines, after which the unit vector $\bar{i}_1', \bar{j}_1', \bar{k}_1'$ will move into directions $\bar{i}_1'', \bar{j}_1'', \bar{k}_1''$ (respectively, they coincide with the directions of axis OX'', OY'', OZ''), at the same time vector $\bar{k}_1''$, which coincide with vector $\bar{k}_1$, defines the position of axis OZ_1 in final position. By expressing vectors $\bar{i}_1'', \bar{j}_1'', \bar{k}_1''$ via $\bar{i}_1', \bar{j}_1', \bar{k}_1'$ we obtain:

$$\begin{aligned} &\bar{i}_1'' = \bar{i}_1'; \\ &\bar{j}_1'' = -\bar{j}_1'\cos\theta + \bar{k}_1'\sin\theta; \\ &\bar{k}_1'' = -\bar{j}_1'\sin\theta + \bar{k}_1'\cos\Theta. \end{aligned} \tag{2}$$

By operating matrix theory, transition from gear wheel point coordinates is produced (for example, of the roller centre D), given in the mobile system of co-ordinates $OX_1Y_1Z_1$ to the coordinates of the same points in the immobile system $OXYZ$. After some modifications we obtain:

$$\begin{aligned} &X_D = R\cos\delta\left[-\cos\psi\sin(Z_1/Z_2) + \sin\psi\cos(Z_1\psi/Z_2)\right] - \\ &-R\sin\delta\sin\psi\sin\theta; \\ &Y_D = -R\cos\delta\left[\sin\psi\sin(Z_1/Z_2) + \cos\psi\cos(Z_1\psi/Z_2)\right] - \\ &-R\sin\delta\cos\psi\sin\theta; \\ &Z_D = -R\cos\delta\cos(Z_1\psi/Z_2)\sin\theta - R\sin\delta\cos\theta \end{aligned} \tag{3}$$

Point D moves at the spherical surface by radius R with its centre in the precessional centre O (figure 1). Being familiar with the trajectory of roller centre motion, the position of the contact point by central wheel tooth is determined, which family in a

precessional cycle represent the shape of the wheel tooth (Bostan, 1992).

After some modifications we obtain:

$$\xi = X_E'' \cos\frac{\pi}{Z_1} + \left[R_D \cos(\delta+\beta) + Y_E''\right]\sin\frac{\pi}{Z_1};$$

$$\zeta = X_E'' \sin\gamma \sin\frac{\pi}{Z_1} - \left[R_D \cos(\delta+\beta) + \right. \qquad (4)$$

$$\left. + Y_E'' \cos\frac{\pi}{Z_1} + \left[R_D \sin(\delta+\beta) + Z_E''\right]\cos\gamma.\right.$$

Were:

$$\sin\gamma = tg(\delta+\beta) \Big/ \left[\cos^2\frac{\pi}{Z_1} + tg(\delta+\beta)\right]^{1/2};$$

$$\cos\gamma = \cos\frac{\pi}{Z_1} \Big/ \left[\cos^2\frac{\pi}{Z_1} + tg\,(\delta+\beta)\right]^{1/2}.$$

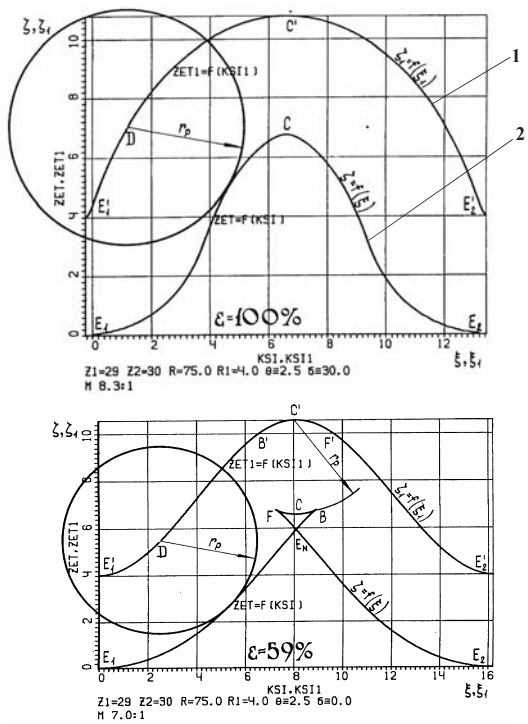

Fig. 2. *The diagrams of teeth with convex-concave profile.*

In Figure 2 the diagrams of teeth profile, obtained for the various geometrical parameters of gear are shown. The analyses of diagrams demonstrate the lever and direction of influence upon the angle of conical axoid δ, medium radius of wheel R_m, rollers radius R, conical angle of rollers β and correlation between number of teeth Z_1 and Z_2.

3. Gear manufacturing technology

3.1. Kinematics of the realizing mechanism for the teeth generating method

To realise the method of teeth processing we have elaborated the mechanism (Figure 3, Figure 4). In the elaborated mechanism the node, which involves the tool into precessional motion, is fixed not to rotate round the common axis of the principal shaft - semiproduct shaft with a binding mechanism.

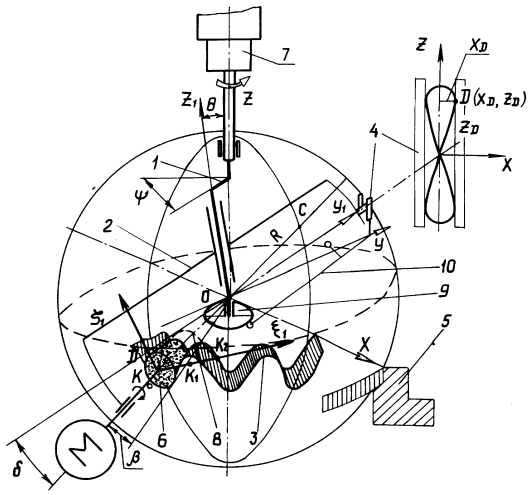

Fig. 3. *Spatial scheme of the realizing for the processing method by rolling using precessional tool.*

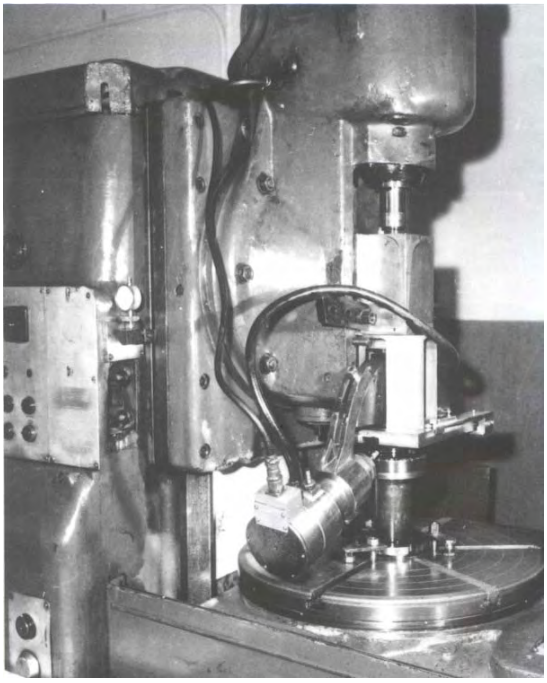

Fig. 4. *The device of the realizing for the teeth processing method by rolling using precessional tool.*

The constructive execution of the tool binding mechanism with the shaft ensures the continuity of the transmission function $\omega_1/\omega_3 = const.$ and is determined by the motion trajectory of point C which belongs to the movable part. Setting up the position

function of the binding mechanism and the motion equation of the generating wheel and using the matrix device for transferring from the movable system of coordinates $X_1Y_1Z_1$ to the immovable one *OXYZ,* we determined the coordinates of point *C:*

$$\begin{aligned} X_c &= R_c(1-\cos\theta)\cos\psi\,\sin\psi; \\ Y_c &= R_c\left(\sin^2\psi + \cos\theta\cos^2\psi\right); \\ Z_c &= R_c\,\sin\theta\,\sin\psi. \end{aligned} \tag{5}$$

These equations (5) represent the parametric equations of the supporting surface of the binding mechanisms, inserted in the device. The shape of this device ensures the continuity of the transmission ratio of the cinematic chain to the spindle axis-semiproduct shaft.

3.2. Determination of the tool motion trajectory

For the angle of the conical axoid of the teeth wheel $\delta = 0$ the equation of tool motion are identical to the equation (4), having only opposite values.

In the case of toothed wheels processing with an angle of the conical axoid $\delta \triangleright 0$ the centre of the tool will have the co-ordinates in the movable system $OX_1Y_1Z_1$:

$$X_{1D} = 0; Y_{1D} = -R\cos\delta; Z_{1D} = -R\sin\delta.$$

Then the equation of tool motion in the immovable system of coordinates $OXYZ$ will be:

$$\begin{aligned} X_D &= -R_U\cos(1-\cos\theta)\cos\psi\,\sin\psi - R_U\sin\delta\,\sin\psi; \\ Y_D &= -R_U\cos\delta\left(\sin^2\psi - \cos\theta\cos^2\psi\right) + R_U\sin\delta\cos\psi; \\ Z_D &= -R_U\cos\delta\cos\psi - R_U\sin\delta. \end{aligned} \tag{6}$$

The motion trajectory of point D (curve 1, Figure 2) for $\delta = 0$ presents a symmetrically closed curve related to the big axis whose shape changes according to the angle value of conical axoid δ. Curve 2 (Figure 2) presents the motion trajectory of tool's centre in the movable system of coordinates $OX_1Y_1Z_1$.

3.3 Determination of the family wrapping of tool surfaces

Tooth profile of the processed wheel represents the family wrapping of the generating contour profiles of the tool.

The wrapping is determined by the equations of the working surface of the generating tool and by the relative motion parameters while wrapping.

To make easier the determination of wrapping we pass to the tool centre co-ordinates in the movable system of co-ordinates, bound to the semiproduct:

$$\begin{aligned} \overline{X} &= X_D\cos\psi_3 + Y_D\sin\psi_3; \\ \overline{Y} &= -X_D\sin\psi_3 + Y_D\cos\psi_3; \\ \overline{Z} &= Z_D. \end{aligned} \tag{7}$$

Where: $\overline{X}_D, \overline{Y}_D, \overline{Z}_D$ are the coordinates of the tool centre in the movable system of co-ordinates; $\psi_3 = \psi / i$ is the rotation angle of the semiproduct; *i* - is the transmission ratio of the cinematic chain "principal shaft - semiproduct". The equations (7) define the motion trajectory of tool centre, evaluated on the sphere. Then we determined the equation of wrapping on the sphere (Figure 5).

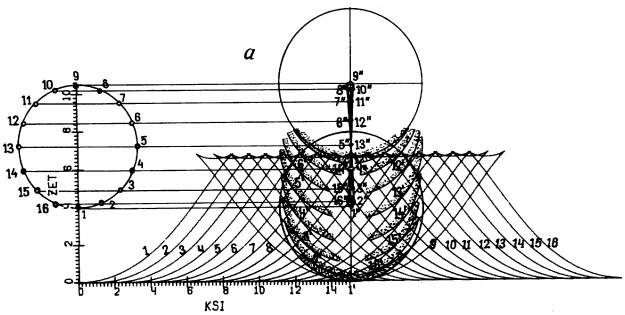

Fig. 5. *The family wrapping of tool surfaces.*

The analyses of diagrams demonstrate the lever and direction of influence upon the angle of tool insertion δ by the rotation axis of the semiproduct, tool radius *R* and transmission ratio *i* of the cinematic chain "principal shaft - semiproduct " on processed tooth profile.

4. The elaboration of precessional reducers

The elaboration of working machines driving mechanisms is based on the diagram of precessional transmissions, presented in Figure 6.

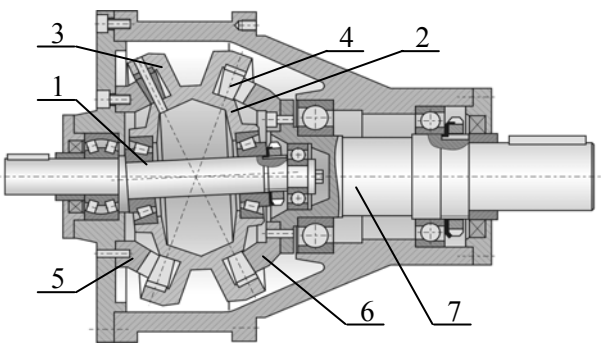

Fig. 6. *Precession reducer.*

The rotating motion of the crank shaft 1 is transformed into sphere-spatial motion of the block pinion 2 with two teethed crowns 3 and 4, which are rolling without sliding on the immovable and driven toothed wheel teeth 5 and 6. Due to the minimum difference between the numbers of teeth $Z_5 = Z_3 - 1, Z_6 = Z_4 - 1$, $Z_3 = Z_4 + 1, 2, 3...$ the transmission ratio is:

$$i = \pm \frac{Z_3 Z_6}{Z_5 Z_4 - Z_3 Z_6}; \qquad (8)$$

The teeth of crowns 3 and 4 are manufactured in the shape of conical rollers installed on axis having the possibility to rotate round them, and the teeth of central wheel 5 and 6 have non-standard convex-concave profile (Figure 2).

References

[1]. Bostan I. *Precessional transmissions with multi-pair gearing*. Stiinta Publishing House, 1991, 356p.

[2]. Bostan, I., Babaian I., Precessional gear-engagement / Patent RU nr. 1455094 (patent MD 560), 1990

[3]. Bostan, I., Dulgheru V., Vaculenco M. Precessional gear-engagement and method of its realisation/ Patent MD 1886, 2001.

[4]. Bostan, I., Dulgheru, V., Grigoraş, Ş., *Planetary, precessional and harmonic transmissions*, Bucureşti - Chişinău, 1997.

MATHEMATICAL MODELLING OF STEEL CONTINUOUS CASTING HYDRODYNAMICS (1)

Viorel MUNTEANU[1], Simona SAVA[2]
[1]"Dunarea de Jos" University Galați,
[2]S.C. Uzinsider Engineering S.A. Galați,
e-mail: viorel.munteanu@ugal.ro

ABSTRACT

The quality increase of steel continuous casting and a reliability indices of afferent installations imposes the automation systems adoption of machines of continuous casting of steel.

In this paper enters original solution of automatic settlement of liquid steel debit and level in tundish and analyses the behaviour in dynamics behaviour of automatic installation.

KEYWORDS: steel continuous casting, automatization, tundish, mathematical modeling, sliding gate mechanism

1. Introduction

The quality increase of steel continuous casting and of afferent installations reliability indices imposes the automation systems adoption of machines of continuous casting of steel. In the framework of those systems, automatic settlement curl of level in tundish has an particular important, as conditions, in good measure, the correct running, under technological aspect of continuous casting machine.

The manual casting management purpose permanent supervision of steel level, process which trains nervous blood-pressure and a growing weariness of operator, which it generates rigging bugs and spoilages of continuous casting installations.

A level too heaved in tundish can turn out overrunning in overflow vein and a level too allows carry forword dross in mould, turning out the line punch. It results, therefore, the automatic settlement necessity of liquid steel level in tundish, for the increase yield of metal, the quality improvement slab and the incidences avoidance of casting, which manage to the machines productivity decrease of continuous casting.

The spatial mechanism for closing with case represents an element of automatic settlement system of level in tundish [2]. In the ones what follow enter an original solution of automatic settlement of level in tundish and analyses the behaviour in dynamic behaviour of automatic installation.

2. The automatic settlement algorithm of liquid steel level in tundish

To the automatic settlement system adoption pushed along from realization requirement to a reliable mechanism, taking account of running highly the heavy conditions of this.

The use of a settlement system with continue action should lead a practically permanent running of element execution, which it holds the spatial mechanism, resulting a pronounced wear of this.

The basic idea of proposed system consists in running behaviour relief of execution mechanism, what it works in environmental highly heavy conditions (mechanical and thermic various), demand by the adequate adoption of electric system command, which it works in running pars.

This idea managed to the adoption to a settlement system with sampling. Sampling period, T, it adopted equal to 10 s.

At a some discrete value of time kT, (k = 0, 1, 2, ….), it does the next processes what compare the reaction purveyed signal of transducer, with the reference signal; if the resulted error in absolute value, it surpasses a imposed limit, it the short period displacement command with a assignment quantity, of container case of casting, in a different meaning, contingent on the error mark; if the error is smaller than imposed limit, the mechanism is not acted. Between the sampling periods, the mechanism stands able of rest.

From the ones featured result as proposed algorithm frames in settlement tripozitional systems class with sampling. As it showed, the essential advantage of solution consists in the insurance to a time how smaller of call of acting mechanism. Though it should utilize a proportional command, the sampling adoption lowers with 80% acting time of mechanism. The tripozitional command used in proposed draft, spliced with the signal sampling, it lowers the acting time in a bigger proportion.

Tenet draft of settlement system of liquid steel level in tundish is given in figure 1, in which: 1 is pressure traductor, 2 – hydraulic drum, 3 – tundish, 4 – command element by impulses (with sampling), 5 – execution element, 6 – closing appliance with sliding case.

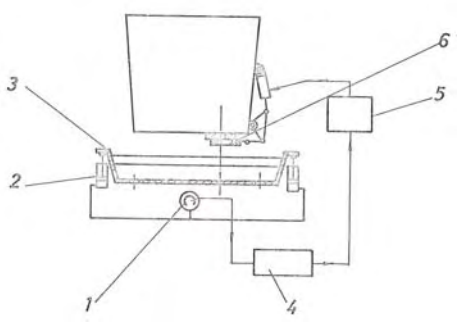

***Fig. 1**. Tenet draft of settlement system of liquid steel level in tundish*

The move and sustenance vertically of machine tundish of continuous casting does by the agency of to a hydraulic indited installations from a behaved electric pump and four hydraulic drums with lifter rods and pistons, dispositioned on the sustenance support of tundish tundish-car. Assigned uniform task on the sustenance pistons of tundish creates in the hydraulic drums a pressure which can be metered.[1]

The level variation in the machines tundish of continuous casting translates in the pressure variation from the hydraulic drums of tundish sustenance, which it transmits to transducers in unified system or pressure-gauges with electric contacts.

The reaction signal, given by transducers is transmitted by impulses to the command element, which it is a tripozitional controller with sampling. Delicate purveyed command by the controller applies hydraulic execution element, which it acts the rectifying mechanism of passage reach.

The running tenet of automatic settlement system of level in tundish is ilustrated of given diagram in figure 2, in which it enters the indicial reply of h(t) system, to an applied variation of reference, the execution size action x_m (the settlement organ opening), and also the delicate purveyed commands controller.

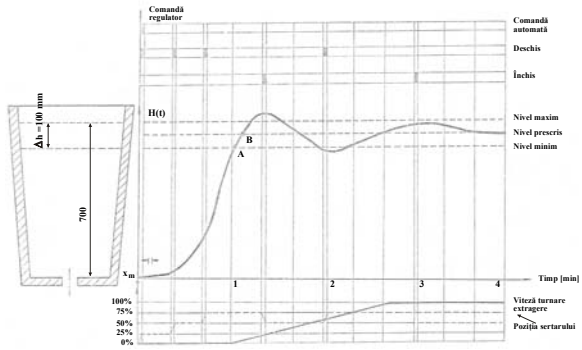

***Fig. 2**. The running tenet of automatic settlement system of liquid steel level in tundish*

3. Automatic dynamics installation study

For the controller parameters fitting, for procurance to some imposed performances of automatic settlement system whole, it is needed automatic dynamic installation knowledge, which it includes the spatial mechanism acting. This is imposes mathematical modelling of tuned installation, in stabilization behaviour of liquid steel level.

The representation by input-output sizes of formed installation is given in figure 3, in which: h is the level (the output size), x_m – case opening (execution size), x_{p1} – liquid steel level in the casting container, x_{p2} şi x_{p3} – settlement organs position to the exhaust from tundish, x_{p4} – metal temperature, x_{p5} – steel quality etc. (x_{pk}, k = 1, 2, …, are disturbed sizes).

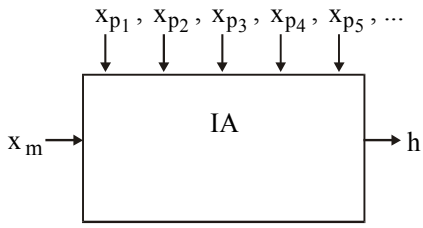

***Fig. 3**. The formed installation representation by input-output sizes.*

The mathematical pattern of automatic installation is formed from state equation, representing the material balance-sheet in tundish and from the relations which explain the intermediate variables which appear in the state equation.

The material balance-sheet equation is:

$$\frac{d(V\rho)}{dt} = Q_1 - Q_2 \qquad (1)$$

in which:

V is the liquid steel volume;

ρ – steel consistency

Q_1 and Q_2 – input debits and, respectively, the output debits.

It does the next hypotheses, according to the physical process:

- The liquid steel temperature variation is negligible, therefore, ρ = constant;
- The interest variation of free surface liquid, in the stabilization behaviour of level, it is negligible.

For a given quality of steel, the disturbed sizes which it intervene are: x_{p1}, x_{p2} and x_{p3}.

From the relation (1), with the espoused hypotheses, results:

$$A \cdot \rho \frac{dh}{dt} = Q_1 - Q_2 \tag{2}$$

where, A is the free surface area of liquid.

The input debit in tundish is:

$$Q_1 = S(x_m) \cdot \rho \cdot 60 \sqrt{\frac{2gh_1}{2 + \lambda \frac{L}{D}}} \tag{3}$$

in which:

$S(x_m)$ is constructive characteristic of settlement organ to the steel exhaust from the casting container;

h_1 – liquid level from the casting container;

D – rated diameter of outflow orifice;

λ - endurance ratio (constant);

L – by-pass span.

The relation (3) it also can put down under form:

$$\begin{aligned} Q_1 &= k_1 \cdot S(x_m) \cdot \sqrt{h_1} = \\ &= k_1 \cdot S(x_m) \cdot \sqrt{x_{p_1}} \end{aligned} \tag{4}$$

where, k_1 is a ratio depending the static running point parameters on settlement organ characteristic.

Alike, it infers the debit relation to the exit from tundish:

$$Q_2 = k_2 \cdot \sqrt{h}\left[S_1(x_{p_2}) + S_1(x_{p_3})\right] \tag{5}$$

in which $S_1(x_{p_2})$ and $S_1(x_{p_3})$ are the constructive characteristics of settlement organs to the steel exhaust from tundish, while k_2 is a suchlike ratio k_1.

The non-linear pattern of automatic installation is:

$$\begin{aligned} A\rho \frac{dh}{dt} &= k_1 S(x_m)\sqrt{x_{p_1}} + \\ &+ k_2 \sqrt{h}\left[S_1(x_{p_2}) + S_1(x_{p_3})\right] \end{aligned} \tag{6}$$

As the installation functions in stabilization behaviour of level, the mathematical pattern can be lineared around rated running point. Considering as all the physical sizes from system hold a constant component (the par) and a variable component, relative small toward the par, namely:

$$\begin{aligned} h &= \bar{h} + \Delta h \\ x_m &= \bar{x}_m + \Delta x_m \\ x_{p_k} &= \bar{x}_{p_k + \Delta x_{p_k}}, k = 1,2,... \end{aligned} \tag{7}$$

where the pars are barred, linearization supposes the relations subrogation (7) in equation (6) and hold the first two terms from the serial development Taylor of non-linear terms

$Q_1 = Q_1(x_m, x_{p_k})$ şi

$Q_2 = Q_2(h, x_{p_2}, x_{p_3})$.

It results as:

$$\begin{aligned} Q_1(x_m, x_{p_1}) &\cong \bar{Q}_1 + \frac{\partial \bar{Q}_1}{\partial x_m} dx_m + \\ &+ \frac{\partial \bar{Q}_1}{\partial x_{p_1}} dx_{p_1} \end{aligned} \tag{8}$$

$$\begin{aligned} Q_2(h, x_{p_2}, x_{p_3}) &\cong \bar{Q}_2 + \frac{\partial \bar{Q}_2}{\partial h} dh + \\ &+ \frac{\partial \bar{Q}_2}{\partial x_{p_2}} dx_{p_2} + \frac{\partial \bar{Q}_2}{\partial x_{p_3}} dx_{p_3} \end{aligned} \tag{9}$$

in which:

$\bar{Q}_1 = Q_1(\bar{x}_m, \bar{x}_{p_1})$,

$\bar{Q}_2 = Q_2(\bar{h}, \bar{x}_{p_2}, \bar{x}_{p_3})$,

while barred derivatives entails in the rated running behaviour.

Taking account of the expressions (4) and (5), it results:

$$\begin{aligned} Q_1 &= \bar{Q}_1 + \frac{\partial \bar{S}}{\partial x_m} \bar{k}_1 \sqrt{\bar{x}_{p_1} \Delta x_m} + \\ &+ \frac{1}{2} \frac{\bar{k}_1}{\sqrt{\bar{x}_{p_1}}} S(\bar{x}_m) \Delta x_{p_1} \end{aligned} \tag{10}$$

$$\begin{aligned} Q_2 &= \bar{Q}_2 + \frac{1}{2} \frac{\bar{k}_2}{\sqrt{\bar{h}}} \left[S_1(\bar{x}_{p_2}) + S_1(\bar{x}_{p_3})\right] \Delta h + \\ &+ \bar{k}_2 \sqrt{\bar{h}} \left[\frac{\partial \bar{S}_1}{\partial x_{p_2}} \Delta x_{p_2} + \frac{\partial \bar{S}_1}{\partial x_{p_3}} \Delta x_{p_3} \right] \end{aligned} \tag{11}$$

In fixed behaviour, are the valid relations:

$$\bar{Q}_1 = \bar{Q}_2 = \bar{Q} \tag{12}$$

$$\frac{dh}{dt} = \frac{d\Delta h}{dt} \tag{13}$$

$$\bar{k}_1 = \frac{\bar{Q}_1}{S(\bar{x}_m)\sqrt{\bar{x}_{p_1}}} \quad (14)$$

$$\bar{k}_2 = \frac{\bar{Q}_2}{\sqrt{\bar{h}}\left[S_1(\bar{x}_{p_2}) + S_1(\bar{x}_{p_3})\right]} \quad (15)$$

and from the relations (10) and (11) it calculates grafo-analytic, utilizing the constructive characteristics plots of settlement organs.

$$\frac{\partial \bar{S}}{\partial x_m} = \frac{\Delta S}{\Delta x_m}\bigg|_{\bar{x}_m} = S_1 \quad (16)$$

$$\frac{\partial S_1}{\partial x_{p_{2,3}}} = \frac{\Delta S_1}{\Delta x_{p_{2,3}}}\bigg|_{\bar{x}_{p_{2,3}}} = S_{2,3} \quad (17)$$

Replacing the relations (13) and (17) in equations (10) and (11), it results:

$$Q_1 = \bar{Q} + \frac{\bar{Q}}{\bar{S}} s_1 \Delta x_m + \frac{1}{2}\frac{\bar{Q}}{\bar{x}_{p_1}} \Delta x_{p_1} \quad (18)$$

$$Q_2 = \bar{Q} + \frac{1}{2}\frac{\bar{Q}}{\bar{h}}\Delta h + \frac{\bar{Q}}{\bar{S}_{1,2} + \bar{S}_{1,3}}\left(s_2 \Delta x_{p_2} + s_3 \Delta x_{p_3}\right) \quad (19)$$

where are utilized the notations:

$\bar{S} = S(\bar{x}_m)$,

$\bar{S}_{1,2} = S_1(x_{p_2})$ and

$\bar{S}_{1,3} = S_1(x_{p_3})$.

Pursuant to the relations (13), (18) and (19), the state equation of automatic installation becomes:

$$A \cdot \rho \cdot \frac{d\Delta h}{dt} = \frac{\bar{Q}}{\bar{S}} s_1 \Delta x_m + \frac{1}{2}\frac{\bar{Q}}{\bar{x}_{p_1}}\Delta x_{p_1} - \frac{1}{2}\frac{\bar{Q}}{\bar{h}}\Delta h - \frac{\bar{Q}}{\bar{S}_{1,2} + \bar{S}_{1,3}}\left(s_2 \Delta x_{p_2} + s_3 \Delta x_{p_3}\right) \quad (20)$$

It observes as all the ratios from the lineared pattern equation (20) it expresses contingent on the constructive characteristics or the parameters of installation, as well as contingent on the pars of physical sizes ($\bar{Q}, \bar{h}$ etc.), to the numeric values computation of those ratio is a highly simple problem.

Utilizing the notations:

$$T = \frac{2 \cdot A \cdot \rho}{\bar{Q}} \cdot \bar{h} \quad (21)$$

$$k_1 = \frac{2 \cdot \bar{h}}{\bar{S}} \cdot s_1 \quad (22)$$

$$k_2 = \frac{\bar{h}}{\bar{x}_{p_1}} \quad (23)$$

$$k_{3,4} = \frac{2 \cdot s_{2,3}}{\bar{S}_{1,2} + \bar{S}_{1,3}} \cdot \bar{h} \quad (24)$$

the linear pattern of automatic installation becomes:

$$T\frac{d\Delta h}{dt} + \Delta h = k_1 \Delta x_m + k_2 \Delta x_{p_1} - k_3 \Delta x_{p_2} - k_4 \Delta x_{p_3} \quad (25)$$

whereupon it correponds flow-process chart from figure 4.

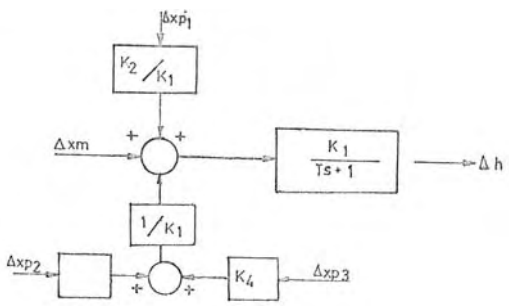

***Fig. 4**. Flow-process chart of lineared pattern of automatic installation*

The lineared pattern ratios computation did in hypothesis as the sizes from system have small variances around pars. This hypothesis is valid for all the sizes from the analysed process, excepting size $x_{p_1} \equiv h_1$. The analytic relation use (23) manages to an incertitude looking the value adoption $\bar{x}_{p1}$. For the exceeding of this problem utilized the curves families which give the debit Q_1, contingent on h_1 and of equivalent diameter D of outflow reach. In the equation (18), the variable ratio x_{p1} entails average slope of curves which give the debits. In this kind, the relation (18) becomes:

$$Q_1 = \bar{Q} + \frac{\bar{Q}}{\bar{S}} s_1 \Delta x_m + \alpha \Delta x_{p_1} \quad (26)$$

where α it entail chart:

$$\alpha = \frac{\Delta Q_1}{\Delta h_1} \cdot \bar{D} \quad (27)$$

In the final equation, the ratio k_2 will entail with the relation:

$$k_2 = \frac{2\alpha\bar{h}}{\bar{Q}} \tag{28}$$

The mathematical pattern of pressure transducer is formally:

$$T_T \frac{dx_r}{dt} + x_r = K_T \Delta h \tag{29}$$

where T_T and K_T are the roll parameters of apparatus.

The mathematical modelling of hydraulic execution element did pursuant to the acquainted methodology establishment of dynamics equations for a tundish system – hydraulic drum. Considering the cynetic energy filling in the elements found in movement and taking account of noted delay [1] with T_m, in the command transmission electro-hydraulic, the execution element equation is:

$$T' \frac{d^2 \Delta x_m(t)}{dt^2} + \frac{d\Delta x_m(t)}{dt} = \\ = k \cdot x_C(t - T_m) \tag{30}$$

where x_C is given command date of controller.

Flow-process chart of settlement system of level in tundish, with details of mathematical pattern of managed process, is given in figure 5.

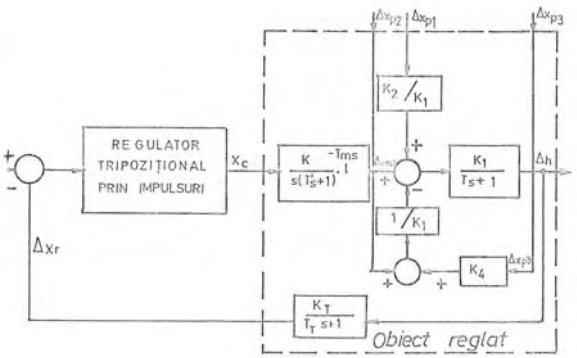

***Fig. 5**. Flow-process chart of settlement system of level in tundish*

4. The settlement level system realization in tundish and tests data

The proposed settlement system performances study did by numeric simulation and by experiments on the physical system realized. Analysis on the numeric computer had as the main syock-holders environment number fixing objective of mechanism with case, for dimensions sundries of mould and technological casting parameters. The chased aim is to obtain a number how smaller of stock-holders, for the tax life equals increase, in preservation conditions in imposed limits of level variances. Logical draft of command system on normal function is given infigure 6, while logical draft command of controller by impulses is given in figure 7, in which PA_{max} is the maximum acting pressure, PA_{min} – the minimum acting pressure, DSS – distance between centers, P_{min} and P_{max} – pressure chosen limits.

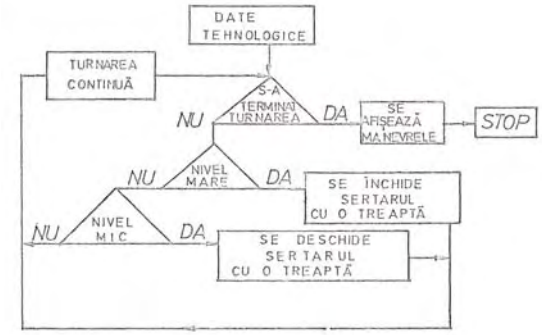

***Fig. 6**. Logical draft of command system on the normal function.*

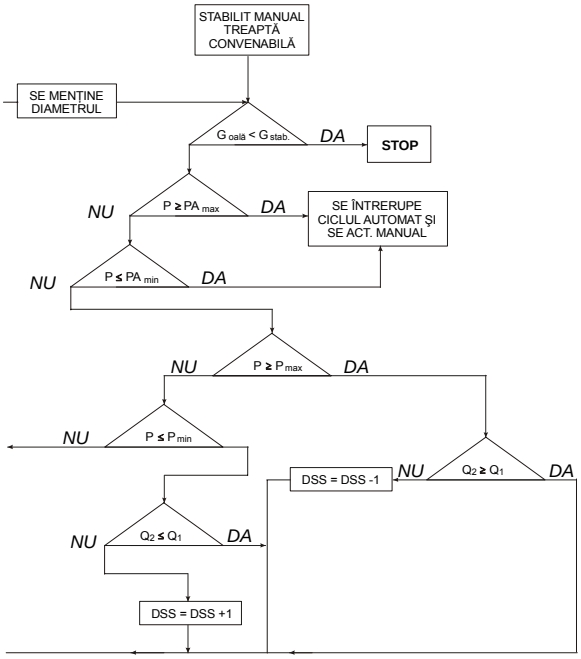

***Fig. 7**. Logical draft of controller by impulses*

In virtue of those logical draft, it realized the programme for the numeric simulation of automatic settlement system function.The obtained outcomes are synthesized in the table 1, looking the stock-holders number of mechanism with case and in the table 2, looking the others technological parameters. It distinguishes the minimal number stock-holders of

[1] The delay period determination T_m was realized by experimental way, analytic evaluations are qualitatively.

spatial mechanism closing with case, which it acknowledges the owned premises in view to the tenet solution establishment.

5. Conclusions

The obtained results by continuous casting timing satisfy quite all the quality conditions and technological operation: the level variation stands in admissible limits, the stock-holders number is lowered pursuant analysis on the numeric computer, the level record allows the control as technological document of installation function. In figure 8, are given records of level variation, in manual settlement behaviour and in automatic settlement behaviour, resulting in decisive mode, the performance indices increase to the automatic settlement, by the realized system. During on the all experiments, the automatic settlement appliance adduced a good reliability of operation.

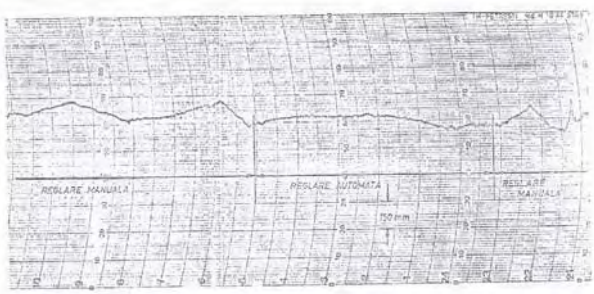

***Fig. 8**. The liquid steel level in tundish in manual and automatic settlement behaviour*

The realization of automatic settlement system of liquid steel level in tundish has importance issues looking the continuous casting slab quality (under the purity aspect in non-metalic inclusions) as well as looking the line punches avoidance, with bearings over indices of output and productivity of continuous casting machines.

***Table 1.** Casting time and the stock-holders number of function case of mould tipo-dimension and casting speed*

The width of mould (mm)	1,600	1,000	1,300	1,600
The thickness of mould (mm)	250	200	250	300
Speed (m/min)	0.650	1	0.7	0.5
Casting time (min)	35	46	39	36
The stock-holders number of mechanism with case	8	6	4	8

Table 2.

The thickness (mm)		0.150		0.200		0.250		0.300	
The width (m)	Steel group	Speed [m/min]	Debit Q [t/min]	Speed [m/min]	Debit Q [t/min]	Speed [m/min]	Debit Q [t/min]	Speed [m/min]	Debit Q [t/min]
0.7	1	1.5	1.13	-	-	-	-	-	-
0.7	2	1.7	1.25	1.25	1.23	-	-	-	-
0.7	3	1.7	1.25	1.60	1.60	1.05	1.29	-	-
1	1	1.5	1.58	1.00	1.40	0.70	1.23	-	-
1	2	1.7	1.79	1.20	1.68	0.80	1.40	-	-
1	3	1.7	1.79	1.30	1.82	1.05	1.84	-	-
1.3	1	1.35	1.84	1.00	1.82	0.70	1.59	-	-
1.3	2	1.35	1.84	1.00	1.82	0.80	1.82	-	-
1.3	3	1.35	1.84	1.00	1.82	0.80	1.82	-	-
1.6	1	-	-	0.8	1.79	0.65	1.82	0.50	1.68
1.6	2	-	-	0.8	1.79	0.65	1.82	0.55	1.85
1.6	3	-	-	0.8	1.79	0.65	1.82	0.55	1.85

References

[1].Munteanu V. – *Instalaţie de autoreglare a nivelului oţelului lichid în distribuitorul maşinilor de turnare continuă*, Brevet de invenţie nr. 78734 - România;

[2].Orănescu A., Munteanu V., Bocioacă R. - *Structural Optimizing of the Sliding Gate Nozzle Devices for Casting Ladles*. Buletinul Universităţii din Galaţi, 1982, pag. 49-55;

[3].Munteanu V., Orănescu A., – *Posibilităţi de optimizare a procesului tehnologic de turnare a oţelului.* Simpozion cu tema „Reducerea consumului de materii prime, combustibili şi energie" Galaţi 8-9 aprilie, pag. 237-243.

EXPERIMENTAL EQUATION OF DEFORMATION BEHAVIOUR OF A CONCRETE STEEL

Nicolae Cananau, Gheorghe Gurau, Petrica Alexandru, Gheorghe Corobete
"Dunarea de Jos" University
email: ncananau@ugal.ro

ABSTARCT

The plastic deformation behavior is defined by the function of the deformation strength according to the strain, strain rate and temperature as the factor of the deformation process. The behavior law establishes by the experimental way, using the torsion test method. The paper shows the results of the researches for establishing of the equation of deformation behavior of steel destined of rolled wires for reinforced concrete.

KEYWORDS: plastic deformation, concrete steel

1. Introduction

The plastic deformation of a metallic material is described by the equation [1]:

$$\sigma = \sigma(\varepsilon, \dot{\varepsilon}, T) \qquad (1)$$

In this equation σ is the stress intensity in the really deformation conditions, ε - strain intensity, $\dot{\varepsilon}$ - strain rate intensity, T – temperature.

The knowledge of this equation of plastic deformation behavior is necessary for the evaluation, programming, modeling, simulation and optimization of the plastic deformation processes, by applying in the calculus program of the constitutive equation [1,2].

$$\dot{\varepsilon}_{ij} = \frac{2}{3} \cdot \frac{\dot{\varepsilon}_0}{\sigma_0} \cdot S_{ij} \qquad (2)$$

in this equation $\dot{\varepsilon}_{ij}$ - is the component *ij* of the strain rate tensor, $\dot{\varepsilon}_0$ - is the strain rate intensity in the really deformation conditions, σ_0 - the intensity of the stress, S_{ij} - the component *ij* of the deviator tensor of stress state. This equation is defined by:

$$S_{ij} = \sigma_{ij} - \delta_{ij} \cdot \sigma_m$$

in equation σ_{ij} is the component *ij* of the stress tensor, δ_{ij} – Kronecker's symbol, σ_m – mean normal stress of the stress tensor.

In this paper it presents the results of researches effectuated for establishing of the equation of plastic deformation behavior of steel for wires destined to reinforced concrete.

2. Experimental conditions

The constitutive equation is established through experimental way using a torsion testing machine. In figure 1 is presented a general view of the testing machine equipped with a data acquisition system [3].

The researched material has the chemical composition rendered in table 1. The form of active zone of the sample is cylindrical and has the dimensions $(\phi 6 \pm 0.02) \times (36 \pm 0.1)$mm.

Table 1. *Chemical composition of steel, [%]*

C	Mn	Si	P	S	Cr	Ni
0,18	1,23	0,35	0,037	0,035	0,21	0,15

The torsion testing installation is equipped with: electro-hydraulic system for action of sample with the power of 5kW, the revolution is 1 – 2000 rpm, data acquisition system type Spider 8, heating system, maximum temperature of 1100 ^{0}C and precision ±5 ^{0}C [3,4].

Fig. 1. *General view of the torsion testing machine.*

As result of the torsion test we obtain the torque diagram $M(t)_{\dot{\varepsilon},T}$ where *t* is the time, which may be transformed in strain. Thus we obtain the $M(\varepsilon)_{\dot{\varepsilon},T}$ diagram. In figure 2 is presented an example of the torsion moment diagram. The research program must cover a temperature area, according to the researched material and a domain of the strain rate values. A test corresponds at a certain strain rate value and certain temperature according to the established research program. In the aim of the testing we must regulation the revolution of hydraulic system, then it mounts the sample in the action device and we put in the function the heating system. Also it is put in the function the data acquisition system. When the temperature of the sample becomes equal at the programmed temperature, the action system is coupled and the deforming process it is made until the tearing of the sample. As result the data acquisition system registers a torsion moment diagram. In the figure 2 it is presented an example of the torsion moment diagram.

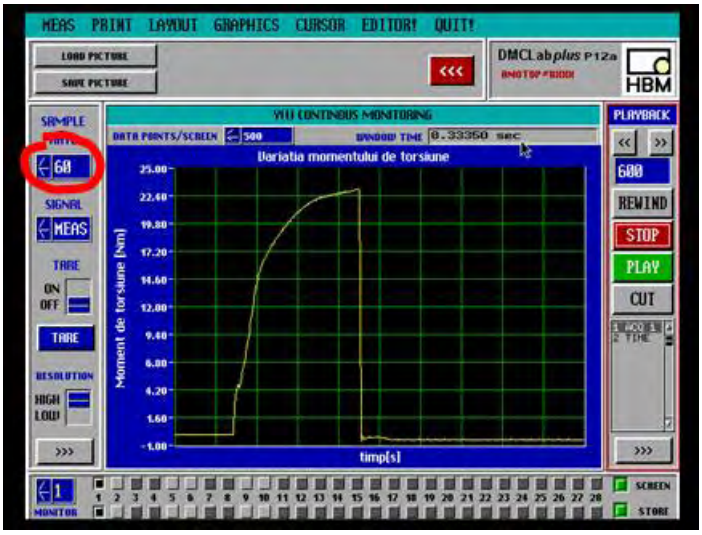

Fig. 2. *Experimental torsion moment diagram [3].*

3. Experimental researches

The research program consists in: research temperatures of 1023K, 1073K, 1123K, 1173K and the revolution of 25, 107, 400 rpm.

The application of the research program leaded at the torsion moment diagrams rendered in the figure 3, 4 and 5.

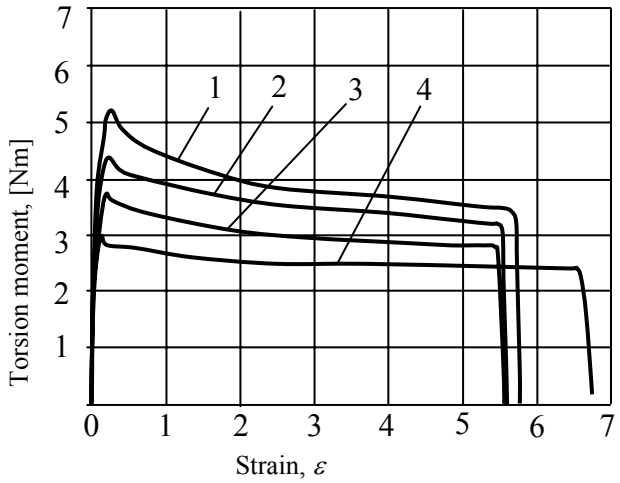

Fig. 3. *The torsion moment diagram – strain for the revolution of 25rpm: 1-1023K, 2-1073K, 3-1123K, 4-1173K.*

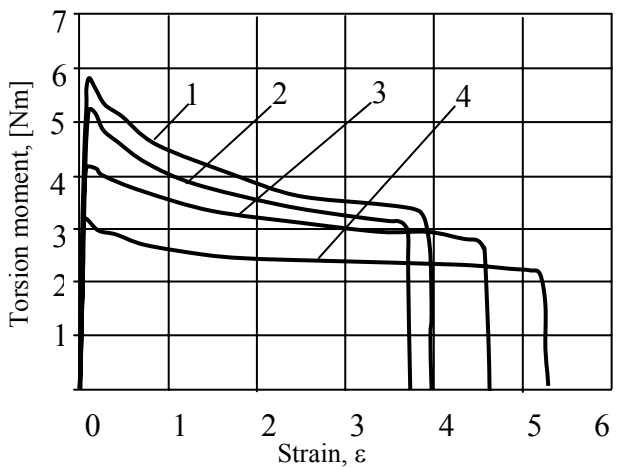

Fig. 4. *The torsion moment diagram – strain for the revolution of 107rpm: 1-1023K, 2-1073K, 3-1123K, 4-1173K.*

The function of the torsion moment is depended of the deformation degree (ε), strain rate ($\dot{\varepsilon}$) and the temperature (T). The mathematical expression of the torque is:

$$M = M(\varepsilon, \dot{\varepsilon}, T) \qquad (3)$$

In differential form the expression (3) becomes:

$$dM = \frac{\partial M}{\partial \varepsilon} \cdot d\varepsilon + \frac{\partial M}{\partial \dot{\varepsilon}} \cdot d\dot{\varepsilon} + \frac{\partial M}{\partial T} \cdot dT \qquad (4)$$

For the maximum values of the torque the expression (4) becomes:

$$dM_{max} = \frac{\partial M_{max}}{\partial \dot{\varepsilon}} \cdot d\dot{\varepsilon} + \frac{\partial M_{max}}{\partial T} \cdot dT$$

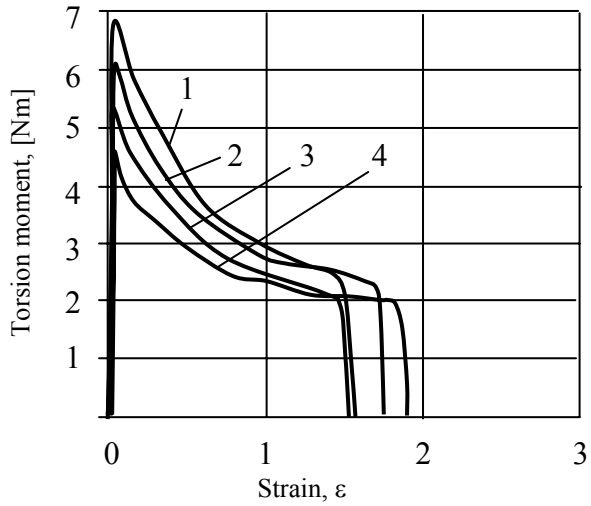

Fig. 5. *The torsion moment diagram – strain for the revolution of 400rpm: 1-1023K, 2-1073K, 3-1123K, 4-1173K.*

Selecting the maximum values of the torque, which correspond at the research program, according to the strain rate and temperatures values we obtain the diagrams rendered in figure 6. The analysis of the diagram shows that at the increasing of the strain rate the deformation resistance of material increases and its deformability decreases. At the increasing of the temperature the deformation resistance decreases and the deformability increases. At the temperature of 1073K it is manifest a trend of decreasing of the plasticity. The deformation strength of the metallic materials varies with the strain ε by a hardening law (power or exponential law), with the strain rate $\dot{\varepsilon}$ by a power law and in function of temperature through an exponential law.

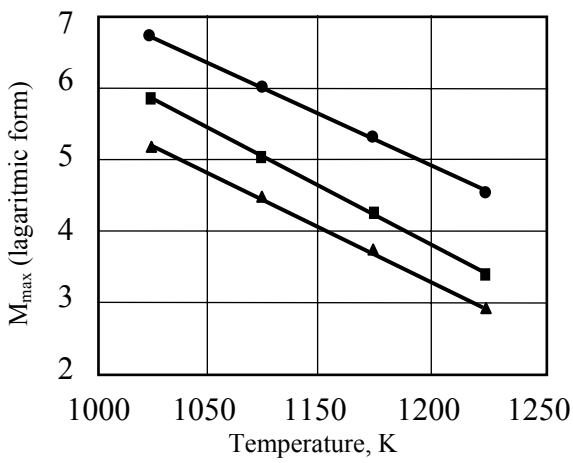

Fig. 6. *The torsion moment diagram in logarithmic coordinates: 1-25rpm, 2-107rpm, 3-400rpm.*

The general mathematical expression of the torsion moment, frequently used for description of the function of the torsion moment the following [2,4,5]:

$$M_{max} = A_2 \cdot \dot{\varepsilon}^m \cdot \exp\left(\frac{m \cdot Q}{RT}\right) \qquad (5)$$

In (5) *m* is the coefficient of the sensibility of deformation strength at the strain rate, Q – activation energy of deformation process, R – the ideal gas constant, T – temperature, in Kelvin, A – experimental constant.

We transformed the relation (5) in the linear form and applied a regression calculus program with two independent variables and one dependent variable and we obtain the results rendered in table 2.

Table 2. *Regression data at the equation (5).*

Standard Error of the Estimate = 6,56297855244627E-02				
Coefficient of Multiple Determination (R^2) = 0,9415813889				
Regression Variable Results				
Variable	**Value**	**Standard Error**	**t-ratio**	**Prob(t)**
a	-2,299048475	0,405759417	-5,666038497	0,00031
b	0,119960921	0,016731242	7,16987528	0,00005
c	4687,084251	484,3296201	9,677467692	0,0

The constants which are included in the expression (5) have the values:

$A_2 = 9{,}964$;
$m = 0{,}119961$;
$Q = 325{,}858$ kJ/mol

The mathematical expression of the maximum torsion moment is the following:

$$M_{max} = 9{,}964 \cdot \dot{\varepsilon}^{0,119961} \cdot \exp\left(\frac{4687{,}08}{T}\right) \qquad (6)$$

Admitting the Voce function for the hardening factor the equivalent stress may be defined by equation [2,5]:

$$\bar{\sigma} = \begin{cases} A \cdot \left[1 - \exp(-n\bar{\varepsilon})\right] \cdot \left(\dot{\bar{\varepsilon}}\right)^m \cdot \exp\left(\frac{mQ}{RT}\right) & \text{pentru } \varepsilon \le \varepsilon_0 \\ \sigma^* \cdot \left(\dot{\bar{\varepsilon}}\right)^m \cdot \exp\left(\frac{mQ}{RT}\right) & \text{pentru } \varepsilon > \varepsilon_0 \end{cases} \qquad (7)$$

ε_0 is the value of the strain which corresponds at the maximum value of the torsion moment. This factor is, also, a function of the strain rate and temperature.

4. Conclusions

The knowledge of the constitutive equation of the material is necessary form the modeling, simulation and optimization of the plastic deformation process. The best method for establishing of constitutive equation is the torsion testing. Applying a research program at the torsion testing machine in the Plastic deformation laboratory at the Faculty of Metallurgy and materials science from *Dunarea de Jos* University of Galati it established the constitutive equation of a steel for wears destined at the reinforcing of the concrete.

References

[1]. Cănănău N., *Teoria deformării plastice*, Universitatea Dunarea de Jos din Galati, 1994.

[2] Dumitrescu A.T. - *Contribuţii la modelarea laminarii in calibre*. Teza de doctorat, Institutul Politehnic Bucureşti, 1986.

[3] Corobete, G. - *Contribuţii la cercetarea procesului de laminare a sârmelor din otel cu caracteristici mecanice superioare*. Teza de doctorat, Universitatea Dunărea de Jos din Galaţi, 2006.

[4] Moussy F., Franciosi P. - *Physique et mecanique de la mise en forme des meteaux*. Presses du CNRS, Paris, 1990, ISBN 2-87682-023-4

[5] Cananau N., Petrea I, Corobete G. - *Modelling of the flow and deformation fields at the profiles rolling by field lines method*, The Annals of "Dunarea de Jos" University of Galati, Fascicle IX, Nov. 2005

ON THE KINETICS OF SOL GEL Al:ZnO THIN FILMS CRYSTALLIZATION ON SILICON SUBSTRATE

Viorica MUŞAT[1], Joao CANEJO[2]
Catalina ITICESCU[1]
[1]"Dunarea de Jos "University of Galati
[2] Faculty of Science and Technology, CENIMAT, New University of Lisbon
email: Viorica.Musat@ugal.ro

ABSTRACT

Recently, there is a growing interest in applying ZnO thin films on silicon buffer substrates for p-n junction devices, optical wave guide, etc.

A sol gel process is very attractive technique for obtaining oxide thin films, due to easy control of film composition, easy fabrication of large area thin films with low cost and the ability to coat-specific shapes substrates.

This paper presents a kinetic investigation of the crystallization (550-650°C) of high preferential c-axis oriented ZnO thin films on p-type (100) silicon wafer substrate, from XRD data.

KEYWORDS: Al-doped ZnO, thin films, sol-gel, X-ray diffraction, atomic force microscopy, kinetic curves

1. Introduction

Zinc oxide (ZnO) based thin films are inexpensive n-type, wide band gap (3,2eV) semiconductor materials with high transmittance in VIS-NIR region and electrical (resistive or conductive) properties depending on the doping element(s) and microstructure. Transparent and conductive Al:ZnO thin films on glass substrate with high c-axis orientated crystalline structure along (002) plane are extensively studied for various applications including transparent conducting electrode for different electronic devices such as solar cells and electroluminescence displays [1-5]. Recently, there is a growing interest in applying n-type conductive doped-ZnO thin films on p-type silicon buffer substrate for p-n junction devices [6], optical wave guide [7] and ultraviolet (UV) photoconductive detector [8]. Between the most important applications of UV detection are missile warning system, air quality monitoring, accurate measurement of radiation for the treatment of UV irradiated skin, etc [9-10] With the use of wide band-gap semiconductors such as ZnO (UV) photoconductive detector, the need for costly filters to attenuate unwanted and IR radiation would be eliminated [11]. As transparent conductive oxide (TCO), doped ZnO films are very promising alternative materials to tin oxide and indium tin oxide because of their superior abundance in nature, nontoxicity and the excellent stability in hydrogen plasma which is an unavoidable processing ambient in silicon-related fields [12].

A sol gel process is very attractive technique for obtaining oxide thin films, because the advantages of easy control of film composition, easy fabrication of large area thin films with low cost and the ability to coat-specific shapes substrates.

Only few quantitative kinetic studies concerning the crystallization of oxide thin films are presented in the literature. The kinetic parameters of the crystallization of $Sr_{0.7}Bi_{2.3}Ta_2O_9$ (SBT) [13-14], $Sr_{0.7}Bi_{2.3}Ta_2O_9$-$BiTiTaO_9$ (SBT-BTT) [13], $Pb_{0.53}Zr_{0.47}Ti$ (PZT) [15-16] and TiO_2 [17] thin films were evaluated. To date, no papers about the kinetic parameters of sol-gel Al:ZnO thin films crystallization have been found.

This paper presents, based on XRD data, qualitative kinetic study (variation of XRD curves parameters of annealed films as a function of the annealing time) of the crystallization (550-650°C) of Al(2wt%):ZnO thin films deposed on silicon substrate by sol-gel method.

2. Experimental

The thin films used as samples for the kinetic study were prepared via a non-alkoxide route and a spin-coating technique at 1500 rpm (rotation per minute) on p-type (100) silicon wafer substrate.

The thin films deposition was performed using a sol prepared with $Zn(CH_3COO)_2 \cdot 2H_2O$ 99.5%, $AlCl_3 \cdot 6H_2O$ 98% as cation sources and ethanol as solvent. The concentration of metal ions in the solution was 0.50 mol l^{-1}. In order to study the kinetics of crystallization, the as-deposed thin films samples were stabilized by preheated in air for 5 min at 400ºC. In order to study the kinetics of crystallization, different pieces of stabilized thin films were annealed for different times (10, 20, 30, 40, 50, 60, 90 and 120 minutes) at 550, 600 or 650°C; three series of eight samples corresponding to the three values of the crystallization temperature have been obtained .

After the annealing (crystallization) treatment, the X-ray patterns of the samples were recorded in 2θ = 30-37 degree range, at room temperature using a Rigaku diffractometer (model RAD IIA) with CuKα radiation.

The kinetic plots present the values of (002) peak intensity, net area and FWHM of the annealed samples that were normalized taking into consideration the ratio between its surface area and the surface area of the biggest sample.

The thickness of the crystallized thin films was measured using a Sloan Dektak 3D surface profilmeter. The final postheated films have a thickness of about 180 and 200 nm for samples annealed at 650 and 550 °C, respectively.

The morphology on the surface of the films was analyzed using an AFM microscope. Tapping mode AFM experiments were performed in a Nanoscope IIIa Multimode AFM microscope (Digital Instruments, Veeco). Commercial etched silicon tips with typical resonance frequency of ca. 300 Hz (RTESP, Veeco) have been used as AFM probes.

The electrical resistivity of the films was measured in dark, using a KEITHLEY 617 Model Programmable Electrometer.

3. Results and discussions

Figure 1 shows the XRD patterns of the films crystallized at 550, 600 and 650°C in air for different periods between 10 min and 120 min, and the normal random orientated ZnO pattern. The XRD patters of the crystallized films (Fig. 1) show a most important (002) peak, indicating a preferential c-axis orientated würtzite type, comparative to the normal random orientated wurtzite structure characterized by (101) most intense peak.

The film crystallized at 600°C show the highest preferential c-axis orientation. Characteristic to c-axis orientated crystalline structure are the grains uniformly perpendicular to the substrate surface.

The AFM micrographs (Fig. 2) confirm this orientation and show non-porous and cracks free films morphology with average grain size depending on the speed of film deposition. Higher speed deposition, higher grain size.

The surface roughness mean square (rms) of the films, estimated from AFM measurements, rises from ~12 nm to ~26 nm when the deposition speed increases from 1500 rpm to 3000 rpm, respectively.

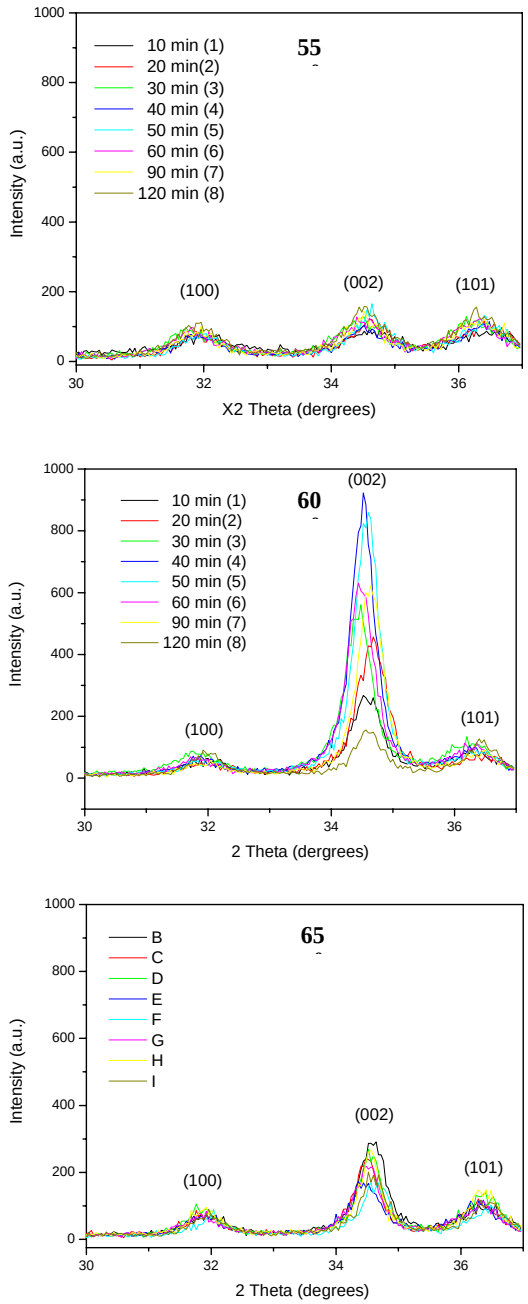

***Fig. 1**. XRD patterns of the thin films annealed in air at different temperature values.*

Figure 3 shows the variations, during annealing, of the net area, FWHM and inter-planes distance (*d*) related to the most intense (002) peak for samples annealed (crystallized) at 550, 600 and 650°C.

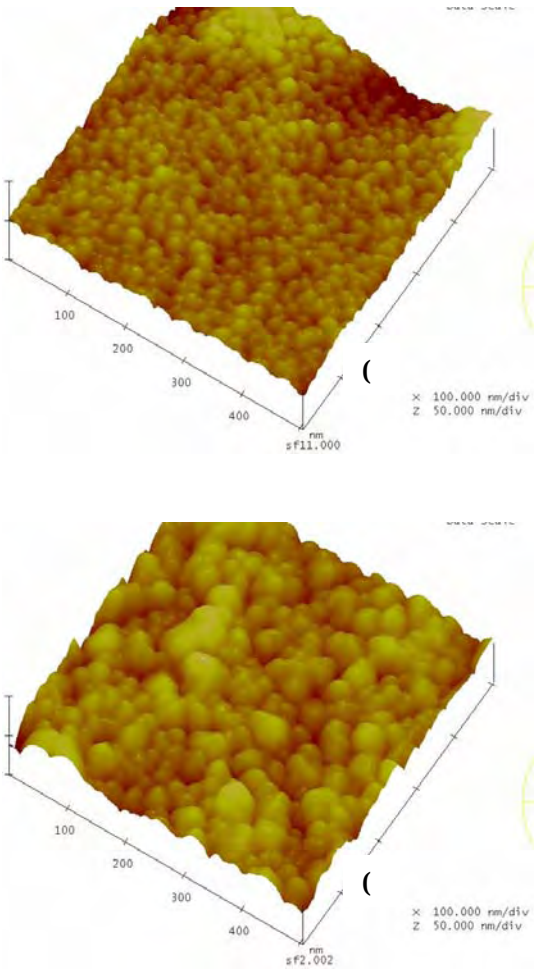

***Fig. 2**. AFM images, 3D surface topology, of thin films deposed at 1500rpm (a) and 3000rpm (b) after crystallization in air at 650C.*

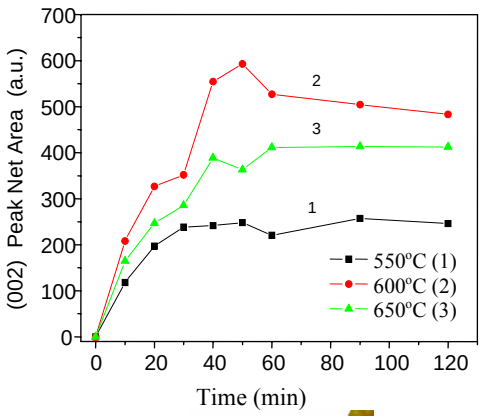

***Fig. 3**. The variation of the net area related to the most intense (002) peak, during the annealing at 550, 600 and 650°C.*

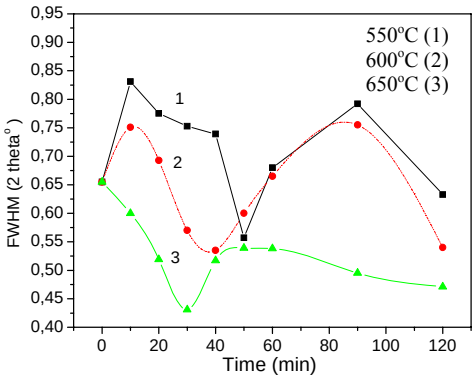

***Fig. 4**. The variation of the half width FWHM of the most intense (002) peak, during the annealing at 550, 600 and 650°C.*

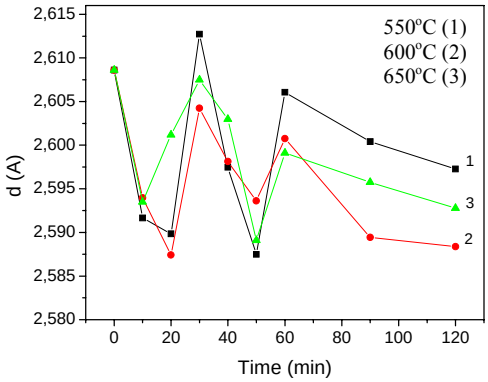

***Fig. 5**. The variation of the interplanar distance, d, related to the most intense (002) peak, during the annealing at 550, 600 and 650°C.*

From figure 3 one can see that during the first period of annealing (0-40 min), the net area of (002) peak continuously increase. The increase is the most important for the sample annealed at 600°C, smallest for the sample annealed at 550°C. The increase of (002) net area during annealing is an indication that the films crystallized at 600°C consist of a significantly larger amount of volume of crystalline phase, crystalline phase that is oriented perpendicular to the surface. Between 50-60 min annealing, the net area of the peaks decreases and after that, no significant variation occurs.

Generally, the decrease in FWHM of (002) peak confirms the improvement in the texture and quality (grain size) of c-axis orientated crystalline structure of the film. Figure 4 shows FWHM variation curves with minimum values and a shift of these minimum values depending on the crystallization/annealing temperature. Higher the annealing temperature, lower the minimum FWHM values (higher crystallite size) reached at shorter annealing time.

The variation of the interplanar distance according to (002) peak as a function of annealing time is presented in figure 5. This variation differs from the variation of the others parameters, each curve is characterized by two minimum and two maximum values situated at the same time values, for all the three series of samples annealed at 550-600 and 650°C. This variation shows that the mechanism of crystallization is complex and the rate determining step changes several times during annealing. The decrease of d during the first 20 minutes can be attributed to the total release of the organics from the stabilized films.

The film annealed in air at 600°C show the highest degree of crystallization and the highest preferential c-axis orientated crystalline structure. These results are in agreement with the literature data that recommend one hour annealing at 600°C in air for the crystallization of ZnO thin films deposed on silicon substrate [7-12].

The electrical measurements on the crystallized films showed very resistive films. A resistivity of 3.9×10^6, $8,7\times10^6$ and 3.9×10^7 Ωcm were obtained for the films crystallized at 550, 600 and 650°C, respectively.

The thickness of the thin films ranges between 250-300 nm and 200-250 nm for samples postheated at 450 and 500ºC respectively.

4. Conclusions

A qualitative kinetic study of isothermal crystallization, in the temperature range 550-650°C, of ZnO:Al (2wt%) thin films deposed on p-type (100) silicon wafer substrate was performed, based on X-ray diffraction patterns recorded at room temperature.

The crystallized films show a preferential c-axis orientated würtzite type structure with dominating (002) peak.

The variation of the net area, FWHM and inter-planes distance (d) related to the most intense (002) peak imply that the mechanism of films crystallization is complex and the rate determining step changes during annealing.

The film annealed in air at 600°C shows the highest degree of crystallization and the highest preferential c-axis orientated crystalline structure, in good agreement with the literature data that recommend one hour at 600°C annealing for the crystallization of ZnO thin films deposed on silicon substrate.

The crystallized films in air are resistive. Resistivity values of 3.9×10^6, $8,7\times10^6$ and 3.9×10^7 Ωcm were obtained for the films crystallized at 550, 600 and 650°C, respectively. After annealing in reducing atmosphere, the films turn in conductive.

References

[1]. S. Fujihara, C. Sasaki, T. Kimura, Applied Surface Sci. 180 (2001) 341.
[2]. M. Ohyama, J. Am. Ceram. 81 (1998) 1622.
[3]. D. Bao, H. Gu, A. Kuang, Thin Solid Films 312 (1998) 37.
[4]. J.F. Chang, W.C. Lin, M.H. Hon, Applied Surface Sci. 183 (2001) 18.
[5]. E. Fortunato, P. Nunes, A. Marques, D. Costa, H. Aguas, I. Ferreira, M.E.V. da Costa, M.H. Godinho, P.L. Almeida, R. Martins, Adv. Eng. Mater. 4 (2002) 610.
[6]. M. Purica, E. Budianu, E. Rusu, , Thin Solid Films, vol. 383, 2001, pg. 283.
[7]. F.C.M. Van de Pol, Ceram Bul*l*., 69 (1990) 1959.
[**8]. Z. Q. Xu, H. Deng, J. Xie, Y. Li and X.T. Zu,** Appl. Surf. Sci. (2006, in press, www.sciencedirect.com).
[9]. H. Otha and H. Hosono, Mater. Today 7(2004) 42.
[10]. T.H. Moon, M.C. Jeong, W. Lee and J.M. Myoung, Appl. Surf. Sci. 240 (2005) 280.
[11]. Y.C. Lee et al, Appl. Surf. Sci. 249 (2005) 91.
[12]. S.Y. Kuo et al, Journal of Crystal Growth, 285 (2006) 78-84
[13]. W.C. Kwak and Y.M. Sung., J. Mater. Res., 17(2002),1463.
[14]. I. M. Sung, J. Mater. Res., 7(2001), 2039.
[15]. Z. Huang, Q. Zhuang and E.W. Whatmore, J. Appl. Phys., 86 (1999), 1662.
[16] Z. Huang , Q. Zhuang and E.W. Whatmore, J. Appl. Phys., 85 (1999), 7355.
[17]. G.J. Exarhos and.M. Aloi, Thin Solid Films, 193 (1990), 42.

THE ANNALS OF "DUNAREA DE JOS" UNIVERSITY OF GALATI
FASCICLE IX METALLURGY AND MATERIALS SCIENCE, ISSN 1453 – 083X. N^0. 2 – 2006

RESEARCH ABOUT THE VIBRATION PARAMETERS FOR A COLD ROLLING MILL MACHINE

Stefan DRAGOMIR, Georgeta DRAGOMIR, Marian BORDEI
"Dunarea de Jos"University of Galati
email: sdragomir@ugal.ro

ABSTRACT

By using the equipments of vibration measurement we can fight against the damages (strip undulation and thickness variation on the length) who is show in while of mill work. The amplitude of vibration parameters determine the apparition of patterns on laminated strip.

The researches about the vibration parameters are essential for a product quality. To directly introduce by a milling program, the roll force and the other parameters, these must be in correlation with amplitude acceleration, frequency and velocity vibration.

KEYWORDS: cold rolling mill, strip, vibration, prediction, undulation.

1. Introduction

The monitoring by vibration for a cold rolling mill is very important because we can see in time the malfunction of parts (box gear, coupling, engine…). In the same time it is possible to verify, by comparing an initially signal with a work signal the good functionally of rolling mill. The roll forces have an important influence on the deformation resistance ($R_{p0,2}$), thickness (H_i and H_o), backward and forward tension (T_b and T_f), friction coefficient (μ), and other constants.

The first four factors (thickness and tension) are constant and impose and it is important do not exist variations. These variations can be registered by vibration monitoring system.

The rolling mill stands, press a strip of steel using upper/lower rolls to a desired thickness.

The gap between upper/ lower rolls determines how much pressure or force is applied. Force, thickness, speed and tension are measured while the strip is processed.

The parameters predictions involve many other factors whose exact relations are not well understood and the mathematical model is far from perfect.

Recent studies about the roll force tension and coil width prediction were made in improving of a mathematical model

The rolls forces, the coil tension, the coil width and the speed sheet were measured with specifically tools and than we draw the next curves by a mathematical model prediction.

Another way for controlled the good functionary at the cold rolling mill for strip is to do a monitoring by vibration for the moving parts of mill machine.

2. Monitoring system by vibration. Experiments.

The system configuration used for measuring and enrolled of vibration parameters (displacement, velocity, acceleration, and frequency) are shown in figure no 1.

This system work like an alarm which automatically determines the incident that has occurred on basis of measured values and notifies the operator accordingly, a diagnostic function to estimate check times from past measurement data, and a database of apparatus repair times.

The measurement system have the next parts: accelerometer, amplifiers, signal selector, measuring, sequencer and display like in figure no. 1.

The system displays this information graphically on the screen.

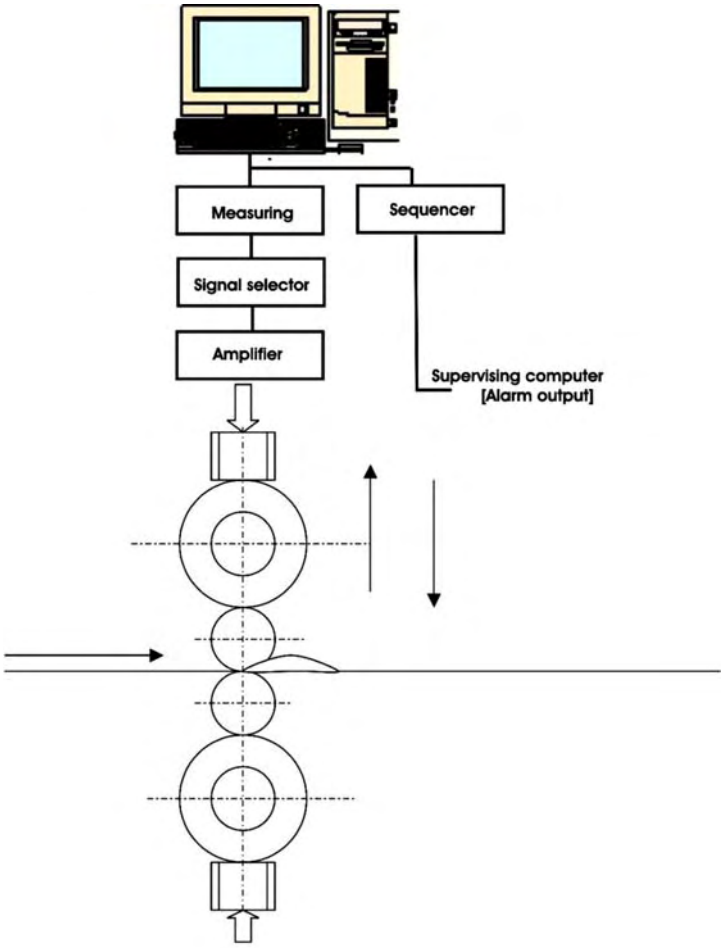

Fig.1. *The vibration monitoring system (accelerometer mounted on each stand)*

In the next figure (no.2) it is shown a parallel registered for each of five stands. It observes that the highest level of vibration is registered at stand number five.

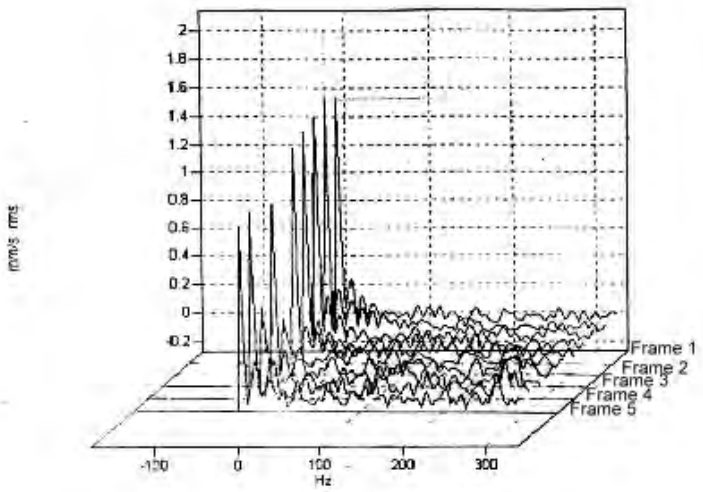

Fig.2*. Level of vibrations registered at each stand of the rolling mill.*

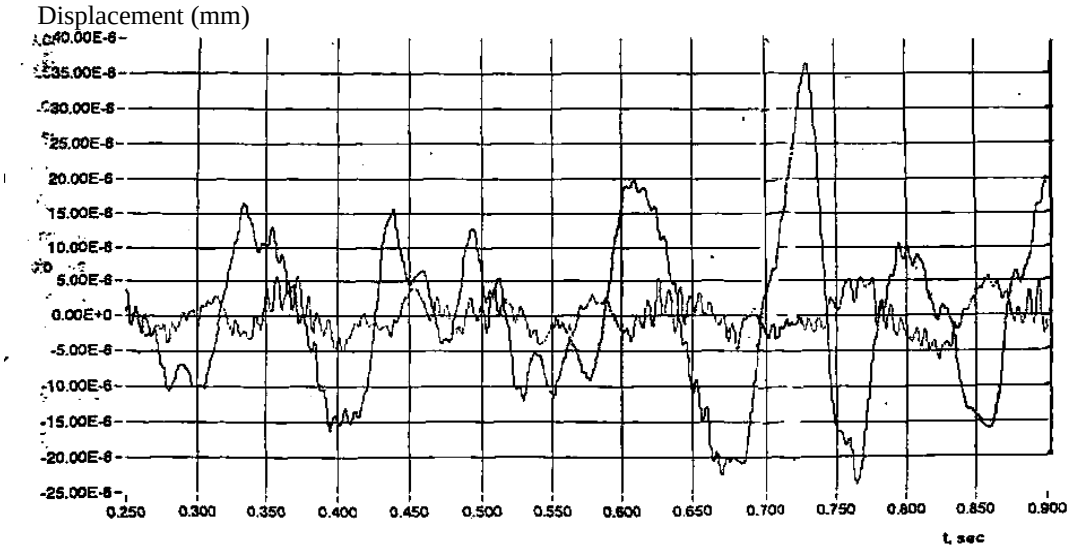

Fig.3. *The gap between the beginning of work period and after six month function (power spectrum).*

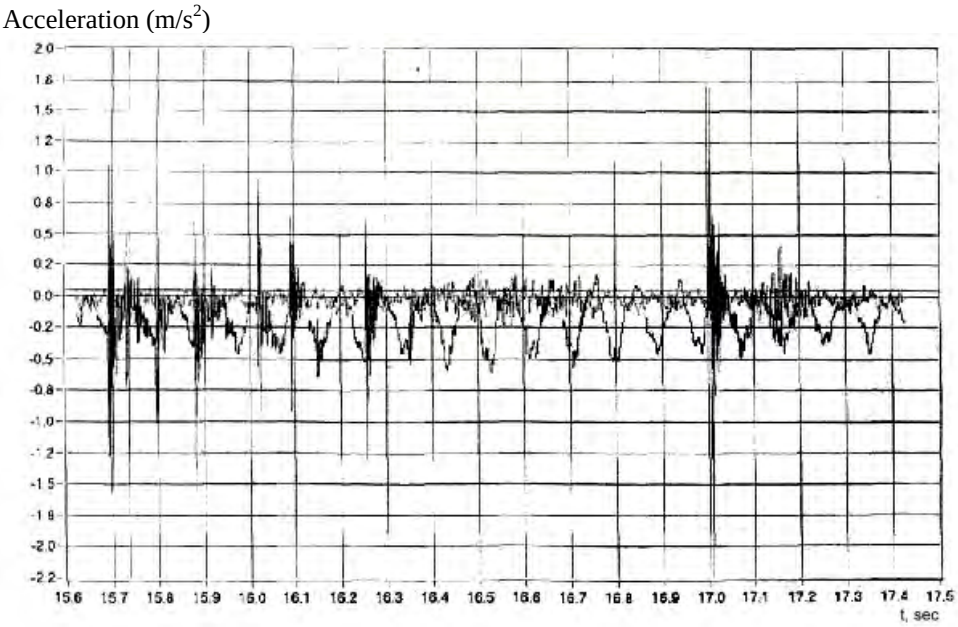

Fig.4. *Comparing between the basic acceleration signal (measured) and the signal after six month work.*

In figures 3, 4 we show (partially) the recordings by comparing the parameters of vibrations at the beginning of work period and after six month in function. Because the wear who appears in bearings, box gear, bar of coupling, the amplitude of vibration increase and determine the "out" of initially work parameters for the cold rolling mill machine .The model directly predicts all work parameters, while the corrective model produces a correct coefficient, which is then multiplied to the mathematical models prediction. Additional variables which were not used in the mathematical model were found to be necessary for the substitutive model only.

The networks of parameters (forces, tensions between stands(cages), speed, can be easily retrained if necessary as all the data from the processed coils are automatically saved in a workstation located next to the process computer.

The retraining period does not have to be fixed such as monthly or yearly .It will be more proper to determine it dynamically by monitoring the trend of prediction error.

The-network models are planned to be used in daily operation. One difficulty is to estimate the monetary savings resulting from the improved quality and decreased off-gauge.

Using the network of parameters-based roll force –prediction models show that the prediction errors of the currently used mathematical model reduced by 30-50%. The substitutive model directly predicts the roll force, while the corrective model produces a correct coefficient, which is then multiplied to the mathematical models prediction.

The networks can be easily retrained if necessary as all the data from the processed coils are automatically saved in a workstation located next to the process computer. The retraining period does not have to be fixed such as monthly or yearly .It will be more proper to determine it dynamically by monitoring the trend of prediction error.

The -network of parameters models are planned to be used in daily operation. One difficulty is to estimate the monetary savings resulting from the improved quality and decreased off-gauge

The networks of parameters (milling process force, tension between cages(stands) have a potential to improve the accuracy of the computation be substituting or correcting the mathematical model.

From the effectuated experiments it can conclude the fact that, the highest values for displacement, velocity, acceleration and power spectrum (on the direction of the action system) have been recorded at the3, 4 and 5th frame of the rolling mill machine (the causes that determinate these important values for the measured made are great tension into the strip between mill cages ;high speed of strip while the milling process or the variation of those ;abrupt change for the rolling mill work parameters; types or different quality for the emulsions used in work; the decrease of reduced number when the strip pass between the work rolls; unpredictability for one of work parameters.

At rolling mill's speed between 600 – 1250 m/min and frequencies of vibration measured that do not excel hadn't recorded of marks, undulations and abrupt variations of the strip thickness after milling process.

At vibration's frequencies between 450 – 1150 Hz, we observed undulation at strip's surface with the gap between 2- 40 mm, big wear of shell of work rolls and into the bearings of work rolls.

4. Conclusions and results

After this study we can extract the next conclusions:

-the vibrations are in each equipments and installations of cold rolling mill by different type.

By an ample study and perform experiments – with modern gear – it result a series of aspects:

- the quality of surface and geometry of cold rolling strip;
- the correct command of milling process
- the prominence of causes and the oscillation's effects, vibrations, shocks, etc. – owing the own system of rolling mill cages and the parts of kinematics action fluxes;
- the fix measures for control, decreasing, command ;
- the increase of productivity, the reduce of costs ;

The experiments made between 2005-2006 at a number of over 100 coils of cold milling strip, which in fact were measures and vibration's analyses, the have been established the following series of characteristics frequencies:

- vibrations in series of frequency between 5-90 Hz, for coupling, couplings bars, gear boxes with defects into their bearings;
- vibrations in series of frequency between 125-300 Hz for the strip which is being milling, for the gaps of positioning system, the wears into the backup and work roll bearings, lubricant used;
- vibrations in series of frequency between 500-980 Hz, wear's afferents accentuated backup and work rolls shell of these encampments, determination the appearance of hallmark and undulation on the surface of strip.

The experiments in the functionality for rolling mill machine show the tendency of vibrations amplitude at the increase of milling speed. We record a increase of milling speed with 50% at each cages of the rolling mill, the vibration's amplitude record a increase 35 % at each cage) by the other way, at strip with small breadth and with high toughness is manifested the same tendency of increasing of vibrations amplitude.

References

[1]. Sungzoon Cho,Yongjung Cho, Sungchul Yoon, "*Reliable Roll Force Prediction in Cold Mill Using Multiple Neural Network*" IEE TRANSACTIONS ON NEURAL NETWORK, Vol 8,Nr 4 1977.

[2]. C. Bishop, "*Neural Networks for Pattern Recognition*". Oxford,U.K:Oxford Univ. Press. 1995.

[3]. D.Cohn, L. Atlas, R.Ladner, "*Improving generalization with active learning*", Machine Learning,vol.15 no.2, pp.201-221,1994.

[4]. Pohang Iron and Steel Company Tech. Rep.2nd Cold Mill Contr. Equipment (PCM part), POSCO, Korea, 1989.

[5]. W. Lee, "*Improvement of set-up model for tandem cold rolling mill*", Tech. Rep. POSCO Res.Inst.Sci.Technol., 1994.

[6]. N. Pican, F.Alexandreand.P.Bresson, "*Artificial neural networks for the presetting of a steel temper mill*", IEEE Expert,vol.11,no1.pp.22-27.1996.

[7]. N.Portman. "*Aplication of neural nerworks in rolling mill automation*", Iron and Steel Eng.,vol.72 ,no.2, pp.33-36.1995.

[8]. B. Rosen, "*Ensemble learning using decorrelated neural networks*", Connections Sci.,vol.8,pp.373-384,1996.

[9]. C. Bishop, "*Neural Networks for Pattern Recognition*". Oxford, U.K: Oxford Univ. Press. 1995

[6]. N. Pican, F. Alexandre and P. Bresson, "*Artificial neural networks for the presetting of a steel temper mill*", IEEE Expert,vol.11,no1.pp.22-27.1996.

[7]. N.Portman. "*Aplication of neural nerworks in rolling mill automation*", Iron and Steel Eng.,vol.72 no.2, pp.33-36.1995

PROTECTIVE AND DECORATIVE VACUUM'S COATINGS ON WARES OF ARTISTIC CASTINGS

V. GRECHANYUK, I. GRECHANYUK, N. GRECHANYUK
Kiev National University of Building and Architectures
Kiev, Ukraine

ABSTRACT

The problem of environmental protection is extraordinarily important, and its actuality will increase with every year. In this aspect, processes of depositing of coatings in vacuum have got serious advantages before wide-spread galvanic method, as the last requires building of the special cleansing building, which cost in general balance of covering's process can arrive till 60 %. It should be noted that preliminary preparation of surface which, as is generally known, has the important value at the method of metallization in vacuum often execute by the smoldering discharge (by the «dry method»).

KEYWORDS: vacuum coatings deposition, electron-beam melting.

Methods of deposition of coatings in conditions of rarefaction (vacuum), depending on the features of transformation of material of coating in the vaporous state with subsequent condensation on the protected surface it is possible to divide into three kinds: cathode sputtering, thermal spray, and ion plating [1].

What from the indicated methods of coating's deposition in vacuum has definite advantages and failing. So, the method of cathode sputtering, differing by large universality, is limited comparatively by low speed of depositing of coatings. Thermal spray in vacuum is characterized by high performance, but had the substantial failing – low coefficient of the using of evaporated material. The method of the ion plating, allowing to obtaining of coatings with high degree of homogeneity of their thickness and with good adhesion with basis, is limited by difficulty of stabilization of plasma's discharge, and difficult equipment.

Most expressly criterions of progressiveness of any technological process are formulated in paper [2]:

1) universality, possibility of conducting of major of operations of production cycle by the identical technological receptions;
2) continuity of row of technological operations of production cycle in combination with group treatment of wares or billets;
3) high speed of conducting of basic operations of technological process, possibility of their intensification;
4) reproduced of parameters of every operation and high percent of output of suitable wares;
5) well technological construction, responding to request the automatic-ability of producing;
6) formalization, possibility of drafting of mathematical description (algorithm) of every technological operation with subsequent creation of the automatically system of technological process control;
7) competitiveness of process and possibility of quick to reconstruct the equipment for making of new types of wares without substantial expenditures.

Attempt of quantitative comparison of different methods of coverage's deposition in vacuum made by authors of paper [3], thus in each of methods their varieties are taken into account. Comparison of different methods of coverage's deposition is conducted on properties of the got films (degree of purity, density, adhesion, accordance of composition of films and evaporated alloy and etc.); on the technological features of process (sizes and form of substrate, speed of condensation, operative of process, substrate's temperature, time of cycle and etc); on the features of material, which coatings are obtained from, including cost and coefficient of using, and also - the cost of equipment.

The results of the indicated comparison taking into account present development of methods of coverage's deposition are resulted in the table 1. The following five-mark's system of estimation of the compared methods is chosen:

1) the index 5 indicates on the highest quality the tapes, most high technological and lowest cost;
2) the index 4 means that in a process the tapes of good enough quality can be got, a process is technological and the equipment has a low cost relatively;

3) the index 3 means that the considered method takes some advantages either as tapes, or in the technological features of process, or in its economy;
4) the index 2 indicates that the compared aspects of process are already found on verge of unacceptability of them for practical realization;
5) the index 1 means complete useless or unacceptability of the given method from point of one or another from the compared descriptions.

Analysis of resulted showed in table 1 data of testify of methods of thermal spray and ion plating are satisfied to all basic criteria of progressiveness. It, in particular case, behaves to the continuous processes of metallization. Of course, the resulted data in table are very relative, however a research value is unquestionable, as it allows to conduct the correct choice of method for the concrete case.

Table 1. *Comparison of different methods of coverage's deposition in vacuum*

Description of the compared methods	**Thermal spray**			**Cathode (ion) plating**		**Ion plating**			
						direct voltage		**radio frequency**	
	resistive method of heating	**electron-beam method**	**explosive evaporation**	**radio frequency dispersion**	**same + negative potential on substrate**	**resistive method of heating**	**electron-beam method**	**resistive method**	**electron-beam method**
A. Property of films:									
- degree of purity	3	4.5	3	5	5	3	4	3	4
- density	3	4.5	3	4.5	5	4	4	5	5
- adhesion	3	4	3	5	5	4.5	4.5	5	5
- homogeneity	3.5	3.5	3,5	4.5	4.5	5	5	5	5
possibility to cover the details of difficult type	2	3.5	2	4.5	4.5	5	5	5	5
possibility to obtain from alloys	1	3	5	5	5	1	3	1	3
B. Features of technologies:									
- size and shape of substrate	5	5	5	3	3	4.5	4.5	4.5	4
- holder of substrate	3.5	3.5	3,5	5	5	3	3	2.5	2
- application of masks	5	5	5	2	2	4	4.5	4	4
- speed of deposition	4	5	4	2	2	4.5	3.5	3.5	3
- complexity of operations	5	3.5	4	4	3.5	5	5	5	5
- motion, moving of substrate	5	5	5	1	1	1	2		2
- temperature of substrate	2.5	3	2,5	3	3	5	5	5	5
- time of cycle	3.5	3.5	3,5	2.5	2.5	5	5	5	5
- time of alteration of process	5	4	3,5	3	3	5	3	3	3
C. Material of coatings:									
- required form and shape	5	5	3	2.5	2,5	5	5	5	5
- coefficient of using	5	5	2	2.5	2.5	5	5	5	5
- cost	2.5	3.5	4	5	4.5	2.5	3	2.5	3
D. Cost of equipment	5	3. 5	4.5	2.5	2.5	4	3.5	3.5	2

Electron-beam influence on metals, resulting in their heating, melting and evaporation, as a new technological direction in area of material's treatment intensively develops from middle of the XX century. Essence of process of electron-beam influence is that kinetic energy of formed that or other method electronic bunch (impulsive or continuous) grows into thermal in the area of treatment.

Because the ranges of power and concentration of energy in the electron-beam are great, it is possible receipt of practically all types of thermal influence on materials: heating to the set temperatures, melting and evaporation with ever-higher speeds.

Presumably, history of process of electron-beam influence begins from 1852 year, when U. Grove in the lecture read in Royal Scientific Society, first indicated on possibility of the electron-beam heating. The first electron-beam melting of platinum anode in a cathode-radial tube was shown at 1879. At that time it was not known yet, that cathode rays were the stream of electrons. At 1907 the first Patent on the process of the electron-beam melting of metals is given out.

Fig. 1. *General view of EB-coating unit L-1*

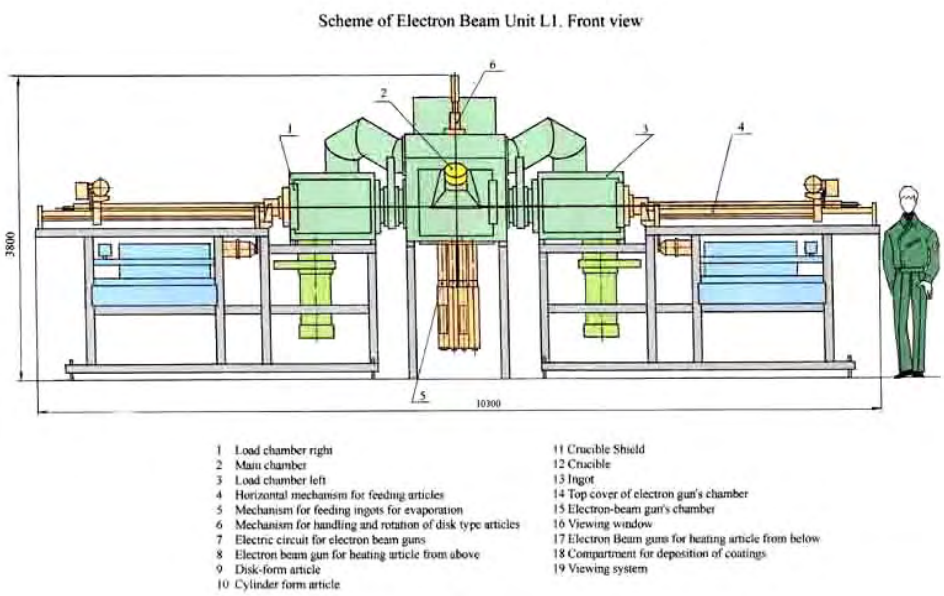

Fig. 2*. The scheme of EB-coating unit L-1.*

In Scientific-production enterprise «GEKONT» the industrial electron-beam unit L-1 for deposition of protective and decorative vacuum's coatings on different wares is developed. Photo of equipment is showed on fig. 1.

The scheme of equipment is showed on the fig. 2. The technological scheme of equipment is showed on the fig. 3. Technical descriptions of facility is resulted in the table 2.

Table 2. *Technical parameters of the industrial EB-coating unit L-1*

Denomination:	**L–1**
1. Dimensions of evaporated articles (ingots), mm diameter length, max	 70 500
2. Dimensions of surfaces of condensation, mm right-angled plane round plate (diameter) cylindrical: diameter length	 550 × 360 750 200 550
3. Distance from evaporation's surface to condensation's surface, mm	250…400
4. Number of crucibles	4
5. Lifting capacity of horizontal shaft for bringing of articles, kg	30
6. Lifting capacity of vertical shaft, kg	100
7. Power, kW transformer accessory devices	 250 85
8. Accelerating voltage, kV	20
9. Quantity and power of EB guns for evaporation materials from crucibles for heating of articles from above for heating of articles from below	 4 × 60 2 × 60 2 × 60
10. Level of vacuum in working chamber, Pa	6×10^{-3} - 1×10^{-2}
11. Discharge of cooling water (15°C), m^3 per hour	20
12. Power-supply circuit's voltage (frequency 50 Hz)	380
13. Dimensions of facility, m in plane height	 10.5×10.5 3.8
14. Weight of facility (valuation), ton	30

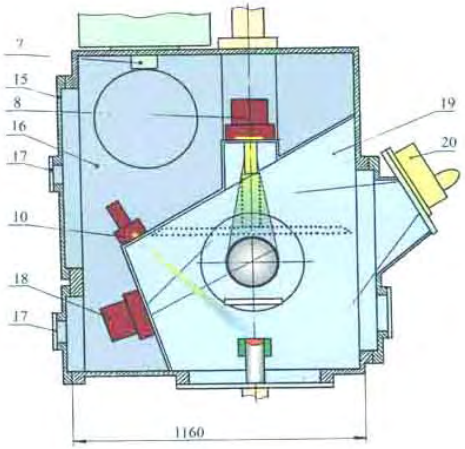

Fig. 3. *The technological scheme of EB-coating unit L.*

EB-equipment is the block of vacuum chambers with mechanisms, devices and systems providing conducting of technological process of coating's deposition on different billets. In the working chamber are located 4 crucibles for evaporation from them of materials of coatings. Evaporation of materials from each of crucibles is produced by the separate individual-guided EB-heaters. Two auxiliary chambers are intended for locking of heated billets. Disjoining of volumes of chambers is produced by 2 vacuum valves. The presence of two auxiliary chambers multiplies productivity of setting. Deposition of coatings on the billets given by turns from two auxiliary chambers takes place without unvacuuming of working chamber. The control by work of equipments is provided by in manual or automatic modes

Presently on the given equipment in industrial scales, are depositing of protective and decorative coatings on different billets from aluminum, copper, nickel, chrome is carried out, aluminum and chromic bronzes by a thickness from 10 till 300 mcm.

References

[1]. Movchan B., Malashenko I., *Heat-protective coatings, depositing in vacuum,* Kiev: Naukova Dumka, 1983. – 232 p. (in Russian)

[2]. Roikh I., Koltunova, Fedosov S. *Deposition of protective coatings in vacuum,* Moscow: Mashinostroeniye, 1976. – 367 p. (in Russian)

[3]. Varga J., Bailey W. *Evaporation, sputtering and ion-plating,* Solid state technology, 1973. – No. 12. – P. 79-86.

SURFACE HARDENING OF 40Cr10 STEEL AFTER SHORT TIME NITRIDING IN FLUIDIZED BED

Adolf BÂCLEA[1], Sorin DOBROVICI[2], Elena DRUGESCU[2], Nelu CAZACU[2], Nelu PREDA[3]
[1]S.C.COSENA S.R.L.Constanța, [2]Universitatea"Dunărea de Jos" din Galați,
[3]Bristol International, Los Angeles, California, USA
email: cazacu.nelu@ugal.ro

ABSTRACT

The paper is based by nitriding in fluidized bed experiments over laboratory plant. Fluidization applications are characterized by high values of mass and heat transfer coefficients. For experiments were used 40Cr10 (Romanian standard) steel specimens. The fluidization and nitriding processes are simultaneously. The results of experiments were investigated by micrograph, hardness and XRD. Micro Vickers investigated micro hardness profiles in section.

KEYWORDS: nitriding, thermochemical treatment, steel

1. Introduction

Fluidized bed is dispersing media (granular solid/gas or granular solid/liquid) that working in a close or open space. Fluid flow having usually an ascending passes 0 0. Relative moving of solid granular and very large exchange relative surface giving all important properties of this media: high values of mass and heat transfer coefficient, high temperature uniformity, high thermal mobility

For majority application of fluidized bed in technologies a solid granular /gas is used.

The complex disperse system is usually depending by two independent phases:

- a continues phase that is formed by granular solid uniform dispersed in a gas
- a dilute phase that appears in anomaly functional stages that represent fine suspension that floating in gas (bubble stage).

Fluidization applications (FBT) in surface engineering (and particularly in heat and thermochemical treatments) are depending by correct functionally of fluidization for resulting global favorable properties 0. A classical application is patented stage for steels wire technology, where fluidized bed is a viable media that changes classical melting lead bath 0. High temperature uniformity and the non-polluting media are the important properties for FBT applications 0. High values for mass and heat transfer coefficient are usually recorded by short time for heat and thermochemical processes, 0.

2. Experimental conditions

Some particularities and limits are important when fluidized beds are used:

- open furnace reducing total time treatments by decreasing time for heating and cooling
- open furnace conduce to simple installation concepts and working procedures with advantage in structure and properties of materials
- combustible gases (hydrogen, rests of ammonia) are burned in air and result normal gasses (water vapour)

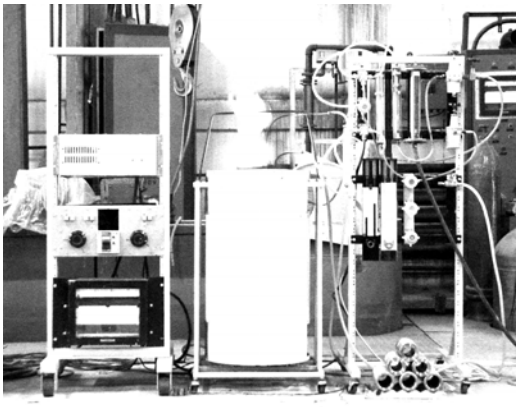

Fig. 1. *Fluidized bed furnace for thermochemical treatments*

For fluidized bed nitriding some functional characteristics are important:

- active nitriding media are functionally identical with fluidization bed

- all basic properties of fluidisation phenomenon having influence over nitruidig processes
- ammonia are source of nitrogen atoms for nitriding

Tab. 1. *Experimental nitriding in fluidized bed regimes.*

Exp.no.	Chemical composition of gas mixture	nitriding temperature	nitriding time
m.u.	%	°C	h
1	$33\%NH_3+67\%N_2$	520	1
2			2
3			3
4		550	1
5			2
6			3
7		580	1
8			2
9			3

In Fig. 1 and in

Tab. **1**, are showing fluidized bed furnace and experimental regimes.

Because nitriding is a final treatment, 40Cr10 steel samples has all anterior heat treatments (quenching and tempering) 0. Solid dimension was 0,10…0,16mm, 0. All anterior nitriding in fluidized bed regimes show 00 three groups of influence factors over nitriding process and finally over nitriding structures and properties for layer:

- nitriding factors (nitriding temperature, nitriding time, and nitrogen media activity)
- materials factors (chemical compositions, dimension and shape pieces, surface quality, etc.)
- nitriding media factors (chemical activity, heat and mass transfer coefficients, toxicity, environment impact, etc.)

3. Results and discussions

Metallographic analysis showed that after nitriding in fluidized bed for different experimental conditions the specific layer was formed (

Fig. 2).

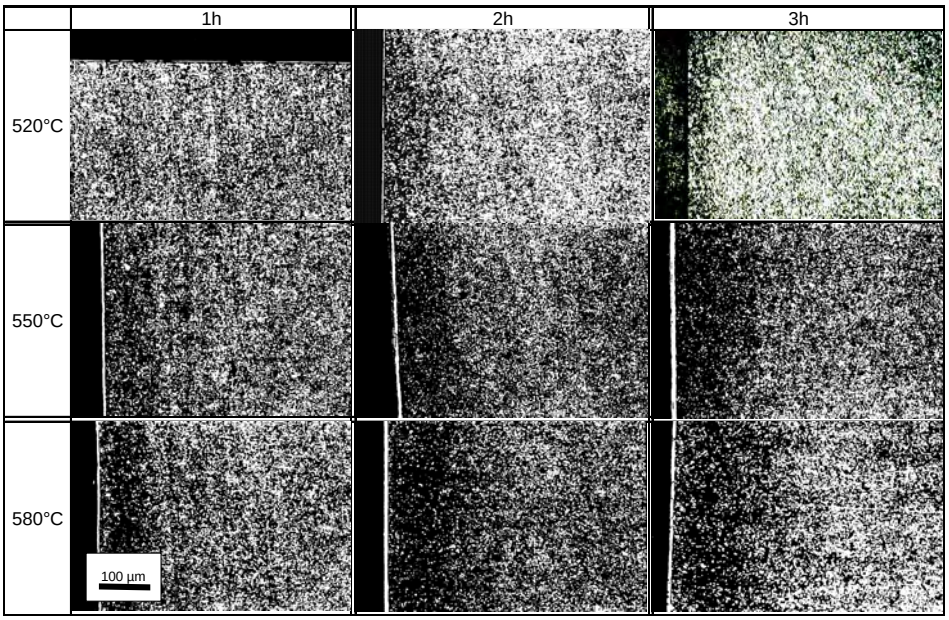

Fig. 2. *Microstructures for 40Cr10 steel specimens after fluidized bed nitriding (etching: nital 2%).*

After etching of all specimens with nital diffusion layer the diffusion zone was formed for all experimental regimes.

Combinations layer (ε+γ') was formed in correlations with high temperature and long time for these treatments. For temperature range 520...580°C the dependence of the total thickness with the process time having a parabolic dependence with nitriding time (Fig. 3). Hardness on the nitride surface of each specimen was measured by Vickers method (MPP-2 with load 5daN). The results are showed in Fig. 4. For all regimes hardness increasing and a maximum values of hardness (HV_5) was obtaining at 550 and 580°C (520...700 daN/mm^2). A parabolic profile of hardness is present.

Measurement of micro hardness (fig) over the thickness of the nitrided layer is usual investigation method for study hardness profile from surface to core of the each specimen. Micro Vickers $HV_{0,05}$ method was used (PMT-3 with load 0.05daN).

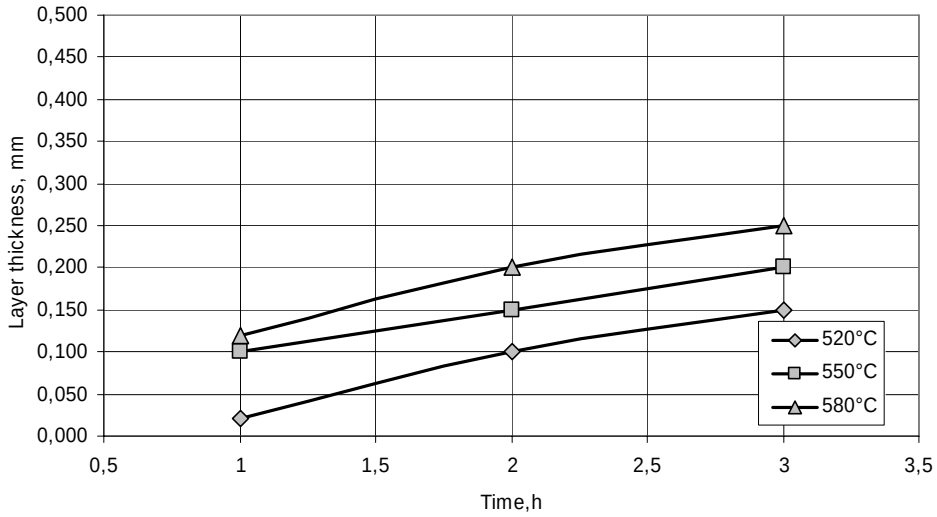

Fig. 3. *Total layer depth for 40Cr10 steel specimens after fluidized bed nitriding and for different temperature.*

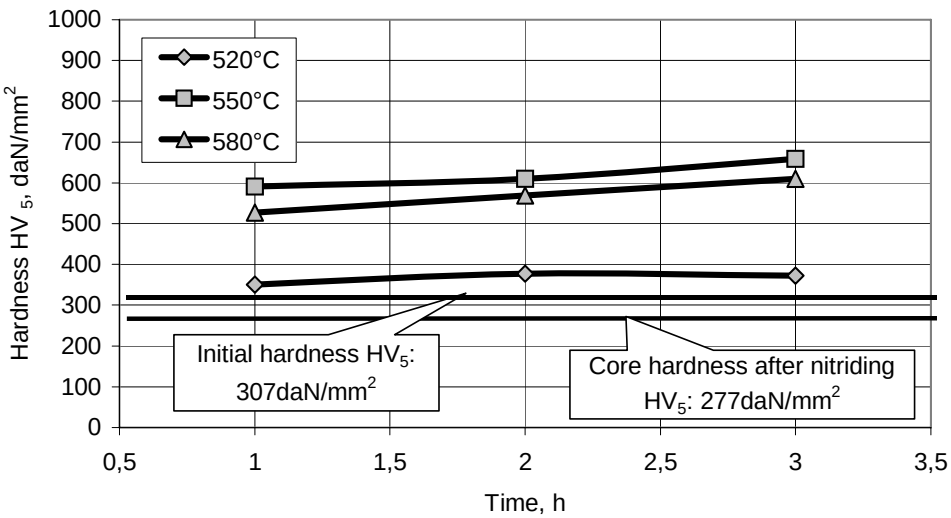

Fig. 4. *Hardness HV_5 over 40Cr10 steel specimens surface after fluidized bed nitriding.*

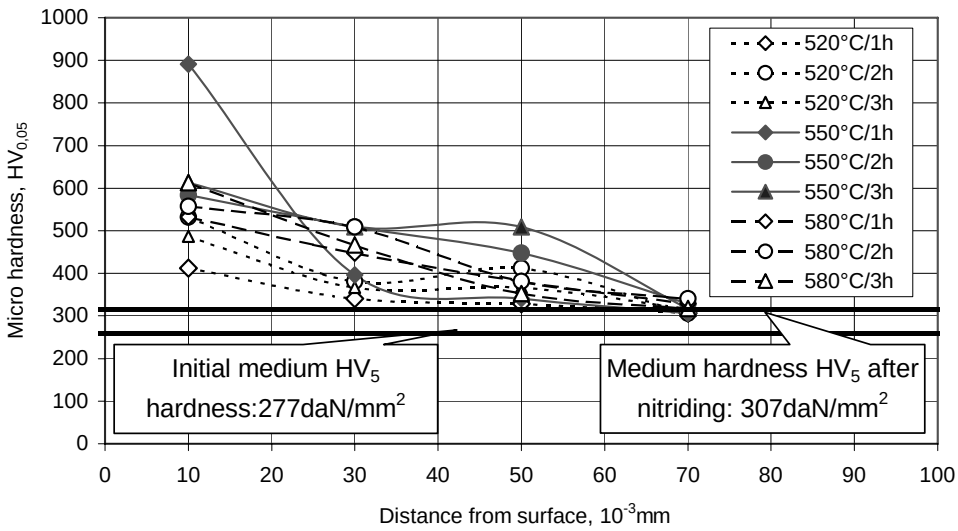

Fig. 5. *Micro hardness $HV_{0,05}$ for 40Cr10 specimens after fluidized bed nitriding..*

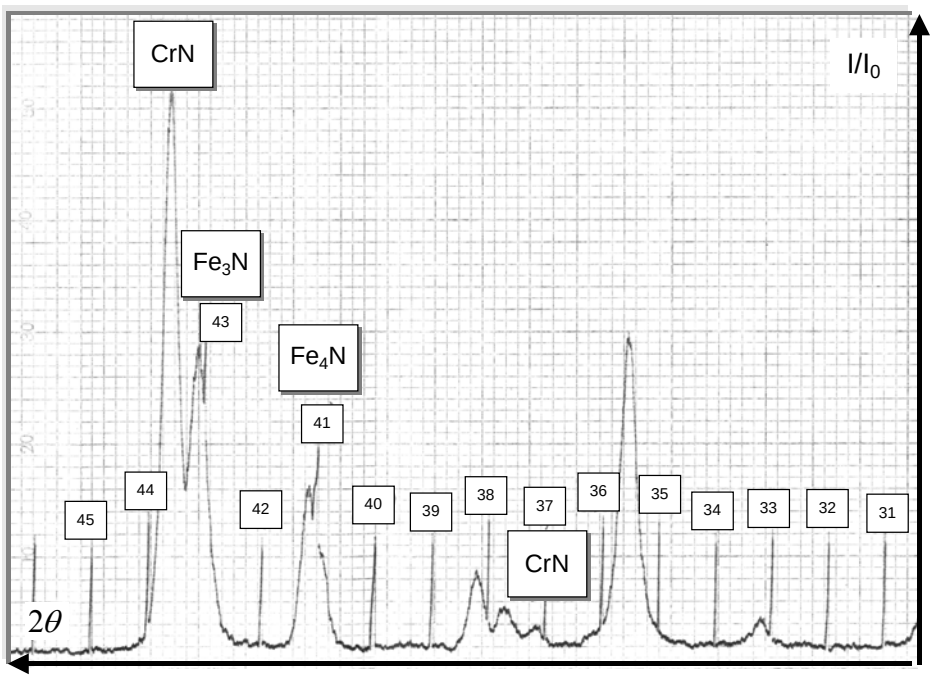

Fig. 6. *Difractogramm for 40Cr10 steel specimens after nitriding in fluidized bed (550°C/3h)*

The measurement results are showed in Fig. 5. Nitrided layer depth obtaining by micro hardness measurements showing:

- 50μm at 550°C temperature a maximum values is obtaining for 3h maintaining
- 70…75μm for 3h maximum titriding time (3h) at 550/580°C nitriding temperature.

XRD measurements (DRON 3.0, Bragg-Bentano method, 30kV and 24mA) showed that the iron and chrome nitride with specific structure were formed (Fe_4N, Fe_2N, CrN). In Fig. 6 is showing difractogramm for 550°C nitriding temperature and 3h nitriding time.

4. Conclusions

Fluidized bed is recognized that active media for thermochemical treatments characterized by high values for mass and heat transfer coefficients 0. For that total time of processes are reduced with maintaining the result values for superficial structures and properties.

For all nitriding experimental regimes was obtained nitriding layers and structure and superficial properties is in direct depending with values of experimental factors.

- The maximum values for hardness was obtaining for 550 and 580°C temperatures
- Hardness increasing can be associated with carbon and chrome contents of steel
- Microstructure and XRD are direct correlated with surface HV_5 hardness and micro hardness $HV_{0,05}$ profile for each regime
- Nitrogen desorbtion are eluded by rapid cooling after treatment

References

[1]. Bâclea A, *Studies and researches regarding fluidized bed nitriding implementation for increasing properties for ship equipment parts*,.doctoral thesis, "Dunarea de Jos" University of Galati

[2]. Bâclea A, Cazacu N, Drugescu E, Dobrovici S, *Nitrurarea in strat fluidizat cu amestec de amoniac si azot aplicata otelurilor aliate cu aluminiu*, Conferinţa Tehnologii şi materiale avansate,TMA 2003, Galaţi 20…22 noiembrie 2003, ISBN 966-549-916-5, pag.266;

[3]. Iacob, C., Vigierre,P., *Traitement thermique de fils d'acier en lit fluidise: solution alternative au bain de plomb*, Traitement thermique, no.310 aout-septembre 1998;

[4]. Kunii D, Levenspiel O, *Fluidization engineering*, John Wiley & Sons, Inc., New York, 1969, 1991;

[5]. Mihailă C., *Procese termodinamice în sisteme gaz-solid şi aplicaţiile lor în industrie*, Editura Tehnică, Bucureşti, 1983;

[6]. Sagon-King, F, *ASM Handbook, Vol. 4, Heat Treating, Fluidized-Bed Equipment*, ASM International, Materials Park, OH 44073-0002, pages 484-491;

[7]. Baladin Y.A, *Surface hardening of die steels by diffusion boronizing, borocopperizing and borochromizing in fluidized bed.* Metal Science and heat treatment, vol47, nos. 3-4, 2005, pg.203

[8]. Samoila C, Ionescu M.S, Drugă L, *Tehnologii şi utilaje moderne de încălzire*, Editura Tehnică, Bucureşti, 1986;

[9]. Vermeşan,G., *Tratamente termice. Indrumăto*r, Editura Dacia Cluj Napoca, 1987, pag.167÷180.

THE INFLUENCE OF POLARIZATION TENSION OF THE GRADING OVER THIN LAYER PROPERTIES OF TiN DEPOSED THROUGH PDV METHOD

Mihai GAITA, Marian BORDEI
"Dunarea de Jos" University of Galati
e-mail: gaita.mihai@yahoo.com

ABSTRACT

The deposits of tough thin layers on pieces and tools through PDV method knew a permanent and constant spreading owing to the great applicability of the resulting coatings which make that the thin layer deposit from the vapour stage to become a strategically industrial technology with great development possibilities, regarding both the materials and the optimization applications of the deposits processes.

In the present paper the PDV coatings studied (TiN obtained through the technology with cathodic arc) has a high hardness, a low friction coefficient and a good corrosion resistance, these properties making them excellent anti wear coatings, they are already used on a large scale in the mechanical industries, aero spatial, optics and biomedicine.

KEYWORDS: PDV method, thin layer, hardness, friction coefficient

1. Introduction

As a result of a rising coating and industrialization of the PDV technology, this one receives a great importance regarding the production costs connected with the optimization of the deposits parameters and the possibility of on-the-spot modification of the process variables according to the properties that the coating has to possess. The present paper has the aim of analyzing the way the mechanical and morphological properties of the TiN monolayer deposit tend to vary depending on the deposit parameters modifying the polarization tension of the grating.

2. Experiments

TiN coating were achieved by using the PDV represented in the figure 1. Two deposits on 10TiNiC180 stainless steel plates were achieved using the cathodic arc technology.

These TiN coatings called TiN-U_o and TiN-U_1 were achieved by modifying the polarization tension of the grating (U_o and U_1 being the two 140 V and 155 V tensions).

***Fig. 1**. The PDV installation (Valahia University of Targoviste).*

***Table 1.** The deposit parameters of the coatings*

Sample	Pressure N_2	T_{max} substratum	Polarization tension	Deposit time
	[10^{-2} mbarr]	[^{0}C]	[V]	[h]
TiN-U_o	1.6	400	140	5.5
TiN-U_1	1.6	400	155	5.5

The coatings obtained were examined and characterized by using the optics and electronic microscopy, the laser profilometry and with inductive sensor, Vickers microhardness meter, block on ring and scratch test tribometer.

3. Obtained results

In the following figures the coatings thickness is presented. They were made by means of the optic microscope in clear field; 120 measurements were made in different zones of the sample in order to obtain a medium significant statistic value.

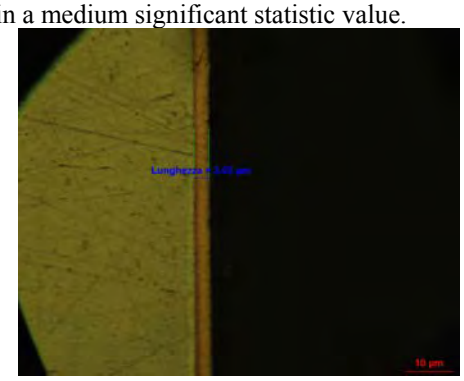

Fig. 2. *Section from sample TiN-U$_o$ layer thickness 3.03 µm.*

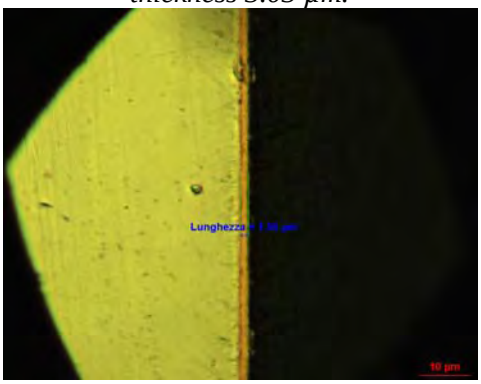

Fig. 3. *Section from sample TiN-U$_1$ layer thickness 1.55 µm.*

In table 2 the medium values and the standard deviations of the measured thickness are presented.

Table 2*. Measured values of the thickness.*

Sample	Medium measured value	Standard deviation
	[µm]	
TiN-U$_0$	2.74	0.33
TiN-U$_1$	1.46	0.16

After these first results were can emphasize the fact that the increase of the polarization tension of the grating led to a decrease of the coating thickness at about half of it.

Profilometries were made on the samples surfaces in order to evaluate the roughness (table 3) and to analyze the defects size. For the quantification of the defects size we resorted to determining some special parameters such as the medium height of the defects (P_c parameter) and the number of defects (of major height of the slated threshold) for the surface unit (SP_c parameter as shown in tables 4 and 5)

Table 3. *Roughness parameters*

Parameter	TiN-U$_0$	TiN-U$_1$
	[µm]	
R$_a$	0.0811 ±/-0.020	0.0582 +/-0.0064
R$_q$	0.17 +/-0.048	0.105 +/-0.0209

Table 4. *Medium height of the defects*

Parameter	TiN-U$_0$	TiN-U$_1$
	[µm]	
P$_c$	0.314 +/-0.234	0.296 -/-0.137

Table 5. *The defects density*

Parameter	TiN-U$_0$	TiN-U$_1$
SP$_c$ (pk$_s$/mm^2) ≥ 0.5 µm	768	386
SP$_c$ (pk$_s$/mm^2) ≥ 1 µm	319	64
SP$_c$ (pk$_s$/mm^2) ≥ 2 µm	48	6

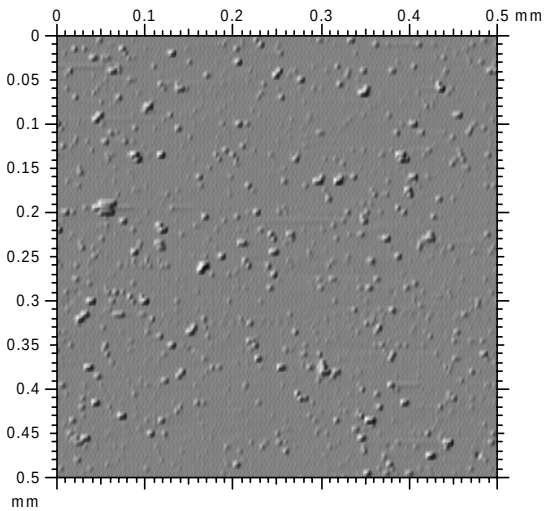

Fig. 4. *The profilometry of TiN-U$_o$ sample.*

We can notice that for the TiN coatings, at the rise of the grating polarization tension, the defects density decreases. In the figures 4 and 5 the superficial defects of the samples are presented. Measurements of microhardness were made on the coating substratum system in order to measure the coating hardness, emphasizing the substratum contribution; for this aim, 4 pre-established models were used (Burnett-Rickerby, Chicot-Lesage, Korsunsky, Puchi-Cabrera).

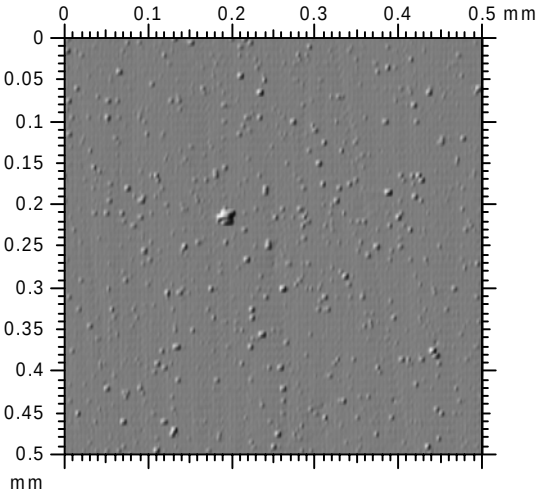

Fig. 5. *The profilometry of TiN-U$_1$ sample.*

In table 6 (Burnett-Rickerby B-R, Chicot-Lesage C-L models) the hardness values are presented according to drive loading.

Table 6. *Hardness according to the drive loading, calculated after Burnett-Rickerby (B-R), Chicot-Lesage (C-L) models.*

Loading	**HV TiN-U$_0$**		**HV TiN-U$_1$**	
[daN]	[daN/mm^2]			
	B-R	C-L	B-R	C-L
0.01	2477.42	2691.59	2565.36	3726.70
0,015	2506.94	2844.46	2116.75	3429.10
0,025	2682.78	3096.64	3240.08	3839.19
0,05	2788.12	3288.06	3175.85	3810.77
0,1	2366.80	2714.06	2833.48	-

Table 7. *Absolute coating hardness through Korsunsky method; k is the value of best fit of the model parameter; r^2 is the correlation coefficient*

	TiN-U$_0$	**TiN-U$_1$**
HV [daN/mm^2]	2872	1414.47
K	14.14	1.42
r^2	0.98	0.95

Table 8. *Absolute coating hardness after the Puchi-Cabrera model; n is the exponent that appears in Meyer law which connects the applied load to the imprint diagonal*

	TiN-U$_0$	**TiN-U$_1$**
HV[daN/mm^2]	2893.66	1433.86
n	1.30	1.54
r	0.96	0.96

In figure 6 one of the imprints measured for determining hardness is shown.

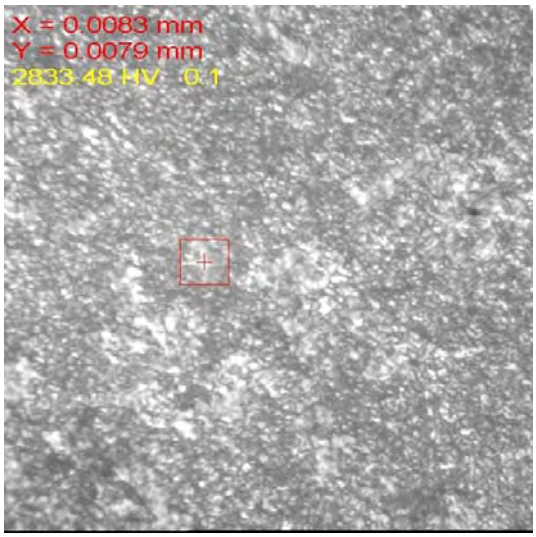

Fig. 6. *The imprint measured for determining the hardness with 0.1 daN load.*

At this point the following appreciations are necessary: no doubt that B-R and C-L models are very dependent on the values of Young model of substratum and coating (which were taken from the specialized references). These limits could be surpassed by determining the elasticity model of the examined coating. On the contrary, Korsunski and Puchi-Cabrera models had the advantage of being totally independent of Young model.

The tribologic samples were made using both a tribometer with block on ring configuration with and without lubrication.

All samples were made by using the following parameters:

- the rotation speed of the hasp: 36 rpm;
- the applied loading: 47 N;
- testing time of the sample: 300s.

The non-lubricated samples emphasized an unexpected crack of the coating.

In table 9, the resulting medium value of the dynamic friction coefficient is presented.

Table 9. *The medium value of the dynamic coefficient (without lubrificant).*

	TiN-U$_0$	**TiN-U$_1$**
Dynamic friction coefficient	0.31	0.29

Lubrication tribologic samples were also made (Hydraunyoil FH 51 lubricant). In the figure 7 we can notice the evolution of the dynamic friction coefficient, and in table 10 their medium values.

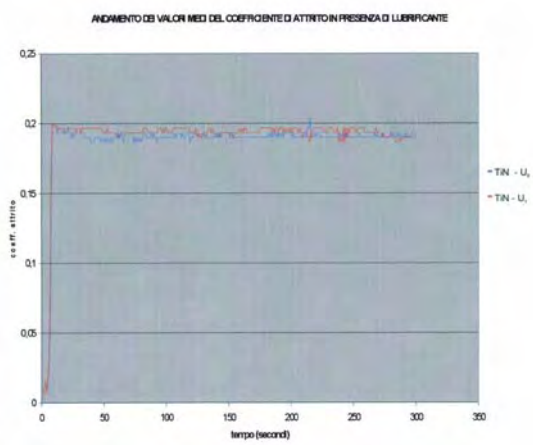

Fig. 7. *The evaluation of the dynamic friction coefficients according with lubrication.*

Table 10. *The medium values of the friction coefficient with lubrication.*

	TiN-U$_0$	**TiN-U$_1$**
Dynamic friction coefficient	0.19	0.19

For the scratch test samples, four destruction successive conditions were individualized (contraction, aliquation easy, aliquation moderate, aliquation heavy) each of them being reached at the applied critical loading.

Two tests were made for each material; the medium values of the critical loading at different degrees of destruction are presented for each material in table 11.

Table 11. *Medium critical (in Newton) corresponding to the scratch tests*

	TiN-U$_0$	**TiN-U$_1$**
Contraction	1.584	1.428
Easy aliquation	10.985	8.970
Moderate aliquation	10.985	8.970
Heavy aliquation	12.570	11.803

From the executed samples confrontation we can draw the conclusion that the TiN coating obtained with polarization tension of the inferior grating behaves better.

4. Conclusions

The obtained results emphases the influence of the deposing parameters, especially the polarization tension of the grating over the mechanic behaviour of the coating. For the TiN coating, a rise of the polarization tension of the grating determines besides a decrease of the final thickness, a substantial decrease of the defects number too, together with good values of the wear hardness and resistance under lubrication conditions.

References

[1]. K.H. Habig – *Chemical Vapor Deposition and Physical Vapor Deposition Coatings, Proprieties, Tribological Behaviour and Application,* J. Vac. Sci. Technol. A4(6) Nov/Dec, 1986

[2]. R.V. Berry – *Thin Film Technology*, Van Nostran & Company, Princeton, New Jersey, Toronto London, 1970.

[3]. E. Moll and E. Bergman – *Hard Coatings by Plasma Assisted PVD Technologies, Industrial Practice, Surface and Coating Technology*, 37, 1989

[4]. Briggs D., Peach M.P. – *Practical Surface analysis* , 1994.

[5]. Wiley J., Sans N. Y.-*Practical Surface analysis*, 1993

[6]. Winand R.-*Application of Polarization Measurements in the Control of Metal Deposition* –Ed. I.H. Warren,Elsevier, 1984

[7]. Bernard J.-*Adsorption on metal surface*, Elsemer, 1993.

ASTM Designation G77-98 *Standard Test Method for Ranking Resistance of Materials to Sliding Wear Using Block-on-Ring Wear Test* .

[8]. ASTM C1327-99, *Standard test method for Vickers indentation hardness of advanced ceramics*, ASTM International.

[9]. Glocker D.A., Shah S.I., IOP Publishing Ltd. *Handbook of Thin Film Process Technology*, Vol. 1,1995

[10]. Korsunsky A.M., McGurk M.R., Bull S.J., Page T.F., Surface and Coatings Technology, *On the hardness of coated systems,*1998

[11]. Puchi-Cabrera E.S. *A new model for the computation of the composite hardness of coated systems*, Surface and Coatings Technology, 2002

[12]. Heinke W., Leyland A., Matthews A., Berg G., Friedrich C., . Broszeit E., *Thin Solid Films Evaluation of PVD nitride coatings, using impact, scratch and Rockwell-C adhesion tests*, 1995

[14]. Santos S.C., Sales W.F., da Silva F.J., Franco S.D., da Silva M.B., *Tribological characterisation of PVD coatings for cutting tools*, Surface and Coatings Technology, 2004

THE ANNALS OF "DUNAREA DE JOS" UNIVERSITY OF GALATI
FASCICLE IX METALLURGY AND MATERIALS SCIENCE, ISSN 1453 – 083X. N^0. 2 – 2006

HARDENED ALUMINUM WITH OXIDE PARTICLES

Florentina POTECASU, Octavian POTECASU, Elena DRUGESCU
"Dunarea de Jos" University,
e-mail: fpotec@ugal.ro

ABSTRACT

The paper presents the effect of size and dispersion degree of the particles of aluminum oxide, on structure, mechanical characteristics and phenomena that take place when heating at different temperatures for recrystallization, for some samples obtained through deformation of superficially oxidized aluminum powder.

The powder necessary for research had a grain size smaller than 40 μm and it was obtained in lab on a pulverization installation with air-jet. The fine film dispersion of oxide in the metallic matrix was obtained as an effect of extrusion with high degrees of the compressed products of superficially oxidized powder (from compressed with diameter of 20 mm to tests with diameter of 3 and respectively of 4 mm). For comparison reasons semi-products of cast aluminum were deformed under the same conditions.

The maintaining temperatures of thermal treatment ranged from 350-550°C. At heating the oxide particles are stable and have a role of barrier against dislocations, therefore delay the interactions among dislocations and thus maintaining high mechanical resistances for the hardened aluminum matrix as compared to cast aluminum (without particles). The hardening effect through dispersion is as much higher as the deformation degree of tests from superficially oxidized powder increased, which determined o more pronounced finishing of the oxide particles and a greater dispersion of the fine oxide particles in aluminum matrix.

KEYWORDS: aluminum, oxide, dispersion, hardening

1. Introduction

The enhanced mechanical resistance, including at high temperatures, for a hardened material through dispersion with non-metallic particles is due to interactions among matrix dislocations and the fine precipitates, interactions that diminish the dislocations mobility. The obstacles that the particles create for moving the dislocations in the alloy's matrix are made on the one hand by the presence of these disperse phases, and on the other hand by the existing stress fields around these ones.

Starting from these reasons, the paper presents the influence of stable Al_2O_3 particles, hardening on structure, mechanical characteristics and the phenomena that take place at heating done at different temperatures for recrystallization, in the case of some deformed tests of superficially oxidized aluminum powder with a grain size smaller than 40 μm.

2. Experimental conditions

The aluminum powder used for experiments was obtained in the lab on a pulverization installation with air-jet. The oxide dispersion in the metallic matrix, was realized through extruding the compressed products of superficially oxidized powder with the grain size of < 40μm, initially compressed and sintered at 550°C. When passing by the calibration zone of the matrix, it occurs a profound deformation due to initial diameter reductions of 20 mm to final diameters of the extruded tests of 4 and respectively of 3mm.

As an effect of this deformation, the particles of fragile oxide that cover the aluminum powder particles, are crumbled and controlled carried along in the aluminum matrix of the extruded tests. Under the same conditions of extrusion the blank tests were obtained of cast aluminum with identical deformation degree, similar to the cases of hardened.

tests with oxide, of ε_1 =25 and respectively of ε_2 = 44. The deformation degree « ε » was determined as a report of the initial section, before deformation and the final section of the extruded test ($\varepsilon = S_0/S_f$).

3. Experimental results

In fig.1 it is presented the microstructure of oxidized powder tests and of cast aluminum, extruded at the diameter of 3 mm (ε_2 = 25).

The cold-hammered tests were heated at different temperatures within the range of 350- 550°C and the structural changes and mechanical properties for applied conditions were analyzed.

In fig. 2 it is presented the graph with the temperature influence of thermal treatment on mechanical resistance and elongation determined at the tensile breaking test both for the samples of aluminum extruded through dispersion and for those of aluminum hardened through dispersion with fine oxide particles.

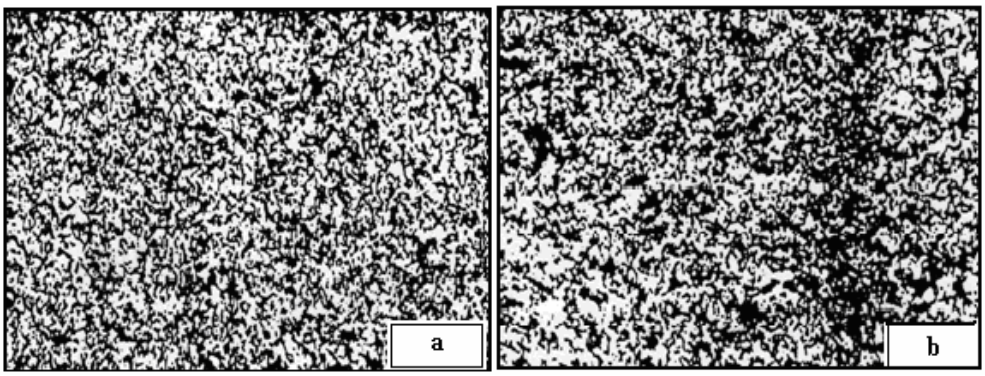

Fig. 1. *Microstructure of cold-hammered samples with ε_2 = 44: a-aluminum hardened through dispersion with oxide particles; b-aluminum (increase: x 250; metallographic attack: 10% HF)*

Experiments highlighted the importance of oxide particles in blocking the dislocations thermodynamic activated by heating. Thus, superior values of mechanical resistance were obtained, for extruded samples with the same deformation degree in the case of aluminum hardened with oxide (curve 3) as compared to those not hardened (curve 1).

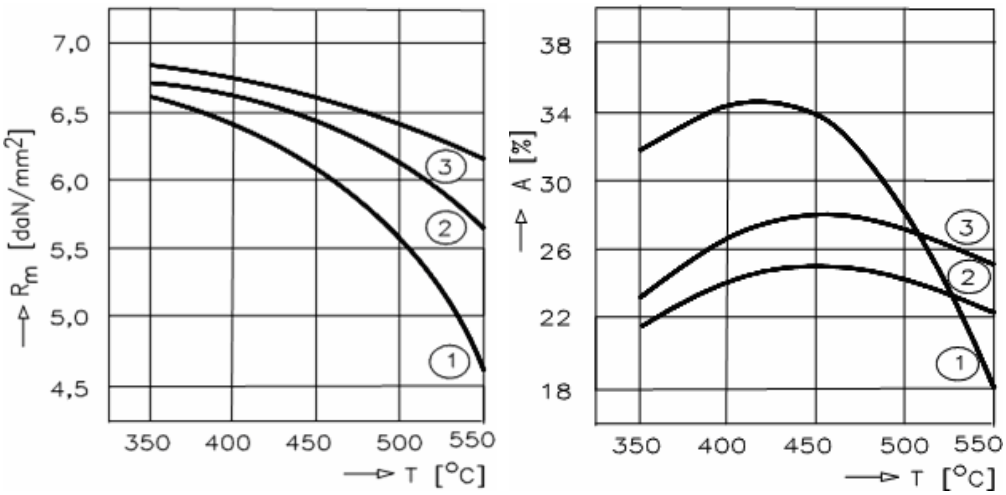

Fig. 2. *The temperature influence of thermal treatment on mechanical resistance and elongation on extruded samples: 1-aluminum (ε_2 = 44); 2 - aluminum hardened through dispersion with oxide particles (ε_1 = 25); 3 - aluminum hardened through dispersion with oxide particles (ε_2 = 44).*

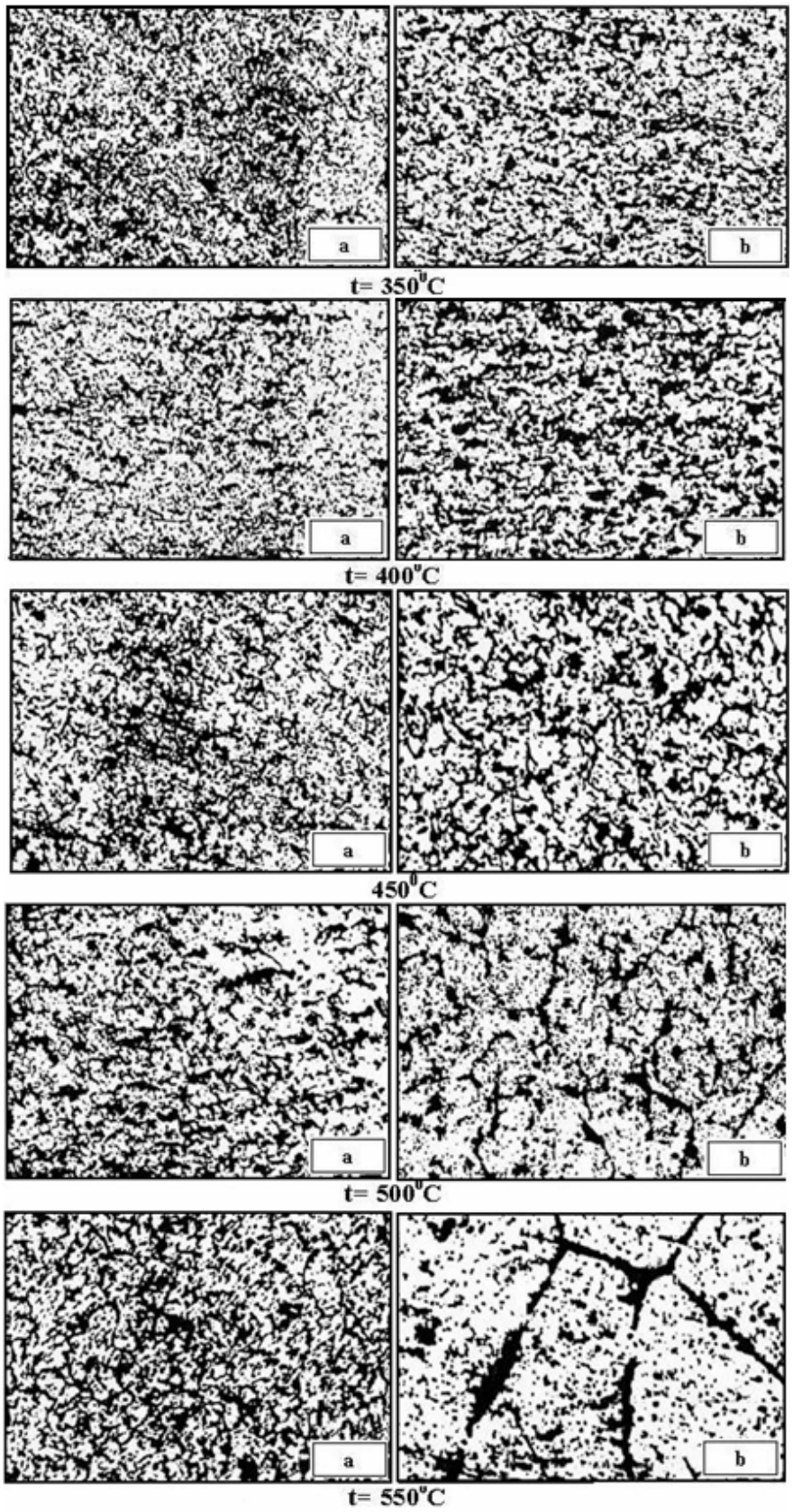

Fig. 3. Microstructure of extruded samples with ε_2 = 44 and maintained for 1 hour at different temperatures of annealing thermal treatment: a – aluminum hardened through dispersion with oxide particles; b – aluminum (increase: x 250 ; metallographic attack: 10% HF)

One can notice also, that when increasing the deformation degree (curve 3) the more pronounced finishing of the dispersed particles (as compared to curve 2) lead to higher number of obstacles against dislocations, which determined a more pronounced hardening of the metallic matrix associated with a better plasticity.

If above 450 ^oC the aluminum softening is speeded, for the hardened aluminum the decrease is diminished.

The results of the mechanical tests are confirmed also by the microstructural analysis presented in fig. 3 for cold-hammered samples, thermically treated at different temperatures within the range of 350-550 ^oC with maintain periods of 1 hour.

4. Conclusions

The experiments presented in the paper showed that the metallic matrices get hardened by extruding with high degrees of the compressed products of superficially oxidized powders.

The hardening of extruded materials through dispersion with fine particles is obtained as a result of crumbling the fragile films of oxide that clothe the powder particles. The dispersed oxide particles are barriers against dislocations and, thus, when heated, the metallic matrix keeps itself a high density of dislocations. This brakes the increase of the grains at thermal treatment of recrystallization and it gives to the extruded products superior characteristics of mechanical resistance and one can notice a good creep behavior also. Products hardened through dispersion of hard and stables particles, can be obtained by deforming from superficially oxidized powders. They have superior mechanical characteristics that can work under higher temperature conditions as compared to the same metallic matrices without hardening phases.

References

[1]. G. Barkleit, A. Grahl, M. Maccagni, M. Olper, P. Scharf, R. Wagner, H.Warlimont - *Electrodeposited, dispersion-hardened, lightweight grids for lead–acid batteries* - Journal of Power Sources 78_1999.73–78

[2]. Surdeanu T. – *Cermeti* – Editura Tehnica, Bucuresti, 1983.

[3]. Jangg G., Woronow S., Rehut D.,Chanduvi C., - Oxide Dispersion Strengthening, Metallurgical Soc. Conf., vol.5, pag.315, 1990.

[4]. Lic Y. Oriani R. A. -- Oxide Dispersion Strengthening, Metallurgical Soc. Conf., vol.47, pag.431, 1968.

[5]. Jangg G., Arnhold V., Hummert K., Brockmann J., Neubing H., im Druck 1988.

[6]. Nagarajan V., Wright I. G., Stringer J. – *A dispersed reservoir approach to the development of protective scales on high–temperature alloys* -- **O**xide Dispersion Strengthening, Metallurgical Soc. Conf., vol.6, pag.333, 1990.

[7]. Gennari U., Kny E., Gartner T., - *Niobium – Titanium oxide alloy; A novel approach to **O**xide Dispersion Strengthening* - **O**xide Dispersion Strengthening Metallurgical Soc. Conf., vol.2, pag.587, 1990.

[8]. Rabenseifer L. – *Tantal und Niob als Implantatwerkstoff*, Sttutgard,1986.

[9]. Zitter H., Plenk H., - Journal of Biomedical Materials Research, 21 pag. 881, 1987.

[10]. Clyne T.W., Withers P.J. - *An Introductions to Metal Matrix Composites*, Cambrige,Unyversity Press,1993.

[11]. Borrowdaile J. B., Ruch W.- *The Secondary Processing of Particles Reinforced Al Composites*, in Inst. of Metals Conf.—M.M.Cs; London, pp.10.1-10.3, 1994.

***[12].* F. Potecasu**, **O. Potecasu, F. M. Braz Fernandes, V. Muşat** *Lead - Hardening by Oxide Dispersion*. - Materials Science Forum; Advanced Materials Forum III, 514-516 (2006) p718-722, ISSN 0255 – 5476, Trans Tech Publications LTD Switzerland, UK, USA.

THE ANNALS OF "DUNAREA DE JOS" UNIVERSITY OF GALATI
FASCICLE IX METALLURGY AND MATERIALS SCIENCE, ISSN 1453 – 083X. N^0. 2 – 2006

THERMODYNAMIC ASSESMENT OF THE Cu - Ti SYSTEM IN MICROALLOYED COPPER BASE ALLOYS

Maria VLAD
"Dunarea de Jos"University of Galati
email: mvlad@ugal.ro

ABSTRACT

The correlations made between thermodynamic and kinetic data of the heterogeneous systems provided insight into the alloys properties. Experimental researches presented in this paper refer to the thermodynamics of Cu-Ti binary system for very low concentrations of titanium in copper from $0.006\cdot10^{-2} \div 0.340\cdot10^{-2}$ *mole fractions at 1372 K, at 1423 K temperatures. By electrochemical method the thermodynamics activities and activity coefficients at 1372 K, 1423 K were determined. The Associated Solution Model (ASM) parameters have been used to describe the thermodynamic properties of the Cu-Ti dilute solutions. Analytical expression has been derived to express the activity of titan in copper and the activity coefficient. The first and second order Wagner's self-interaction parameters were given as a function of ASM parameters.*

KEYWORDS: alloy, thermodynamics, activity.

1. Introduction

The copper based alloys feature very favourable thermal and electrical properties and also excellent mechanical characteristics therefore micro alloying copper with Ti, Cr, Al etc. may be used in all present and future technical fields. Kinetic and thermodynamic data of the melt alloys allow for the equilibrium conditions of the heterogeneous systems to be established and give a complete image upon the structure of the alloy and its properties [1, 2].

In the present study, liquid copper containing titanium at concentrations corresponding with concentration superior limits of authors papers [3-5] have been investigated and experiments have been carried out at two temperatures 1373 K and 1423 K, conditions which may be met at copper micro alloying. Liquid copper containing titanium was brought into equilibrium with molten $\{CuCl_2 + Ti_2O_3\}_{slag}$ saturated with Ti_2O_3 (s). The equilibrium oxygen partial pressure was measured by means of solid-oxygen galvanic cell of the type:

$$Mo/Mo + MoO_2/ZrO_2\ (MgO)/(Cu + Ti)_{alloy} + Ti_2O_{3(s)} + (CaCl_2 + Ti_2O_3)_{slag}/Mo$$

The thermodynamic activity of titan in copper and interaction parameters of the Cu-Ti binary liquid solutions was interpreted using the Associated Solution Model (ASM) Parameters [6].

2. Experimental method

The electrochemical methods based on the galvanic cells of the oxygen concentration with solid electrolytes are the most convenient methods for thermodynamics study of the high temperature metallic melts. The schematic draw of the electrochemical cell with solid oxide electrolyte is illustrated in figure 1.

The thermodynamic equilibrium of galvanic cell corresponds to the chemical reactions equilibrium:

$$2Ti_{(inCu)} + 3/2O_2 = Ti_2O_{3(s)} \quad (1)$$

$$\Delta G^0_{(1)} = -RT\ln K_{(1)} \quad (2)$$

$$\log K_{(1)} = \log a_{Ti_2O_3} - 2\log a_{Ti} - (3/2)\log P_{O_2} = 13{,}48 = 18500/T \quad (3)$$

where: the activities of Ti_2O_3, $a_{Ti_2O_3}$, referred to pure solid Ti_2O_3 are unity, since the ($CaCl_2$ + Ti_2O_3) melts were saturated with pure solid Ti_2O_3.

From Eq (3) results that titanium activity can be determined by the oxygen potential measurements with the following relation:

$$E = \frac{RT}{F}\ln\frac{P^{14}_{O_2(Ref)} + P^{14}_{(-)}}{P^{14}_{O_2(slag)} + P^{14}_{(-)}} \quad (4)$$

where: E is electromotive force, F the Faraday constant and $P_{(-)}$ the oxygen partial pressure when both ionic and n-type electronic conductivity are equal.

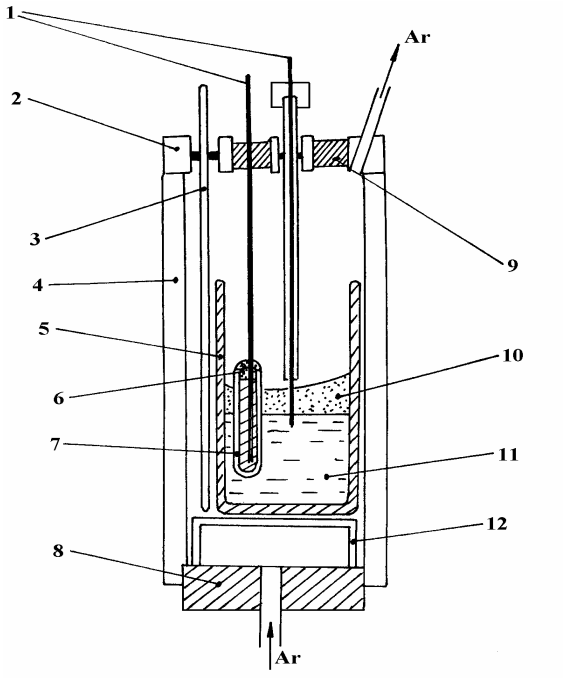

Fig.1. *Experimental cell. (1) molybdenum electrodes, (2) water cooled lid, (3) thermocouple, (4) mullite reaction tube, (5) alumina crucible, (6) zirconia cement, (7) zirconia tube, (8) rubber stopper, (9) rubber stopper, (10) Ti_2O_3 saturated ($CaCl_2$ + Ti_2O_3) melt, (11) Cu-Ti alloy, (12) pedestal.*

The oxygen partial pressure at the Mo+MoO_2, reference electrode, $P_{O_2(\mathrm{Ref})}$ was calculated by using the author's previous results [2]:

$$RT\ln P_{O_2(\mathrm{Ref})} = -576.1 + 0.1692\,T \pm 0.3 \qquad (5)$$

A description of the thermodynamic characteristics of the liquid binary system to infinite dilution of one of the components could be achieved by using ASM (model).

3. Results and discussions

The activity and activity coefficients of the dissolution, respectively, were calculated on base of the measured electromotive forces, for each molar fraction of titanium in copper. The results are presented in Tables 1 and 2.

Analytical expressions of titan activity coefficient and interaction parameters were determined starting from Lupis and Eliot [4] relation's -see equation (5), by the least square method:

$$\ln\gamma_B = \ln\gamma_B^0 + \varepsilon_B^0 X_B + \rho_B^0 X_B^2 \qquad (6)$$

Analytical expressions of titan activity coefficients are:

$$\log\gamma_{Ti} = -1.27 - 57.14X_{Ti} \quad \text{at 1373 K} \qquad (7)$$

$$\log\gamma_{Ti} = -1.26 - 37.14X_{Ti} \quad \text{at 1423 K}$$

Table 1. *Values of activity (a_{Ti}), activity coefficient (γ_i), titanium concentration X_{Ti} and electromotive force E of Cu-Ti binary system at 1373 K.*

Nr. crt.	$X_{Ti}\cdot10^2$	E [mV]	log a_{Ti}	log X_{Ti}	log γ_{Ti}	γ_{Ti}	$a_{Ti}\cdot10^3$
1	0.312	714	-3.986	-2.503	-1.481	0.0330	0.1032
2	0.307	712	-3.987	-2.512	-1.475	0.0335	0.1030
3	0.304	710	-3.989	-2.517	-1.472	0.0337	0.1025
4	0.152	693	-4.170	-2.118	-1.352	0.0444	0.0676
5	0.148	692	-4.176	-2.830	-1.346	0.0451	0.0667
6	0.145	689	-4.178	-2.839	-1.339	0.0458	0.0663
7	0.117	673	-4.248	-2.932	-1.316	0.0483	0.0565
8	0.112	671	-4.262	-2.950	-1.312	0.0487	0.0547
9	0.107	669	-4.280	-2.971	-1.309	0.0491	0.0525
10	0.0579	648	-4.541	-3.240	-1.301	0.0500	0.0287
11	0.0136	628	-5.143	-3.866	-1.277	0.0528	0.00719
12	0.132	627	-5.152	-3.880	-1.272	0.0534	0.00704
13	0.00676	594	-5.420	-4.170	-1.250	0.0562	0.00380
14	0.00674	591	-5.423	-4.171	-1.242	0.0565	0.00377

Table 2. *Values of activity (a_{Ti}), activity coefficient (γ_i), titanium concentration X_{Ti} and electromotive force E of Cu-Ti binary system at 1423 K.*

Nr. crt.	X_{Ti} 10^2	E [mV]	$\log \cdot a_{Ti}$	$\log X_{Ti}$	$\log \gamma_{Ti}$	γ_{Ti}	$a_{Ti} \cdot 10^3$
1	0.331	704	-3.959	-2.480	-1.479	0.0324	0.1100
2	0.326	701	-3.962	-2.487	-1.475	0.0334	0.1090
3	0.164	692	-4.147	-2.785	-1.362	0.0434	0.0713
4	0.159	685	-4.166	-2.798	-1.356	0.0440	0.0682
5	0.153	681	-4.169	-2.816	-1.353	0.0443	0.0677
6	0.127	667	-4.220	-2.896	-1.324	0.0474	0.0602
7	0.120	662	-4.229	-2.920	-1.319	0.0479	0.0590
8	0.166	659	-4.250	-2.935	-1.315	0.0484	0.0562
9	0.0631	641	-4.497	-3.200	-1.307	0.0493	0.0318
10	0.0143	622	-5.132	-3.844	-1.288	0.515	0.00738
11	0.0141	618	-5.133	-3.850	-1.283	0.521	0.00736
12	0.00724	582	-5.405	-4.140	-1.265	0.0543	0.00393

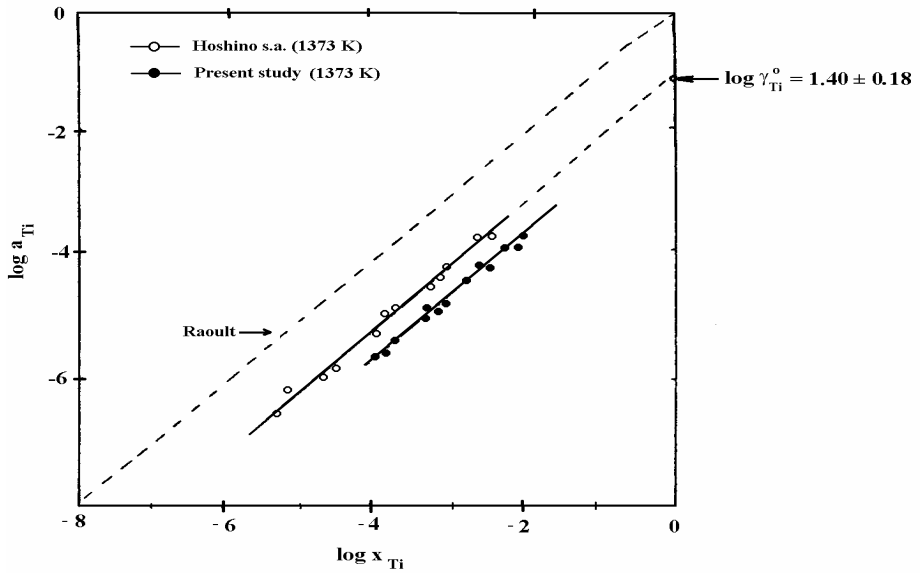

Fig. 2. *Relation between log a_{Ti}, and log X_{Ti}, in comparison with literature data [2].*

Figure 2 shows the study of logarithmic plots between activity a_{Ti} and concentration X_{Ti} for Cu-Ti binary system, in comparison with the literature data. It exhibits the high negative deviation from Raoult law. The negative deviations from ideal solution law indicate that titanium dissolution reaction in copper is exothermic; therefore copper and titan atomic bonding is stronger than those of similar atoms.

3.1. Analytical expression for the titan activity in binary dilute Cu- Ti alloys in terms of Associated Solution Model Parameters (ASM)

A binary solution made of A and B is modeled as a pseudo-ternary solution of "A", "B", and "ApBq" species, constrained by the internal equilibrium reaction:

p "A" + q "B" = "ApBq" (9)

The general analytical expression for $\ln a_B$ is:

$$\ln a_B = \frac{1}{q}[\ln X_B - \ln q + \frac{p+b}{q} X_B + \frac{p+2pq+b^2}{2q^2} X_B^2 - \ln k +$$
$$+1/2(w_{13}+w_{31})\left\{1-2\alpha X_B + \left[(1-p)\alpha^2 - 2\beta\right]X_B^2\right\} +$$
$$+1/2(w_{31}+w_{13})\left\{1-2\alpha X_B + \left[(1-p)\alpha^2 - 2\beta\right]X_B^2\right\} +$$
$$+1/2(w_{31}+w_{13})\left\{1-6\alpha X_B + \left[(9-3p)\alpha^2 - 6\beta\right]X_B^2\right\} +$$
$$+4v_{13}\left\{-2\alpha X_B + \left[(7-p)\alpha^2 - 2\beta\right]X_B^2\right\}] \quad (10)$$

where w_{13}, w_{31}, w_{32}, v_{13} are the solution parameters.

The activity of B diluted substance, of very low concentration, could have normally be expressed by self-interaction parameters in according to relation:

$$\ln a_B = \ln X_B + \ln \gamma_B^0 + \varepsilon_B^0 X_B + \rho_B^0 X_B^2 \qquad (11)$$

where γ_B^0 is activity coefficient of B at infinite dilution and ε_B^0 and ρ_B^0 are the first and second order Wagner's self interaction parameter, respectively.

3.1.1. Results

The thermodynamics characteristics of the binary system of Cu-Ti, with infinite dilution of titanium in copper, could be described considering the two metals an associated species of CuTi. As result $p = q = 1$, $p + q - 1 = 1$, $\alpha = \beta = 1$.

Replacing these values in Eq (10) it has been obtained:

$$\begin{aligned}\ln a_{Ti} &= \ln X_{Ti} + 2X_{Ti} + 2X_{Ti}^2 - \ln k + \\ &+ 1/2(w_{13} + w_{32})(1 - 2X_{Ti} - 2X_{Ti}^2) + \\ &+ 1/2(w_{31} - w_{13})(1 - 6X_{Ti}) + 4v_{13}(-2X_{Ti} + 4X_{Ti}^2)\end{aligned} \qquad (12)$$

$$\begin{aligned}\ln a_{Ti} &= \ln X_{Ti} + w_{Ti} - \ln k - \\ &- (2 + 2w_{13} - 4w_{31} - 8v_{13})X_{Ti} + \\ &+ (2 - w_{13} + 16v_{13})X_{Ti}^2\end{aligned} \qquad (13)$$

Comparing Eqs (11) and (12) it results that:

$$\ln \gamma_{Ti}^0 = w_{31} - \ln k \qquad (14)$$

$$\varepsilon_{Ti}^0 = 2 + 2w_{13} - 4w_{31} - 6v_{13} \qquad (15)$$

$$\rho_{Ti}^0 = 2 - w_{13} - w_{31} + 16v_{13} \qquad (16)$$

The equations (14), (15) and (16) are the analytical expressions for $\ln \gamma_{Ti}^0$, ε_{Ti}^0, ρ_{Ti}^0, representing the ASM parameters.

The analytical expressions of the titanium activity in copper are determined using iterative method and are presented in Table 3.

They were used to study logarithmic plot between a_{Ti} and variation X_{Ti}, at 1373 K (see figure3), and at1423 K (see figure 4).

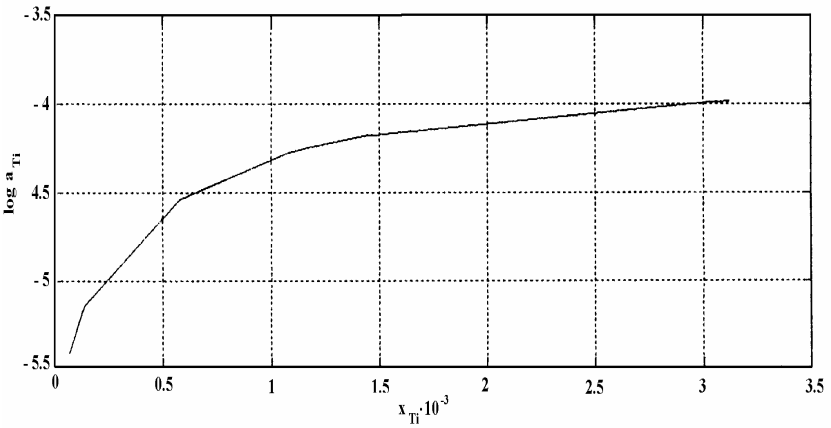

Fig.3. *Relation between log a_{Ti}, and X_{Ti} at 1373 K.*

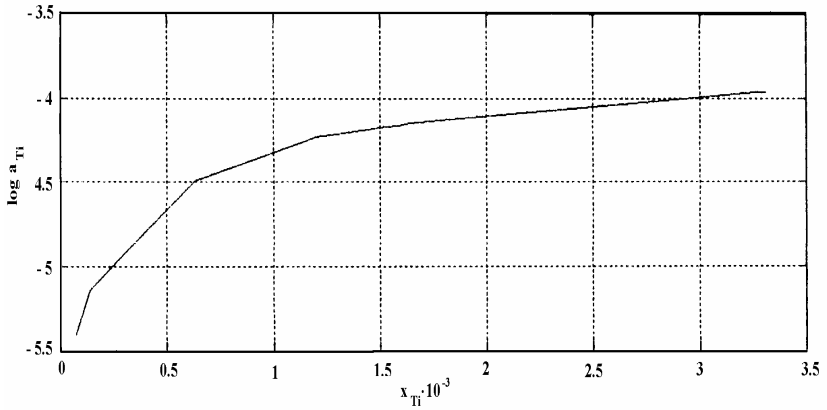

Fig.4. *Relation between log a_{Ti}, and X_{Ti} at 1423 K.*

***Table 3**. Analytical expressions of log a_{Ti} at 1373 K and 1423 K*

log $a_{Ti} = y$	$10^3\ X_{Ti} = x$	Analytical expressions
at 1373 K		
-3.959	3.310	$y = a_0 + a_1 X_{Ti}^2 + \log X_{Ti}$ $a_0 = \log \gamma_{Ti}^0 = -1.280$ $a_1 = \varepsilon_{Ti}^0 = -55.727$ $a_2 = \rho_{Ti}^0 = -2958.1731$ $\log a_{Ti} = -1.260 - 55.737 X_{Ti} - 2956.1731 X_{Ti}^2 + \log X_{Ti}$
-3.962	3.260	
-4.147	1.640	
-4.166	1.590	
-4.169	1.530	
-4.220	1.270	
-4.229	1.200	
-4.250	1.160	
-4.497	0.631	
-5.132	0.143	
-5.133	0.141	
-5.405	0.072	
at 1423 K		
-3.986	3.120	$y = a_0 + a_1 X_{Ti} + a_2 X_{Ti}^2 + \log X_{Ti}$ $a_0 = \log \gamma_{Ti}^0 = -1.2465$ $a_1 = \varepsilon_{Ti}^0 = -50.3097$ $a_2 = \rho_{Ti}^0 = -7898.26$ $\log a_{Ti} = -1.2465 - 50.3097 X_{Ti} - 7898.26 X_{Ti}^2 + \log X_{Ti}$
-3.986	3.070	
-3.987	3.040	
-4.170	1.520	
-4.176	1.480	
-4.178	1.450	
-4.248	1.170	
-4.262	1.120	
-4.280	1.070	
-4.541	1.579	
-5.141	0.136	
-5.152	0.132	
-5.420	0.066	
-5.419	0.067	

4. Conclusions

The following could be drawn:

1. Kinetic and thermodynamic data of melts allow establishing the process equilibrium conditions during alloy processing in order to reach the desired characteristics.
2. The experimental research on the thermodynamics of Cu-Ti system with low concentrations of titanium in liquid copper, at 1373 K and 1423 K, showed negative deviations from Raoult's law. In this case, the dissolution reaction of solid titanium in copper is exothermic.
3. The analytical expression of the titanium activity in copper derived with Associated Solution Model (ASM) parameters are used to express the titan activity, activity coefficient, and the first and second order interaction parameters

References

[1]. L. J. Pan Wei, *Materials Science and Engineering. A* **269**, 104 (1999)
[2]. T. K. Inouye, H. Fujiwara, M. Iwase, *Metallurgical Transactions*, **22B**, 475 (1991)
[3]. H. Hoshino, T. Shimada, M. Yamamoto, M. Iwase, *Metallurgical Transactions*, **23B**, 160 (1992)
[4]. J. P. Hara, M. G. Frahberg, *Metallurgical Transaction*, **23B**, 23 (1992)
[5]. R.Arroyave, T.W. Eagar and L. Kaufman, *Journal of Alloys and Compounds*, **351** (2003) 158-170
[6]. R. C. Sharma, *Metallurgical Transaction*, **18A**, 1641 (1987).

RESEARCH CONCERNING THE INFLUENCE OF HEAT TREATMENT ON PHYSICAL AND MECHANICAL PROPERTIES OF ALUMINIUM BASED ALLOYS

Elisabeta VASILESCU, Marian NEACSU, Ana DONIGA
"Dunarea de Jos" University Galati
email: vasilescu.elisabeta@ugal.ro

ABSTRACT

This work presents the experimental results concerning the behavior on heat treatment of on aluminum based alloy belonging to the class of aluminum alloys deformable and harden by heat treatment.

The laboratory level experiments effected on samples of Al-Zn alloy illustrate the variation of properties depending on the variation of heat treatment technological parameters specific to different variants of heat treatment. In view of the chemical composition of the studied alloy and being aware of the fact that the structure and composition of this type of alloys depend on the proportion Zn/Mg, on the copper and magnesium content as well as on the elements sum(Zn+Mg+Cu), we have experimented more variants of heat treatment in order to establish the optimal variant and to classify the studied alloy according to its use characteristics(high, medium or low strength).

KEYWORDS: heat treatment, quenching in solution and heat ageing, aluminum based alloy.

1. Introduction

Deformable aluminum alloys are alloys containing elements which have a quite high solubility in aluminum (e.g.: Cu; Mg; Zn etc) and the variation of their solubility function of temperature allows heat treatments to be applied.

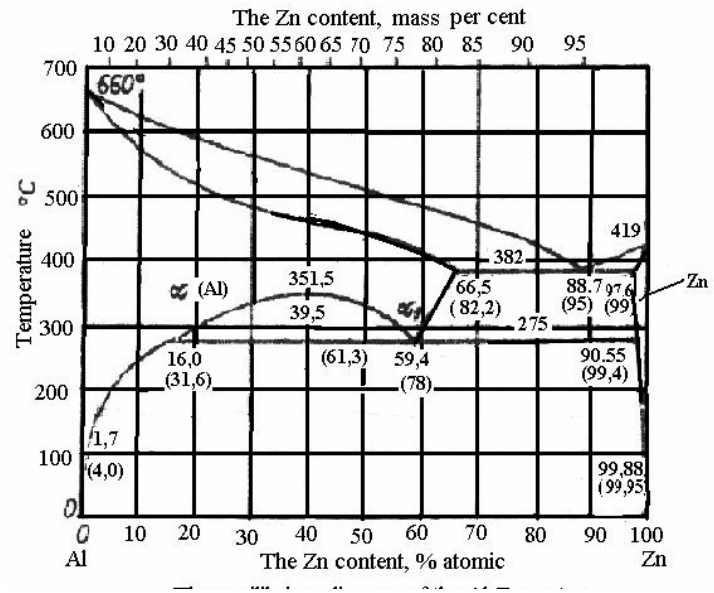

Fig.1. *The equilibrium diagram of the Al-Zn system.*

Among the most used deformable durificable alloys are the alloys in the systems: Al-Cu; Al-Cu-Mg; Al-Mg-Si; Al-Zn-Mg; Al-Zn-Mg-Cu and so on.

The typical representative of these alloys is the Al-Cu alloy containing about 4,0-5.5%Cu and the phenomena accompanying the heat treatments of Al-Cu alloys cam be observed in the case of all aluminum based alloys durificable by heat treatment.

The alloys in the Al-Zn-Mg system belonging to the category of alloys deformable and durificable by heat treatment are characterized by high corrosion resistance.

The structure and the behaviour of these alloys on heat treatment mainly depend on the proportion of the Zn and Mg elements (%Zn/%Mg), its value and the presence of the other alloying or accompanying elements causing the forming of different soluble or insoluble compounds in solid state.

Fig.1. presents the equilibrium diagram of the Al-Zn system.

2. Experimental conditions

The experiments have been made on Al-Zn aluminium alloy having chemical composition shown in table 1.

***Table 1**. Chemical composition of Al-Zn-Mg-Cu(%)*

Cu	Fe	Mg	Zn	Mn	Pb	Si	Al
1,42	0,51	2,32	2,60	0,05	0,05	0,22	Rest

The laboratory experiments have been made of the specific heat treatments: quenching in solution and heat ageing with different parameters (temperature and holding time) in according with table 2.

In order to find the optimal temperature for quenching in solution of the studied alloy six experimental regimes have been effected observing the influence of the quenching in solution temperature on hardness for the same maintaining time and also for the some cooling speed cooling (medium).

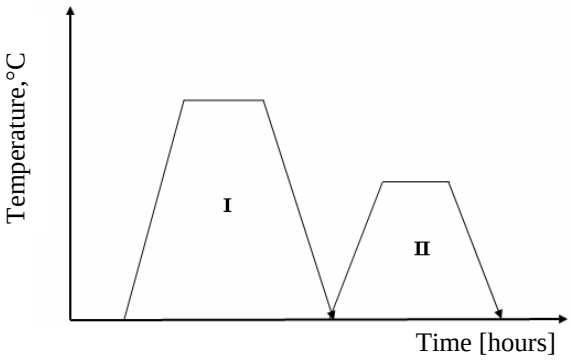

***Fig.2.** The cycle of experimental variants of heat treatment applied on Al-Zn-Mg alloy. I-quenching in solution; II-heat ageing.*

Considering as optimal temperature for quenching in solution the temperature at which the maximum value of hardness is obtained nine more experimental regimes have been effected with a view to establishing the optimal technological parameters for artificial ageing (temperature, maintaining time) for samples of the studied alloy which were in the state of being quenched in solution at a temperature value of 470°C with 1 h maintaining time and cooling in water.

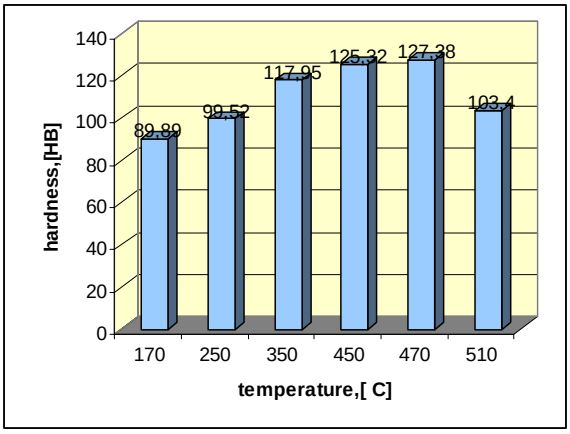

***Fig.3.** The influence of the quenching in solution temperature on the hardness of Al-Zn-Mg.*

Table 2 presents the experimental regimes during which there temperature values were tested (120;150;200) each of them having three maintaining time values(1; 3; 6).

***Table 2**. The experimental working conditions*

Experimental variant number	Quenching in solution		Heat ageing	
	Heating temperature	Hours holding	Heating temperature	Hours holding
	[°C]	[h]	[°C]	[h]
1	470	1	120	1
2	470	1	120	3
3	470	1	120	6
4	470	1	150	1
5	470	1	150	3
6	470	1	150	6
7	470	1	200	1
8	470	1	200	3
9	470	1	200	6

3. Results and interpretations

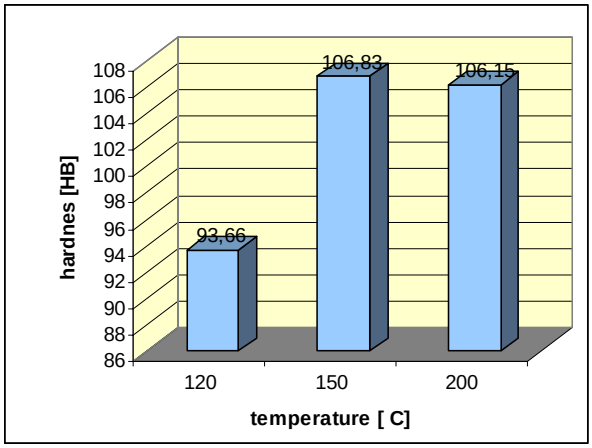

***Fig.4.** The influence of artificial ageing temperature on samples hardness for 1 h maintaining time.*

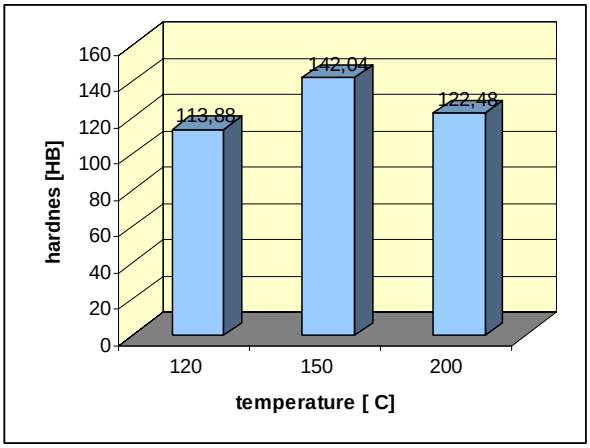

***Fig.6.** The influence of artificial ageing temperature on samples hardness for 6 h maintaining time.*

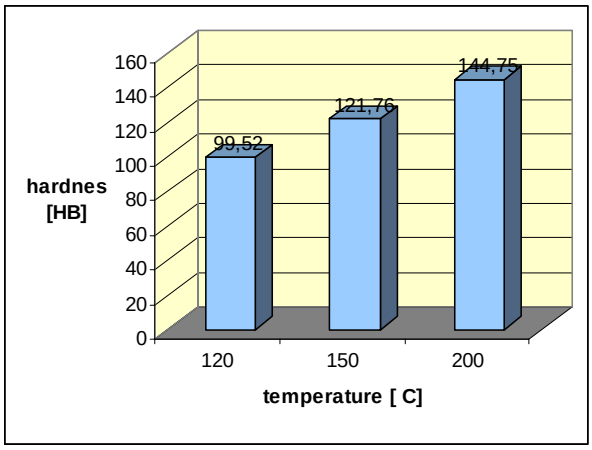

***Fig.5.** The influence of artificial ageing temperature on samples hardness for 3 h maintaining time.*

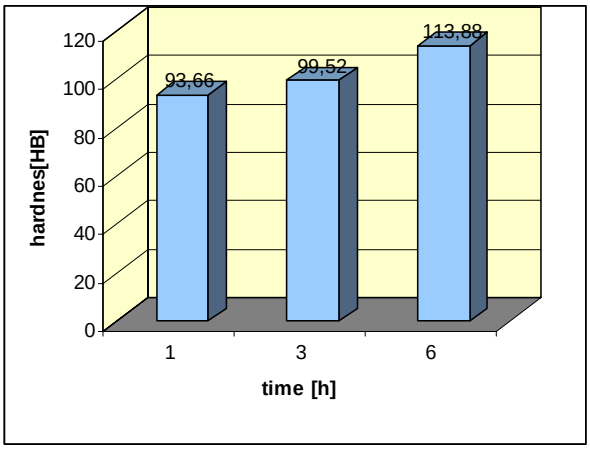

***Fig.7.** The influence of the maintaining time at a 120℃ artificial ageing temperature on samples hardness.*

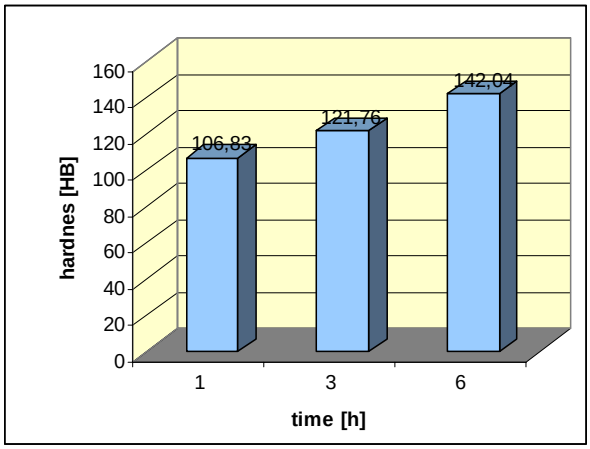

Fig.8. *The influence of the maintaining time at a 150℃ artificial ageing temperature on samples hardness.*

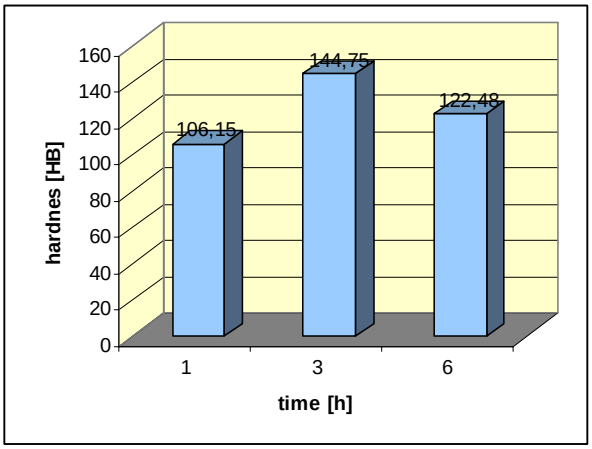

Fig.9. *The influence of the maintaining time at a 200℃ artificial ageing temperature on samples hardness.*

4. Microstructural aspects

Fig.10. *The microstructure of the Al-Zn alloy after quenching in solution and natural ageing (x100, attack natal).*

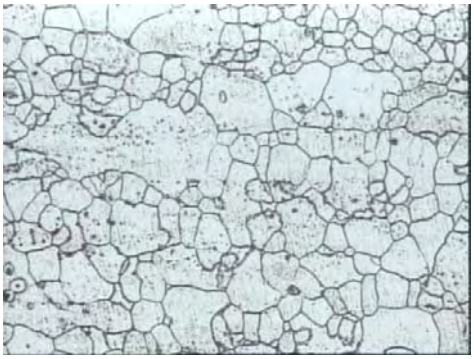

Fig.12. *The microstructure of the Al-Zn alloy after quenching in solution and artificial ageing at 150℃ for 6 hours (x100, attack natal).*

Fig. 11. *The microstructure of the Al-Zn alloy after quenching in solution and artificial ageing at 200℃ for 3 hours (x100, attack natal).*

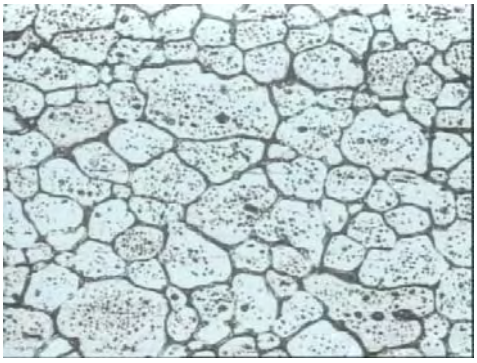

Fig.13. *The microstructure of the Al-Zn alloy after quenching in solution and artificial ageing at 120℃ for 6 hours (x100, attack natal).*

5. Conclusion

This work presents some partial experimental results concerning the behavior of the aluminum-based alloy of a given chemical composition (table 1) to heat treatment considering hardness as a measure for the variation of the mechanical properties.

The temperature for quenching in solution was established at the value of 470°C for a 1h maintaining time.

The study of the influence of the technological parameters for artificial ageing shows that:

a) the alloy hardens increases with the increasing of the ageing temperature until reaching the temperature value of 150°C, after which it begins to decrease at about 200°C

b) for the same ageing temperature, at an ageing temperature value of 120°C; 150°C; the alloy hardness increases with the increasing of the maintaining time (fig.7 and fig.8) bat for an ageing temperature of 200°C, the increase of the alloy hardness takes place at the some time with the increase of the maintaining time only until 3 hours, the extending of the maintaining time over this value leading to a decrease of hardness value (fig.9).

c) the maximum value obtaining of the studied alloy hardness is of 145 HB, value obtained during two experimental regimes:

1. t_{qs}=470°C, τ=1h cooling in water
   t_{aa}=150°C, τ=6h cooling in air
2. t_{qs}=470°C, τ=1h cooling in water
   t_{aa}=150°C, τ=6h cooling in air

regime 2 being recommended.

A future work will present the results of the research concerning the evolutions of mechanical properties function of the technological parameters for the hat treatment of other Al based alloys; by comparison the alloy will be classified according to the value range of resistance.

References

[1]. Geru, N. s.a. - *Materiale metalice*, E.D.P. Bucuresti 1985
[2]. Dulamita, T, Florian, E. - *Tratamente termice si termochimice*, E.D.P, Bucuresti, 1982
[3]. Popescu, N, s.a. - *Stiinta materialelor vol.2*, Editura Fair Partners, Bucuresti, 1999
[4]. Saban, R, Vasile, T, Bunea, D. - *Studiul si ingineria materialelor*, Bucuresti, 2000
[5]. Gadea, S, Protopopescu, M. - *Aliaje neferoase*, Editura Tehnica, Bucuresti, 1965

THE ANNALS OF "DUNAREA DE JOS" UNIVERSITY OF GALATI
FASCICLE IX METALLURGY AND MATERIALS SCIENCE, ISSN 1453 – 083X. N^0. 2 – 2006

STUDY OF THE INCLUSIONS FROM THE ORIENTED GRAINS SILICON STEELS AND THEIR INFLUENCE ON THE TEXTURE

Ana DONIGA, Elisabeta VASILESCU
"Dunărea de Jos"University of Galati,
e-mail: adoniga@ugal.ro

ABSTRACT

The paper presents experimental results concerning the inhibitor phases generation by microalloying elements utilization. It was made experiments on three silicon steel charges. It was observed that the inhibitor phases have a strong influence on steel sheet structure and its texture. So these phases can by considered like "texture nucleus".

KEYWORDS: inclusions, oriented grains, silicon steel, texture

1. Generalities

The extant scattered precipitates in the silicon steels have a decisive role, both: in grain forming, during secondary annealing and Goss texture evolution in the finished strip. The scattered precipitates appear in silicon steels as nitrides: NbN, AlN, as carbides NbC, TiC and sulphides: MnS, against to the added element in the steels to form growth "inhibitors" of the grainsize [1].

In the paper-framework it was watched the influence of the scatter-phase, formed by Niobium and Aluminum adding in the steel, on the evolution of the structure and Goss texture in silicon steels during secondary annealing. The experiments have been made on three steel grades with chemical composition shown in table 1.

Table 1. *Chemical composition of experimental steels*

Steel	State	Chemical composition %								
		C	Si	Mn	S	P	Al	Nb	O_2	N_2
N1	**Casted**	0.040	3.04	0.080	0.017	0.009	0.002	0.090	0.0073	0.0067
A2		0.040	3.02	0.070	0.023	0.013	0.070	-	0.0078	0.0065
M3		0.029	3.04	0.072	0.023	0.009	0.012	-	0.0076	0.0062
N1	**Final plate**	0.004	3.04	0.080	0.015	0.009	0.002	0.090	-	-
A2		0.004	3.02	0.070	0.020	0.013	0.070	-	-	-
M3		0.003	3.04	0.070	0.022	0.009	0.010	-	-	-

Steels N1 (fig.1.a) and A2 have been experimental made by manufacturing of two 50 kg ingots, then rolled and thermal treated in the Metal Rolling Laboratory from Galati University and M3 steel was industrial made by MITTAL STEEL S.A.

2. Experimental Researches

The test-specimen taken from those three steel-grades (hot and cold rolled strips) have been submitted to a complete investigations that watched:

- the nature of the scatter-phases and their role in the grain size growth process during primary recrystallization (after first rolling) and secondary recrystallization (after second rolling)
- the role of the scatter-phase particles in forming and evolution of Goss type crystalographical texture

For study, the optical microscopy, electronically micro probe, X ray diffractometry and electronically microscopy have been used as investigation methods.

In that rolled strip, the optical microscopy distinguished the extant scatter-probe as rare and isolated small inclusions or rows of oxides, silicates and sulphides types.

A more complete analysis was made with electronically micro-probes specifying the nature and complexity of the scatter-phase particles by separation of the main elements in matrix and particles (fig. 1). In fig. 1, N1 steel appear about 1μm complex particle inclusions containing Mn, Al, Ca. Niobium appears isolated or with other elements, forming < 1μm diameter complex inclusions (fig 1a). In A2 steel are present: Al, Si, Mn (fig 1 d). Same type of the complex inclusions, containing Si, Al, Mn, appear in M3 steel. X-Ray diffractometry analyses distinguished crystalline structure of the secondary phase particles and matrix too. The fact of the analyses is that each phase characterized by its own crystalline net is corresponding to a specific system of diffraction lines. The test specimen have been taken from those three experimental steels, from hot rolled strips and submitted to a CoKa radiation. The results are centralized in table 2.

By this analyses, the evidence of the dispersion phase particles, with role of growth inhibitors of the grain size in silicon steel strip shave been watched.

In N1 steel, the microalloying with Niobium is determining the forming of the NbN and NbC precipitates with CFC type crystalline net.

In A2 steel, with Aluminum, AlN Al_2O_3 are formed, both with hexagonal net, but in M3 steel is MnS present, with CFC type net. As literature of specialty shows (2) one of condition that should be carried out by the dispersion phase to be inhibitor is to create a non coherence degree between crystalline net of the particles and matrix. In case of the studied steels between ferrite matrix and dispersion phase particles: NbN, NbC, AlN, Mn, the complex relationship are established due to various crystalline net types and differences between values of the net parameters. These will determinate the net distortions, local elastic deformation and pressure exerted by the particles concentration on the grain borders, which will have as final effect the delaying, or even blocking the growth of the recrystallized grains [3]. Electronically microscopy analyses allowed for study the shape and size of the secondary phase particles in the finished strip.

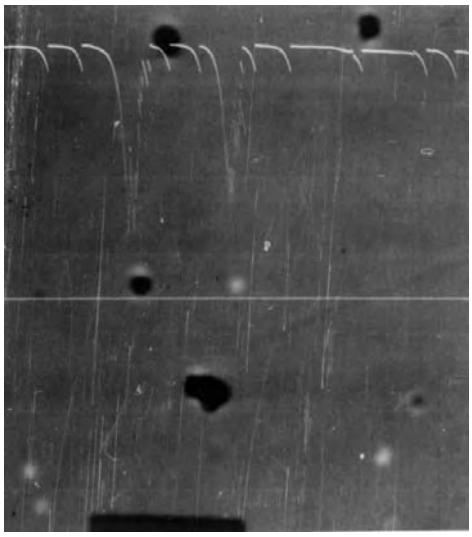

a)

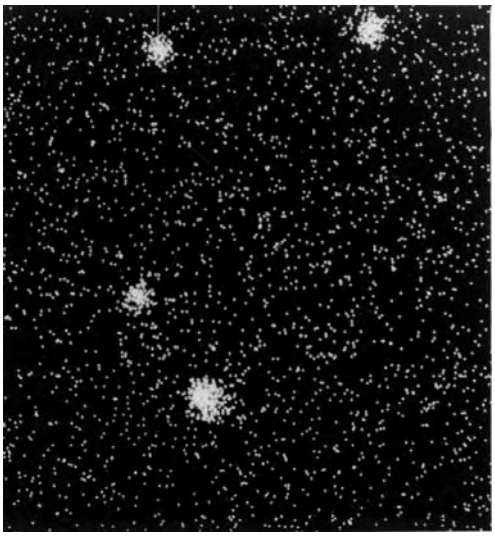

b)

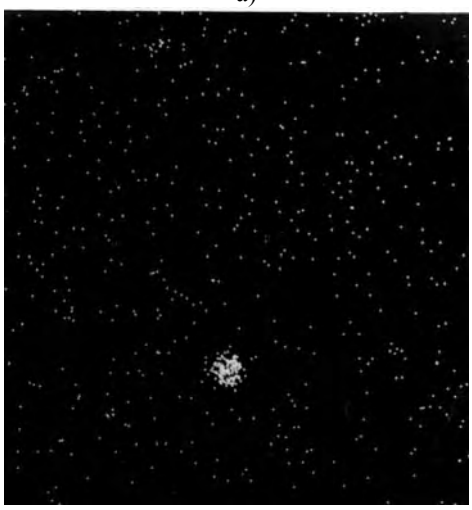

c)

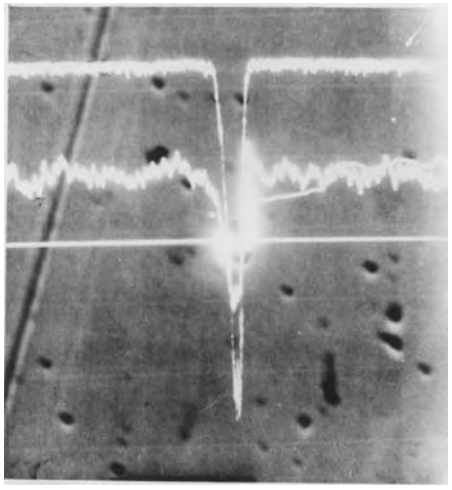

d)

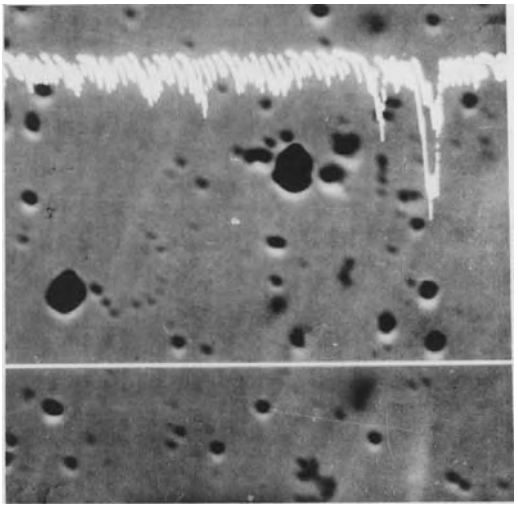

e)

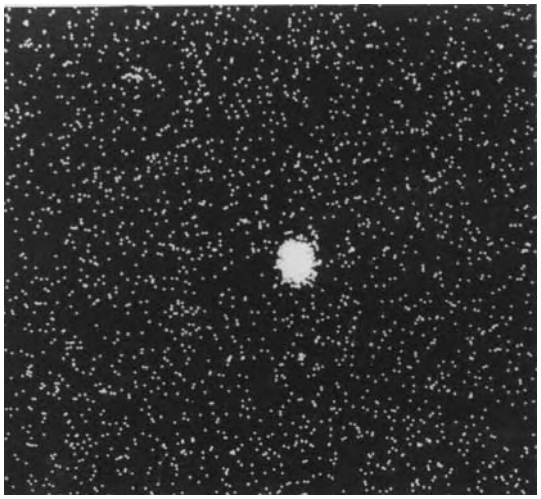

f)

Fig 1. *Complex inclusions in the experimented steels. a) Nb repartition in steel N1; b). Mn repartition in steel N1 c). Al repartition in steel N1; d) variation profile of Si and Al in steel A2; e). variation profile of Mn and Al; f). Al repartition in steel A2 (1200 x increase).*

At temperature increase a suddenly increase of the grain might be produced either due to particle coalescence or their dissolving in matrix. For silicon steel, the distribution variance is wished to get a solid solution with a smallest quantity of inclusions, having in view the magnetic characteristics getting using thin foils method with transmission electronic microscope, the test specimen of N1 steel was analyzed with 33,000 and 100,000x increase.

After secondary recrystallization it was established it was established that NbN precipitates have left as small particle scattered in matrix of about 400Å, round or elongated shape (fig. 2).

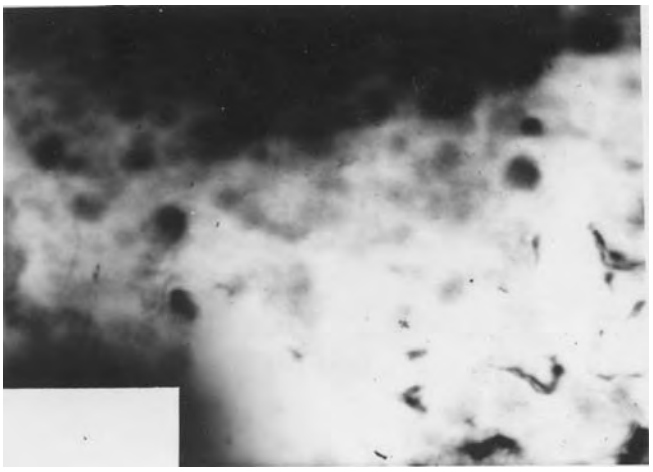

Fig. 2. *Inhibitor particles in finished strip of N1 steel (33,000x increase)*

Selection of a certain inhibitor should be correlated to the temperature of the secondary recrystallization too, to assure an advanced dissolution of the second phase particles, to get a certain grain and stressed Goss texture [4].

In this direction more ranges of secondary recrystallization have been experimented, analyzing, finally the percentage of the gotten Goss texture.

Strip test specimen of 0.35 mm thickness have bees used, which have been thermal treated in Hydrogen atmosphere at 900°C, 1000°C, 1150°C temperature, 6 hours time. Fig. 3 shows the variation way of Goss texture component with secondary recrystallization temperature.

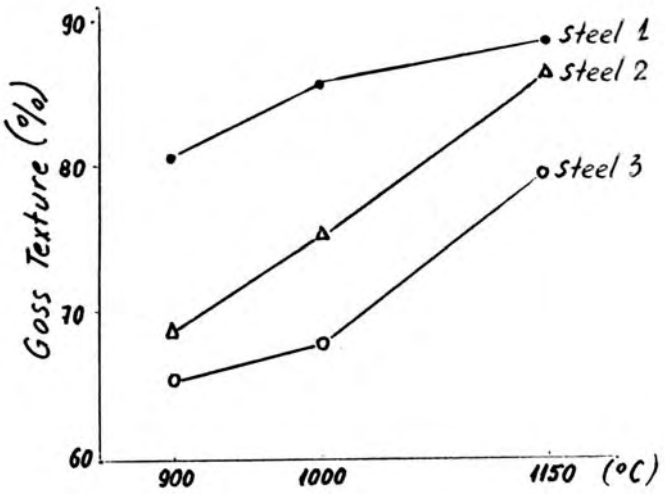

Fig. 3. *Goss texture percentage to the annealing temperature for experimental steels.*

Could be remarked that from those three steel grades, this niobium steel answers the best to the requirements imposed to an inhibitor NbN is less soluble at lower temperatures (900-1000°C) than MnS, therefore, it can keep the grain at small size up to the high temperature. In this time, Goss texture nucleus could be formed, if deformation degree was high enough for (110)[100] texture to store high quantity of energy. At temperature over 1200°C, NbN particles are solving in higher quantity alloying grain growth, characteristic to the secondary recrystallization. At 1150°C, 6-8mm diameter grain size are formed in Nb steel. While in Mn steel (steel M3) very big grain size are forming with 15-20mm diameter. It is possible that, due to dissolution of a higher quantity of MnS particles, at lower temperature (850-900°C), equally, to produce the growth of the other texture components in Goss texture detriment.

These suppositions have been confirmed by the texture measurements made on the experimental test-specimen: a percent of 24.8% texture (112)[100] resulted at 900°C temperature and 18% (112)[100] at 1000°C temperature. AlN particle have a stronger inhibition effect than NbN, dissolving in smaller quantity than NbN, at all temperatures.

As a result, we have remarked that over 1000°C the grains of Al steel (steel A2) remain small enough (under 5mm) and Goss texture is weaker.

In this case, the grain growth process is blocked by the presence of Al_2O_3 particles formed due to oxygen high quantity and very harmful by the negative influence on the magnetically characteristics of the finished strip. Fig 4 shows the macrostructure appearance after secondary annealing.

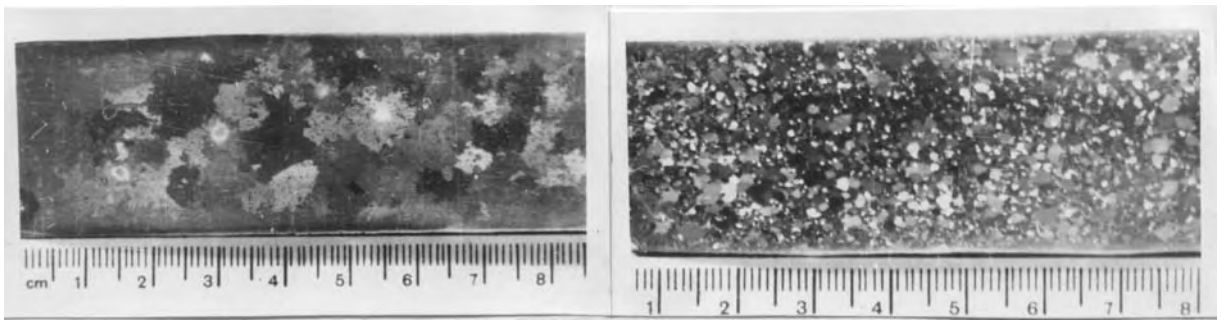

a) b)

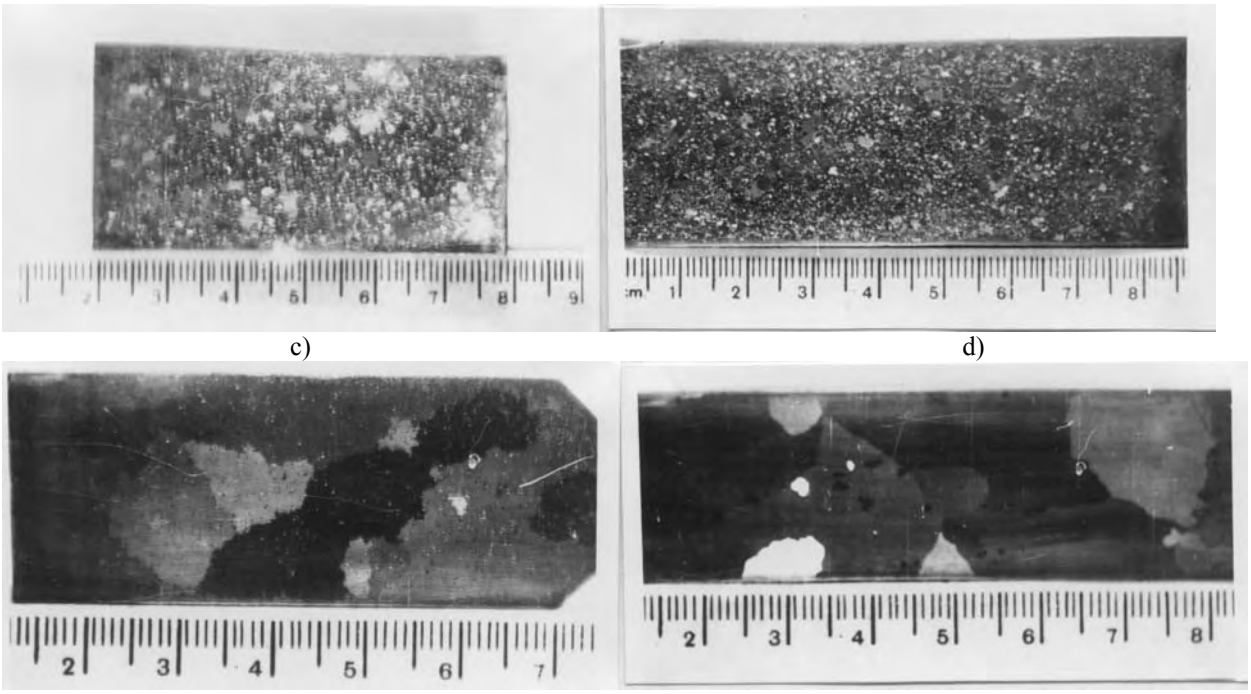

c) d)

e) f)

Fig. 4. *Macrostructure of the strip after secondary annealing*
a). steel N1 – annealing at 1150℃, 6 hours, b). steel N1 - 1000℃, 6 hours, c). steel A2 - 1150℃, 6 hours, d). steel A2 - 1000℃, 6 hours, e). steel M3 - 1150℃, 6 hours, f). steel M3 - 1000℃, 6 hours

Table 2. *Crystalline nets characteristics of the dispersion phase – particles and matrix in the experimental steels.*

Steel	Phase	2 θ (grades)	D/n	hkl	Crystalline net type	Crystalline net parameter
1	Fe_3C	44.08	2.38	(012)	Orthorhombic	-
	Ferită	52.74	2.02	(11)	CVC	2.98
	SiC	86.90	1.31	(201)	Hexagonal	-
	NbN	105.13	1.125	(400)	NaCl cubic type	1.10
	NbC	107.94	1.09	(400)	CFC	4.47
	NbC	130.00	0.993	(420)	CFC	4.47
2	AlN	44.38	2.37	(101)	Hexagonal	5.12
	Al_2O_3	50.97	2.08	(102)	Hexagonal	-
	Ferită	54.00	2.02	(110)	CVC	2.98
	SiC	72.00	1.54	(110)	Hexagonal	-
	AlN	74.25	1.50	(233)	Hexagonal	5.12
	AlN	98.30	1.186	(202)	Hexagonal	5.12
	Al_2O_3	101.96	1.144	(131)	Hexagonal	-
3	Ferită	53.20	2.02	(110)	CVC	2.98
	MnS	58.35	1.85	(220)	CFC	5.22
	Ferită	77.44	1.42	(200)	CVC	2.98
	MnS	89.26	1.12	(42)	CFC	5.22
	SiC	110.30	1.087	(203)	Hexagonal	-

From made researches resulted that inhibitor particles have an important influence on the texture [5]. It is possible that type of the crystalline net net-parameter, generally, non-coherence degree established between particles and matrix to influence, positively, the forming and growth of Goss texture nucleus. By the fact that in Nb steel is remarked the highest level of goss texture, it results that NbC or NbN inhibitor particles have the best influence on Goss texture. From here, could be concluded that the particles so called "inhibitors" of the grain size growth are, in fact "generator" of Goss texture too, acting as "texture nucleus" [6].

From those shown in this chapter results that the existence of the dispersion phases in silicon steels is a complex phenomenon with many implications on the structure and characteristics of the finished products.

Therefore, in the manufacturing process the following aspect, regarding the added elements for dispersion – phase – forming, should be taken into consideration:

- the accurate control of the chemical composition high purity and a very good steel dezoxidation to stumble oxides formation which would limit phase forming with inhibitor role and texture nucleus;
- against to the technology used, chemical element (elements) choosing for dispersion phase forming;
- rigorous control of C and N contents, as dispersion phase to be, mainly, carbide and nitride, these being the most efficient;
- existence of the highest precision equipment to determinate nitrogen and oxygen contents from steel both in making process and finished strip as well.

References

[1]. J. May, D.Turnbull - *Influence of impurities on second recrystallization of silicon iron* - Journal of Appl.Phys. nr.4- 1959

[2]. S. Gadea, M.Petrescu- *Metalurgia fizica si studiul metalelor* vol 3 EDP-Bucuresti 1988

[3]. H. Stuart- Niobium - Proceedings of the International Symposium San Francisco -California 1981

[4]. J. Walter, C. Dunn - *Growth of (110)[100] oriented grains in high purity silicon - a unique form of secondary recrystallization* - Transaction of AIME vo1218 -1960 p.1053

[5]. T. Matsuoka - *Effect of Impurities on the Development* of (110)[100] Secondary Recristallization Texture in 3%Si Iron - Transaction ISIJ vo17, 1967, p19

[6]. A. Doniga - "*Cercetari privind otelurile silicioase pentru transformatoare* " Teza de doctorat -Galati 1998

THE ANNALS OF "DUNAREA DE JOS" UNIVERSITY OF GALATI
FASCICLE IX METALLURGY AND MATERIALS SCIENCE, ISSN 1453 – 083X. N^0. 2 – 2006

ART PIECES CASTING FROM BRASS, DESTINED TO ARTIFICIAL LOCAL LIGHTENING, USED IN ORTHODOX CULT

Ioan CARCEA[1], Florin DIACONESCU[1], Cristian DIACONESCU[2]

[1] Technical University "Gh. Asachi" Iasi, Science and Material Engineering Faculty
[2] Technical College "Gh. Asachi" Iasi

ABSTRACT

In this paper are presented some realizations from SC RANCON SRL Iasi, which regards the casting of lighting local parts from brass, used in orthodox religion. Thus is highlighted the relationship between functionality, technical realization and artistic impression given by these objects from the perspective of the sacred service solemnity.

KEYWORDS:casting, illumination objects, orthodox churches.

1. Introduction

The artificial local illumination supplements the general illumination of cult dwelling or makes evident a certain detail or an interest zone of those who participate at religious service. Also, the local illumination objects, through their beautiful details attract the attention of onlooker and can complete the general image of a cult dwelling. Some local illumination objects (candlesticks), with all that have a limited mobility imposed by the length of feeding cable, can be arranged more advantageous, so they have a much better functionality than are fixed.

For the assurance of ambient frame of cult dwelling, is necessary that around the choice of local illumination objects to realize their judicious arrangement to obtain the maximum illumination efficiency and, not in the last time, a stylistic harmony. The used of styles is in the first hand determined by the architectural frame and the functionality of this. The style represents a synthesis of the all particular and original elements of a certain historic period, of a certain nations or of a certain territory. The appreciation criteria of a style are: the form, the decorative element, the construction details, the materials and the destination of the object.

The form represents the totality of surface lines, ornamental volumes and colors, being related to tradition and artistic taste. The plastic line is given by content and the artistic form of the style from the respective period (trace, proportions, decorations, materials used and the specific finishing methods). The content, determined by the financial and economical aspects of those periods, reflect the life style specifically to their society from that moment.

The orthodox churches have an architecture and iconography to Byzantine inspiration. The Byzantine style (500–1450 a.Ch.) has kept still more century the Roman style, but enriched with new elements inspired from the art of oriental nations and with artistic forms from Christianity.

The decorative Byzantine art, which have a pronounced religious character, is mystical, symbolical and raise the soul bring up him to God. The style takes from Arabic art the abstract geometrical motives and those stylized floral, which are founded at the metallic objects for illumination from church.

The Byzantine art is those of to the transition period, having dual characters and being indissoluble linked to spiritual services. The Byzantine style has exercised a great influence over the Russia and Balkan country (Serbia, Bulgaria and Rumania) and with the time has been integrated in the patrimony of our national art.

The art elements used for the construction and decoration of cult dwelling represent symbols, ideas and feelings springing from the deep of the human soul, which live an elevating approach to God and his saints. At the all services of Saint Church (the Ecclesiastical Praises, The Sacraments and Ierurgiile – services for sanctification, blessing, gratitude and faults remission) are used the illumination objects achievement from metal, with different techniques, with utilitarian and esthetical purposes, which are not just simple art objects, but through the sanctify given by priest according to Molitfelnic Tidiness (Molitfelnic – Liturgical book which contents prayers for sanctification, blessing of man, nature and objects), acquire a religious symbolist aspects.

2. The forms of the local illumination objects

Wall brackets are lighting objects fixed on the vertical walls at height much higher than the men, for a local illumination of certain vertical presentation surface, supplementing thus the general illumination or making obvious an architectural element or a religious scene. These brackets are suspended with two or three fine chains on the wall from pulpit, whence the litanies are said, the Gospels are read or the Christians are blessed.

Wall brackets from figure 1 are with two lights disposed either on the upper parts of the angelic wings or at the end of decorative elements under the form of S letter.

The initial decorative elements have been the pigeon wings, which symbolize the Saint Spirit.

The central pieces, with walls by constant thickness, are molded separately from brass, in a core box with horizontal separation surface, with the decorative face oriented to base for a good imitation of the details and for the avoidance of potential defects, which can brought esthetical prejudices. On the opposite part are fixed with adhesive band the cables for feeding with energy of the electrical terminals.

Fig. 1. *Wall brackets for local illumination.*

*The mass candlestick*s (named in Slavonic language svestĭnikŭ) are religious objects used by Orthodox Church from the ancient times to date for local illumination of the horizontal work surfaces, being necessary for a good visibility of the details and, in special, for reading.

The mass candlesticks can have one, two, three or seven arms, depending by the specifications wished.

The mass candlestick with three lights (figure 2) symbolizes the Saint Trinity and is putting on the saint mass in Altar. He is formed from the support (1), on which is fixed through a M10 thread the body (2) with inside void necessary for the central electrical conductor.

Fig. 2. *Mass candlestick with three lights.*

The support is molding with the prominence oriented downward, in a molding box with sloping surface separation, after the sitting face and circumference is processed. On the body (2) is fixed the arms group (3) horizontal casting in a molding box composed by a metallic cast from aluminum and a false semi-molding box. The trace of the piece is elegant, sinuous, under the S letter shape (symbolizing the sacredness), decorated with vegetal motives. At the end of the arms and in center is fixed the plate (4), one for each arm, in which is placed the electrical terminal (5).

The mass candlestick with seven lights (figure 3) is taken from Jewish religion (MENORA was the candlestick with seven arms which burnt permanently in the temple from Jerusalem).

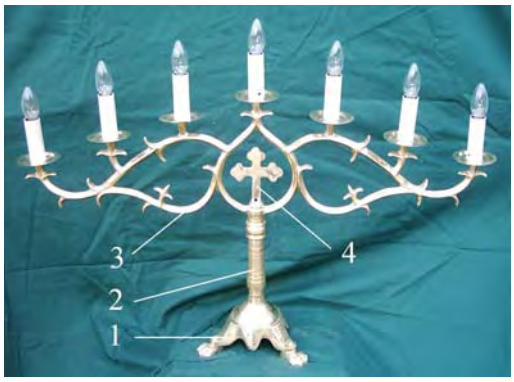

Fig. 3. *Mass candlestick with seven lights.*

This candlestick, which is used in liturgical ritual at Vespers, Saint Liturgy and other services, symbolizes those seven sacraments of the Saint Spirit, and the light relieved, which chase the darkness, signifies on the one hand the presence of Savior in His Church through His Learning and His Divine Grace from Saint Sacraments, till to the end of the

world, by the another hand the light of the Resurrection, which defeat the darkness of the sin, of the death and of the hell. The candlestick with seven arms is set at the sunrise of the Saint Mass from Altar.

The candlestick has a support (1), tripod type, with zoomorphic terminations (lion paws) which, although induce the idea of force and stability, create the impression a plastic representation by still life. This support is casting with the decorated surface downwards, in a molding box with sloping separation surface, executed from the monolithic molding box.

The central body (2) is lathing from massive bar and is designed with inside hole for central electrical conductor. At the ends presents two M10 threaded holes, not completed piercing, for assembling with support (1) and with the arms group.

The arms group (3), named by manufacturer "stag's horns type", is cast separately in a molding box with horizontal separation plane, executed with a monolithic molding box from aluminum, what requests utilization of a semi-molding box. In central part of the arms group is mounted the cross (4), and at the ends of electrical terminals, which are feeding through cables apparent by yellow color, fixed with transparent band.

The mass candlestick with seven lights, presented in figure 4, have a complexity much raised, given by vegetal decorative elements which are formed a real metallic embroidery.

The support (1) has a special artistic configuration with three elements zoomorphic used by Egyptians (XXX century – 30 b.Ch. year) at the furniture for resistance or support pieces, after has took by Mesopotamians (XXXVII – VII century b.Ch.) and by Byzantines, passing till to Italian Baroque (XVII – XVIII century) and Neoclassicism (1770 – 1850).

Fig. 4. *Mass candlestick with seven lights, with vegetal decorative elements.*

The body (2) is confectioned from round profile, which is lathed for realization of the exterior artistic configuration and is drilling for the electric conductor introduction, and after that is finished and polished.

In an attractive contrast with the support, the arms group (3) presents vegetal decorative elements (flowers and stems under the form of the C and S letters), which suggesting the motion and life. The motives, apparently delicate and fragile, are good and equilibrated linked between their, forming a unitary assembly. The arms group is monolithically molded, in a molding box having a horizontal separation plane, executed in an entire metallic molding box from aluminum and with a false semi-box. The electrical terminals (4) are feeding by two insulated conductors, by yellow color, each being fixed on the arms with transparent adhesive band.

The candlestick with foot for candles (figure 5) is situated in orthodox dwelling at each extremity of iconostasis, in front of the church patron icons (right part), in front of the icon of Saint John Baptist, Saint Nicholas or Pious Parascheva (left part), respective in pronave.

This candlestick has at the base a support (1) with three foots, closed with a zoomorphic element (anterior part of a lion), suggesting power and stability. The support is cast in a molding box with sloping separation surface, and the zoomorphic elements are realized using exterior molding box.

In the support (1) is assembled a steel rod, designed at the both ends with M12 thread. After that are mounted alternatively the rosettes (2) and two intermediate bodies (3) casting separately, processed mechanical and finished with felt. Over these constructive elements is mounted the superior body (4) executed from bar through exterior lathing and drilling. The plate (5) presents a border high by 40 mm, is molded separately in a molding box executed with monolithic pattern and is processed similarly to anterior manner.

Fig. 5. *Candlestick with food for candles.*

In the middle of plate is mounted pressing piece (6) which has a double role: realized the fixation of plate having at the inferior part a M12 threaded hole which is fixed on the superior end of the rod and serve as support for a candle much great. Over the plate (5) is mounted a lid (7) with numerous holes for candles, executed in aluminum sheet having 3 mm thickness.

3. Conclusion

The illumination objects produce by S.C. RANCON S.R.L. Iasi emphasize a great riches by decorative elements applied at ancient functions (illumination with candles), but developed according to actual exigencies adapted for electric illumination. These contribute to realization of a harmonious cult dwelling and in the same time with the stylistic personality, if are judicious choice by beneficiaries from range scale proposed by manufacturer, representing a continuation of the past and our traditions.

References

[1]. Petre Vintilescu – *Liturghierul explicat*, Editura Institutului Biblic şi de Misiune al B.O.R. Bucureşti, 1998.
[2]. Ion M. Stoian – *Dicţionar religios*, Editura Garamond, Bucureşti, 1994.

TRIBOLOGICAL BEHAVIOUR OF NITROCARBURIZED SUPERFICIAL LAYER AFTER THERMO-MAGNETIC TREATMENTS APPLIED TO STEELS, DURING FRICTION PROCESS

Carmen Penelopi PAPADATU
"Dunarea de Jos" University of Galati
e-mail: PCARMEN-PENELOPI@email.ro

ABSTRACT

Two types of steels subjected to a nitrocarburized thermo-chemical treatment after thermomagnetic treatments. The contact problems are studied employing the concept of tribosystem and tribomodel. The structural aspects into superficial layer of these steels are studied during friction process by using of an Amsler machine, taking two sliding degrees, different contact pressures and testing time. I tried to determine the durability of these materials, the surface structure evolution at different tests after thermomagnetic treatments. The performed tests allowed establishing the influence of the thermal, magnetic and mechanical parameters on behaviour of these two steels taking in study during friction process.

KEYWORDS: thermomagnetic treatments, tribosystem, tribomodel, superficial layer

1. Introduction

Improved steels mean highly tempering steels. By superimposing a magnetic field over a thermal one, structure modifications and implicitly properties modifications are generated.

Under the influence of the magnetic field, theoretically it is possible [B1], [B2], to modify the material state. The energy state of the ferrous-magnetic material is modified due to a certain magnetic moment, its free energy is increased. This may be a first cause which, under the effect of the magnetic filed, induces structure and physical-mechanical properties modifications in the material (steel). Martensite is decomposed upon tempering (annealing), and the intensity of this process depends on both temperature and duration of the tempering. In addition to the martensite decomposition stages (M), other processes take place upon tempering: transformation of the residual Austenite (Arez.), globalization of Troostite, e.t.c.

According to [B1], [C1], with low tempering of the conventionally tempered steel, the magnetic field slows down the martensite decomposition process, and , if the steel has been tempered in magnetic field, the martensite decomposition is even slower, thus tending to increase the martensite stability. At the same time the magnetic field influences the kinetics of the residual austenite decomposition isothermally upon tempering, accelerating the transformation process. The main cause of the above phenomena is the MAGNETOSTRICTION which causes strains in the microvolumes of the solid solutions – strains that interact with the field of elastic strains characteristic to dislocations.

Magnetostriction is defined as a dimensional variation of a ferrous-magnetic materials under the action of a magnetic field also called Joule effect, which depends on the size and direction of the external magnetic field, the material and the heat treatment previously applied to this material (temperature) [S1], [V1], [S2]. The effect of the magnetostriction decreases with higher temperatures and disappears at the Curie temperature.

Magnetostriction is determined by the influence of the external magnetic field which generates the orientation of the elementary magnetic moments, modifying the balance conditions among the nodes of the crystalline mesh, inclosing variation of the ferrous-magnetic material sample lengths. Under these conditions, the magnetostriction curves can be a result of having measured the ferrous-magnetic sample lengths along the external magnetic field.

In addition to the linear magnetostriction, considered above for plotting the magnetostriction curves with ferrous magnetic materials, it can also be noted a volume magnetostriction which depends on the shape of the piece concerned as well.

Consequences of magnetostriction are:

- - applying alternative magnetic fields causes mechanical oscillations [V1], [B1], [B2] and in the diffusion processes, these (magnetic) mechanical oscillations are quite important because, the strains which are generated by these mechanical oscillations along with the magnetostrictive volume modifications lead to a higher diffusion coefficient;
- of special importance are the local strains in the area of the ferrous-magnetic boundaries. Gradients of the magnetostriction strains occur which further cause higher diffusion coefficients inside the material. They come into contact with the internal strains redistributed by diffusion thus causing a new diffusion influencing factor to appear.

The mechanical oscillations produced by the alternative magnetic fields change the recrystallization conditions especially the germination velocity.

The strains caused by magnetostriction cause elastic and plastic deformations which in turn result in a magnetic texture, thus improving the magnetic and mechanical properties in the direction of the external field ($H_{ext.}$). From this viewpoint the effect of the thermal-magnetic treatment is maximum in the stages of the solid solution decomposition and, especially, upon cooling in magnetic (alternative) field from temperatures higher than Curie point (when orientation of ferrous-magnetic phase particles takes place) [P2], [S1], [V1].

Analysis of the iron-monocrystal magnetostriction [V1],[S1] shows that its sized vary unevenly in different crystallographic directions. Relative elongations $\lambda=\Delta l/l$ have been found as follows: $\lambda_{[100]}= 1,9\ 10^{-5}$, $\lambda_{[110]}= -\ 10^{-5}$, $\lambda_{[111]}= -3,1\ 10^{-5}$, the cube getting deformed into a romboedru (Fig.1).

In spite of these deformations being very small, mentions must be made that the deformations of the martensite crystal upon magnetization in direction [111] cause its rotation inside plan [110] by an angle $\beta=6^{\circ}$.

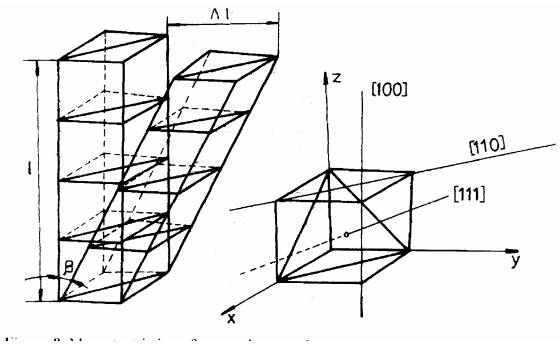

Fig. 1. *The iron-monocrystal sized vary unevenly in different crystallographic directions because of magnetic field applied [S1].*

Magnetostriction may cause local plastic deformations thus determining ecruisation of the residual austenite. This further implies higher material hardness/endurance.

2. Experimental researches

The steels analyzed in this paper are improved steels which should undergo high local variable strains: traction, compression, shearing and therefore certain properties are imperious:

- Higher hardness and homogeneity of the hardness values;
- elimination, if is possible, of the residual austenite ($A_{rez.}$);
- good tenacity;
- high elasticity point, so as to keep the plastic deformations within small limits.

The chemical composition of the materials analyzed according to STAS 791-88, is presented in Table 1.

The chemical compositions of their material samples, according to the lab bulletins, has been established by: spectral analysis, chemical and quantitative analysis presented vs the standards in force, according to Table 2.

Table 1

Steel grade	C	Mn	Si	P	S	Cr	Cu	Mo	Al
	[%]								
42MoCr11	0,38-0,45	0,60-0,90	0,17-0,37	Max. 0,03	0,02-0,04	0,90-1,20	Max 0,30	0,15-0,30	0,02
38MoCrAl09	0,35-0,42	0,30-0,60	0,20-0,45	Max. 0,03	0,02-0,035	1,35-1,65	Max 0,30	0,15-0,25	0,70-1,10

Table 2

Steel grade	C	Mn	Si	P	S	Cr	Cu	Mo	Al
	[%]								
42MoCr11	0,42	0,68	0,33	0,030	0,026	1,02	0,220	0,17	0,02
38MoCrAl09	0,38	0,50	0,25	0,026	0,020	1,38	0,058	0,17	1,18

The content of Ni with steel 38MoCrAl09 is 0,26 %, and with steel 42MoCrV11 is 0,32 %. It is stated that, according to the chemical composition, these steels are in compliance with the prescriptions STAS 329-83 and norms API –Spec 11B-1982. The steels analyzed reach a max score 4,5 from inclusions and a fine grain (score 8-9).

The heat/magnetic treatments applied are:

t1, t1'= quenching (850 ˚C) and high tempering (580 ˚C) applied to steel 42MoCr11 (code V) and quenching (hardening) (920 ˚C) and high tempering (620˚C) applied to steel 38MoCrAl09 (code R);

t3, t3' = quenching (hardening) (850 ˚C) and high tempering (580 ˚C) applied to steel 42MoCr11 (code V) , quenching (hardening) (920 ˚C) and high tempering (620˚C) applied to steel 38MoCrAl09 (cod R), cooling being performed in alternative current magnetic field (H=1300A/m);

t4, t4'= quenching (850 ˚C) and high tempering (580˚C) applied to 42MoCr11 (code V), quenching (920˚C) and high tempering (620˚C) applied to 38MoCrAl09 (code R), cooling being performed in dc magnetic field (H=1300A/m);

T9 = t1(classic)+ plasma nitrocarburation with 42MoCr11 (code V);

T10 = t4+ plasma nitrocarburation with 42MoCr11 (code V);

T11 =t 3 + plasma nitrocarburation with 42MoCr11 (cod V);

T12 = t1'(classic) + plasma nitrocarburation with 38MoCrAl09 (code R);

T13 = t3'+ plasma nitrocarburation with, code R;

T14 = t4'+ plasma nitrocarburation , code R.

Plasma nitrocarburation was performed to treatment temperature of 530 ˚C.

The wear –tests (friction process) were carried out on an Amsler bench from the machine design department „Dunarea de Jos" University of Galați, and the diffractometric analysis were performed by means of a Dron 3 from the same institution.

The curves of variation for phasis distribution and other characteristics in superficial layers because the magnetic field applied before plasma nitrocarburized, function by wear –tests period, are presented in figures: 2 ÷ 19.

Microstructures achieved on heat/magnetic/chemical and plasma nitrocarburation treated samples show that the thickness of the heat/chemically treated surface layer is higher when applying the heat/magnetic treatment (for example, a.c. magnetic field) with steel 38MoCrAl09 (code R), vs. the conventional treatment case- magnetic field - free treatment [3].

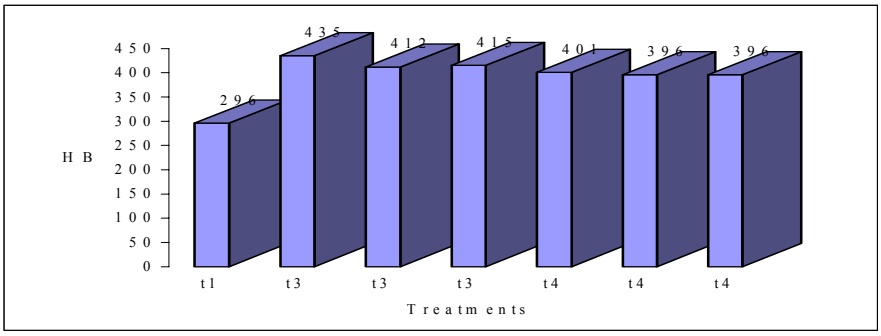

***Fig. 2**. The influence of the magnetic field applied at the cooling regime- before nitrocarburation treatment, on the hardness number, in case of 42MoCr11 steel grade (code V)*

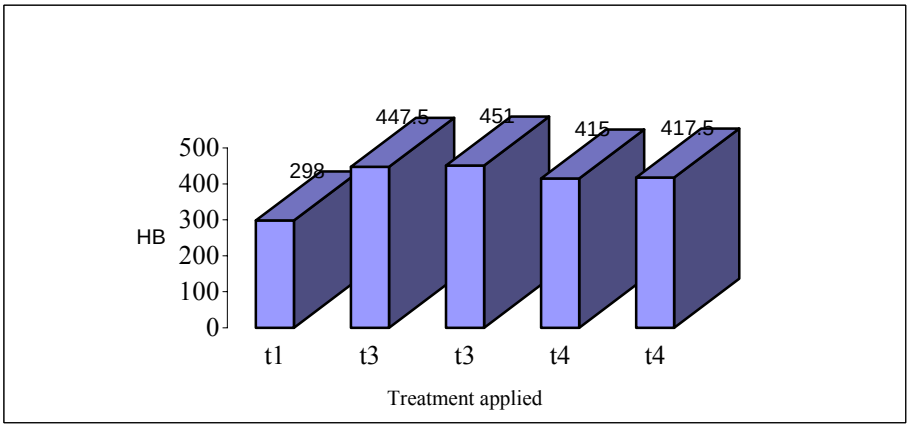

***Fig. 3.** The influence of the magnetic field applied at the cooling regime- before nitrocarburation treatment, on the hardness number, in case of 38MoCrAl09 steel grade (code R)*

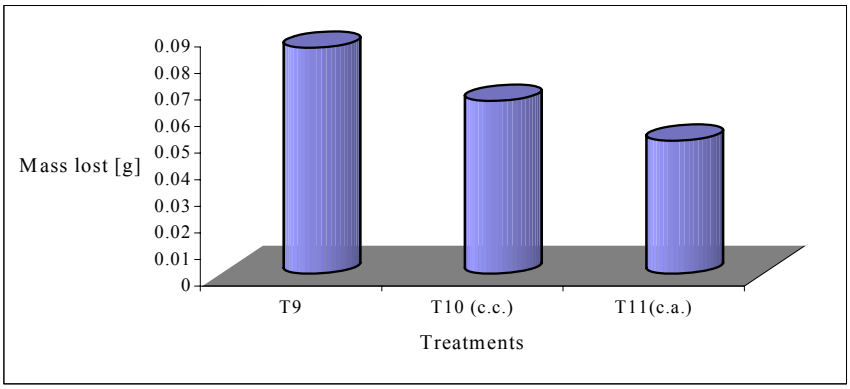

Fig. 4. *The influence of the magnetic field on the average mass loss after 3 hours of wear friction process, strain corresponding to one degree of sliding (by 10%) and the value of the strain are corresponding to Q=150 daN, in case of 42MoCr11 (code V) steel grade (after nitrocarburation treatment) [P1].*

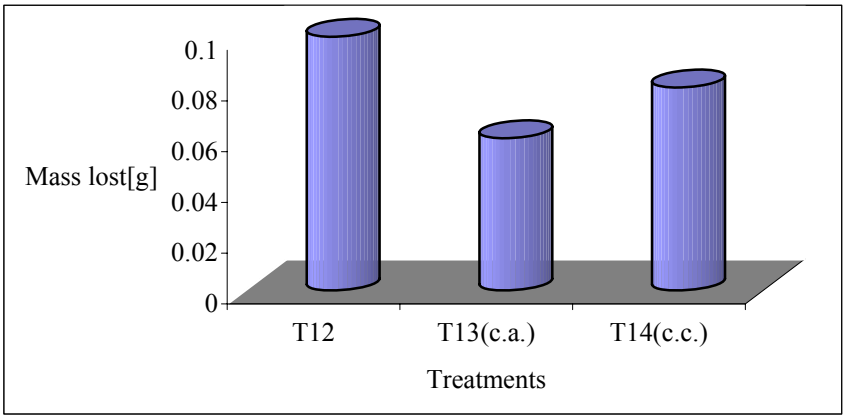

Fig. 5. *The influence of the magnetic field on the average mass loss after 3 hours of wear friction process, which corresponds to a degree of sliding by 10% and the value of the strain are corresponding to Q=150 daN, in case of 38MoCrAl09 (code R) steel grade (after nitrocarburation treatment) [P1].*

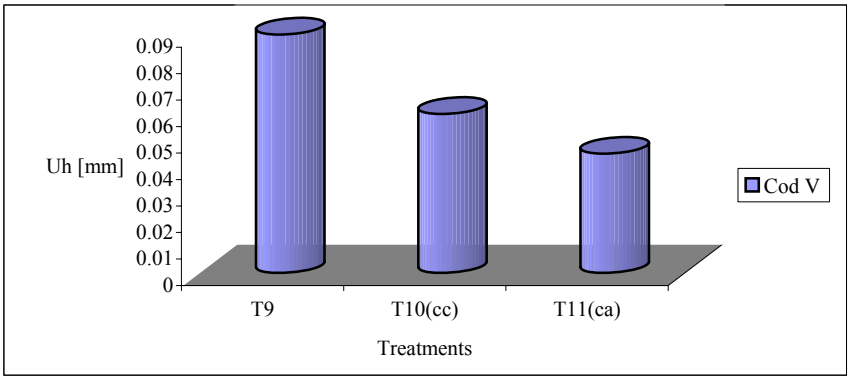

Fig.6. *The influence of the magnetic field on the worn layer depth, after 3 hours of wear friction process, which corresponds to a sliding degree (10%) and the value of the strain are corresponding to Q=150 daN, in case of 42MoCr11 (code V) steel grade (after nitrocarburation treatment) [P1].*

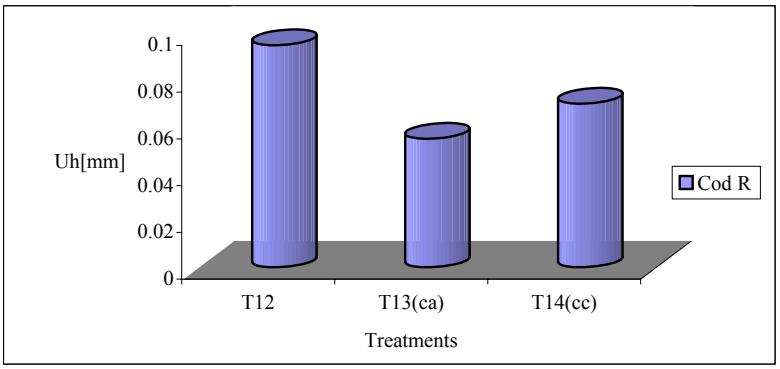

Fig.7. *The influence of the magnetic field on the worn layer depth, after 3 hours of wear friction process, which corresponds to a sliding degree by 10% and the value of the strain are corresponding to Q=150 daN, in case of 38MoCrAl09 (code R) steel grade (after nitrocarburation treatment) [P1].*

Microstructures (figures: 8, 9, 10) achieved on heat/magnetic/chemical and plasma nitrocarburation treated samples show that the thickness of the heat/chemically treated surface layer is higher when applying the heat/magnetic treatment (for example, a.c. magnetic field) with steel 38MoCrAl09 (code R), vs. the conventional treatment case - magnetic field - free treatment

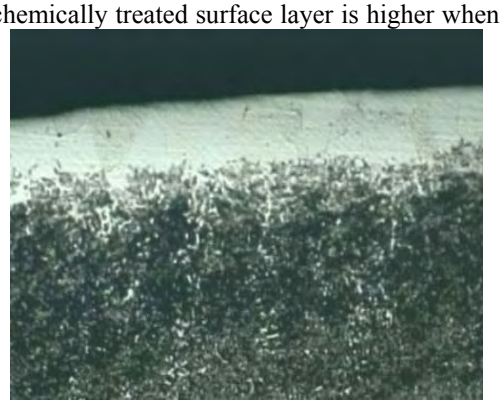

Fig. 8. *Nitrocarburized surface layer on the sample R5 (code R), before wear process tests. Treatment: quenching (t=920˚C) and high tempering (t=620˚C) followed by water cooling in (dc)continuous current magnetic field and plasma nitrocarburation at 530 ºC (7 h)*
(x100)
Nital attack 2%

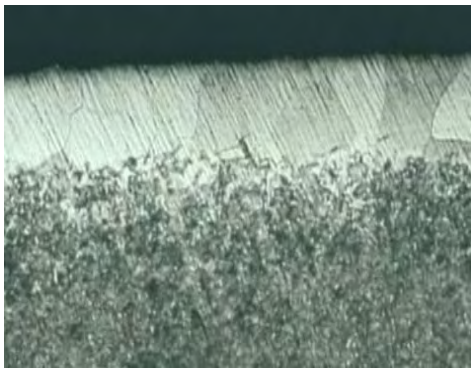

Fig. 9. *Nitrocarburized surface layer on the sample R3 (code R), before of wear process tests. Treatment: quenching (t=920˚C) and high tempering (t=620˚C) followed by water cooling in (ac) alternative current magnetic field and plasma nitrocarburation at 530 ºC (7 h)*
(x100)
Nital attack 2%

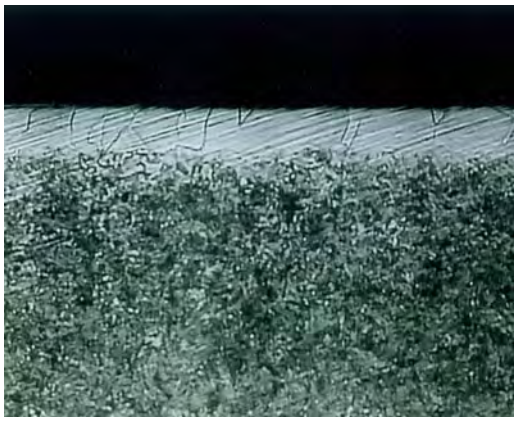

Fig. 10. *Nitrocarburized surface layer on the sample R2 (code R), before wear process tests. Treatment (classic): quenching (t=920˚C) and high tempering (t=620˚C) followed by water cooling - without magnetic field and plasma nitrocarburation at 530 ºC (7 h)*
(x100)
Nital attack 2%

3. Conclusions

For a deeper insight into this theme, the research is focused on pieces from the metallurgical industry (rollers, gears etc.) and on the materials they are made from. At the same time the results achieved under laboratory conditions were used to choose the optimum treatment regimes; depending on the strain conditions the metallurgical pieces are working in, a selection is attempted so that those pieces may be manufactured from the steels investigated and unconventionally treated in this paper. Applying the thermal-chemical treatment implies to make a hard layer into a heat treated (improved) core of a relatively low hardness as compared with the hardness obtained after the thermal-chemical treatment. A first research direction was the improvement of the mechanical characteristics (hardness) in thermo- magnetic treated steels for further applying the diffusion thermo-chemical treatment under the thermo-magnetic treatment

This research is focused on:

a). Improving the wear resistance characteristics of the thermo –magnetic treated surface layer by applying the thermo –magnetic *treatment to the piece core*. The modifications induced by the magnetic field to improve the core, have triggered the modifications of the mechanical and structure properties of the thermo-chemical treated layer. There is an obvious influence of the thermo- magnetic treatment applied to the core on the structure of the thermo-chemical treated surface layer [P1].

b).Continuity of the thermo-chemical treated layer tested to wear resistance and checking the results on three roller-type samples obtained under the same manufacturing and treatment conditions and tested in the same strain conditions for each thermo-chemical-magnetic treatment. Another research direction was the study of the influence of the thermo- magnetic treatment applied before the thermo-chemical treated surface layer when applying plasma nitrocarburation. In a first stage, the samples of microstructures were analyzed after applying the thermo-magnetic treatment and, in the second stage, the microstructures after applying the thermo-chemical treatment of ion nitruration and plasma nitrocarburation, respectively.

It has been shown that, when applying an alternative current magnetic field treatment (for example H=1300A/m), the thickness of the thermo-chemical treated layer increased up to 25% as compared to the conventional thermal, thermo-chemical treatment (H=0 A/m) without a magnetic field. The results from these researches have been compared with those obtained on the classically treated (without magnetic field) samples, while complying with the technological parameters used with the thermal and thermo-chemical treatments in S.C. MITTAL STEEL S.A. Galati.

The novelty of the present paper involves the application of the diffusion thermo - chemical treatment after the thermo-magnetic one, the temperature of the former being lower than that of the latter, except that the thermo-chemical treatment applied after the thermo-magnetic treatment should not modify – due to the high temperature - the improvements of the mechanical properties by the thermo-magnetic treatment.

The positive influence of the volume thermo-magnetic treatment on the surface layer treated thermo-chemically resulted in a higher hardness (see [P1]-subchap.6.1.1.) and the wear resistance by the decreasing the depth of the used layer (see [P1]-subchap.6.4) by approx. 50% - in case of steel 38MoCrAl09 and by 40% - in case of the steel 42MoCr11, which has been proved by the wear tests and the evolution of the mass loss through wear and wet friction.

References

[B1]: Berkowitz, A.E., s.a.- « *Magnetism and Metallurgy* », Academic Press, New York and London, 1969 ;

[B2]: Bozorth, R.M.,- "*Feromagnetism*", New York, Van Nastrand, Co.Inc., 1951;

[C1]: Cedighian, S.,- "*Materiale magnetice*", Editura Tehnica, Bucuresti, 1974;

[P1]: Papadatu, C.-P.- « *Cercetări privind ameliorarea proprietăţilor şi creşterea fiabilităţii unor oţeluri folosite în construcţia utilajelor metalurgice* » - Teza de doctorat, Galaţi, 2005;

[P2]: Popescu, N., s.a.- " *Tratamente termice neconvenţionale*", Editura Tehnice, Bucureşti, pag. :105-117, 1990 ;

[S1] : Stefanescu, I.- *Teza de doctorat*, Galaţi, 1984 ;

[S2] : Stefanescu, I.-« *Contribuţii la studiul influenţei tratamentelor termomagnetice asupra unor caracteristici mecanice ale oţelurilor de rulmenţi RUL1* », Suceava, 1981 ;

[V1] : Vonsovschi, S.V.,-« *Teoria modernă a magnetismului* », Editura Tehnica, Bucureşti, 1956.

SOME ISSUES CONCERNING GEAR WHEELS FABRICATION BY SINTERING

Alexandru OLEVSCHI
"Technical University of Moldavia" Kishinew, Moldova Republic
e-mail: dulgheru@mail.utm.md

ABSTRACT

Powder metallurgy appeared in the XVIII century as result of industrial market demand for electric bulbs filaments made of wolfram. Nowadays powder metallurgy is applied in such fields as: automotive industry (cylindrical or conical gear wheels), fine mechanics (components for calculation devices), toys production industry, electrical engineering (field poles for electrical fittings), machine building industry (filters, gear wheels, levers). In this work some applications of metallic powders in the fabrication of gear wheels are presented. As well the possibilities for their utilization in conical gear wheels of precessional planetary transmissions are described.

KEYWORDS: gear wheels, planetary transmissions, sintering

1. Introduction

The following raw materials are utilized in powder metallurgy: native metal, alloys, metallic and non-metallic mixtures. The advantages that have placed powder metallurgy at such a high level are:

- Short-term technological track. The components have the accuracy and quality of surfaces as it is imposed by the drawing (without any further processing);
- The level of utilization of the material is almost 100%;
- The possibility to produce some components from materials with high melting point, which casting is difficult;
- The products are provided with sensitive and uniform composition and high steadfastness of properties;
- Securing of pseudo alloys achieved by powder mixing. Currently it does not make alloys (CU-graphite, Fe-graphite, etc.);
- Components (filters, bearings) with controlled porosity can be obtained;
- Equipment (homogenizers, mills, furnaces, etc.);
- The process of automation is easy to apply in powder metallurgy;
- The qualifications of personnel are reduced.

But along with these advantages, some disadvantages come:

- High cost of powders;
- Restrictions in the geometrical form and dimensions;
- High cost of moulds.

2. Technology for components fabrication

To make a component from metallic powder mixtures are utilised and the following steps are performed:
1) Sorting; 2) heat treating; 3) splitting up of powder sintering; 4) processing of mixtures.

Depending on the destination of components their moulding is carried out by one of the moulding procedures: application of pressure (cold compressing, hot compressing, sinter moulding, isostatical pressing, powder extrusion, powder rolling, etc.) or without application of pressure (plaster mould casting, metallic mould pressing, vibration moulding, etc.).

Fabrication of components from metallic powders is done in several steps which are presented in fig. 1 [2].

3. Compacting of metallic powders (components moulding)

Depending on the component destination its moulding can be done via two big categories of procedures:
I. Moulding procedures with application of pressing which identifies the next versions: cold compressing; hot compressing; sinter moulding; isostatical pressing, powder extrusion, and powder rolling; (continuous pressing).
II. Moulding procedures without application of pressing on powders. Among these procedures we can mention: plaster mould casting, metallic mould was pressing, vibration moulding.

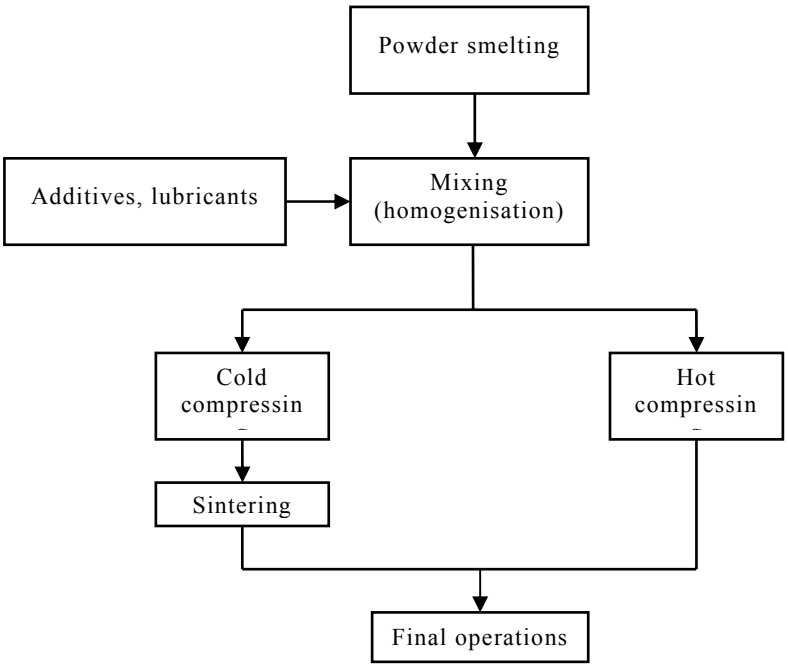

***Fig. 1**. Steps for metallic powders smelting.*

4. Casting of gear wheels by superficial hardening

In many cases the loading generates high stresses at or close to the surface such that full density throughout a part is not required. Such loading situation can be covered by selective surface densification (SSD). This process generates a densified surface layer in the range of 0.2 to 1.0 mm and a density gradient ranging from nearly zero porosity at the surface to typically 10 vol.% porosity in the core of a component. SSD is a processing technology which has been successfully applied to the densification of highly loaded parts such as gears and one-way clutch races.

Highly loaded gears are a most prominent application for SSD. It has been shown that SSD by external transverse rolling supplies P/M gears which have sufficient strength and, simultaneously, reduce the generation of noise.

The present method [3] is intended to characterize the evolution of microstructure, hardness, selective surface densification, pore morphology, geometry (DIN quality) and surface roughness of the helical gear displayed in Fig. 2.

Tooth root strength and pitting resistance are tested on a test rig.

The investigation was carried out on a surface densified helical gear with a 33° helix as shown in Fig. 2. The geometric parameters are summarized in Table 1. The wrought steel version of this gear is presently used as a fixed gear in the 4th speed of a passenger car gear box.

The selection of a P/M material for this gear was based on previous processing experience and on rolling contact fatigue tests. From this information two commercial water atomized, pre-alloyed powders were chosen: ferrous metal powder with 1,5%Cr, 0,2%Mo, 0,1% graphite and wax 0,8%, and ferrous metal powder with 1,5%Mo, 0,2% graphite and 0,8% wax.

The processing sequence employed in the present investigation is:

- pressing of helical gear with over measure;
- sintering to ≈ 90 % of theoretical density;
- turning;
- selective densification by transverse rolling;
- case hardening;
- final surface finishing by honing.

Pressing was performed at 600 MPa on a hydraulic 350 to press (Fig. 3) which is equipped with a gear-box driven adapter to rotate the punch.

Fig. 2. *Gear wheel, made of Metallic powders, with hardened surface and its specifications.*

Table 1

Gear Parameter	Unit	Value
Number of teeth, z	-	39
Normal module, m	-	1,8
Pressure angle, α	°	16
Helix angle, β	°	33
Helix direction	-	Right
Outside diameter, da	mm	88,88
Root diameter, dr	mm	78,38
Pitch diameter, d	mm	83,70

a) *b)*

Fig. 3*. a) Pressing on a hydraulic 350 to press; b) Mo-gears sintered on a belt furnace*

Table 2*. Sintering conditions*

Material	**Furnace**	**Temperature**	**Time**	**Atmosphere**	**Cooling rate**
		[°C]	[min]		[Ks-1]
CrL	Roller hearth	1160	30	N_2/H_2	≈0.2
Mo	belt	1120	30	N_2/H_2	≈0.2

The two materials were sintered with the parameters shown in Table 2. The gears were placed on ceramic plates to avoid distortion (Fig. 3). The dew point in the roller hearth furnace was controlled and kept below 60°C to keep the oxygen content of the chromium containing material CrL below 0,1 wt.%. The average density of as-sintered gears is fairly uniform, i.e. ρ = 6.98-7.02 g/cm³ in the core region. After sintering, the gears were turned to improve concentricity which influences the radial run out Fr and the pitch error Fp.

After machining the gears were selectively densified on a circular force controlled rolling machine. In this process, an as-sintered gear with over measure is put into the center between two mating rolling tools.

The microstructure of Mo- and CrL-gears after sintering shows ferrite and pearlite in both cases as displayed in Fig. 4. The Brinell hardness is 82 HB respectively 77 HB. These low hardness values are prerequisite for cold forming by transverse rolling.

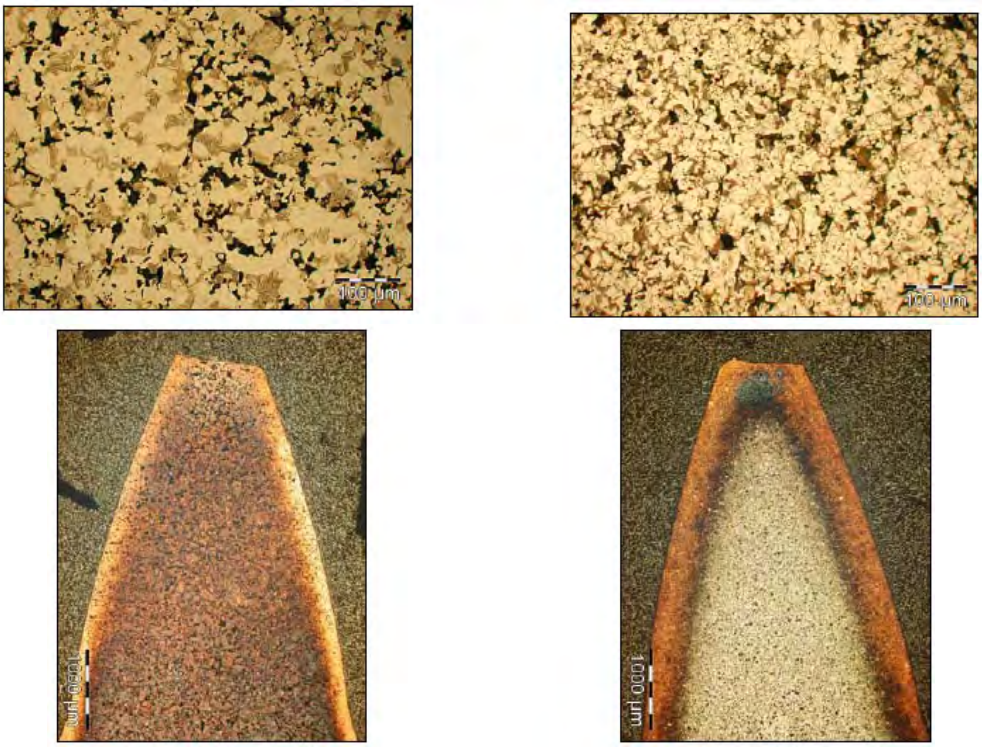

a) *b)*

Fig. 4. *a) Mo-gear after sintering; b) CrL-gear after sintering.*

5. The planetary precessional transmissions

The precessional transmissions of big dimensions include the satellite block with conical roller teeth, placed on an intern cone. The conical rollers, installed on axles with the possibility of rotation around them, replace the sliding friction between the gear elements, impending in the precessional gear, with the rolling friction of the rollers on the surfaces of the central wheels teeth [1].

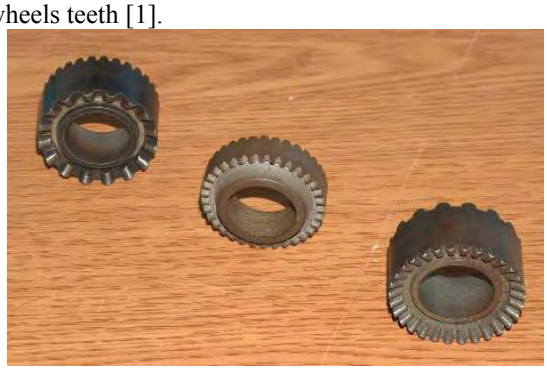

Fig. 5. *Sintered satellites from P/M for precessional transmissions.*

The execution of the conical roller teeth of the satellite block becomes difficult at the decreasing of the precessional transmissions dimensions.

In this case a distinctive interest represents the manufacturing of the toothed gears from metal powder. The reduction of power losses at sliding friction between gear elements is achieved by means of the usage of metal powder containing solid lubricants such as: molybdenum sulphide, graphite etc. There exist some special fields of precessional gear functioning, such as vacuum conditions from cosmos, where the manufacturing of the toothed gears from metal powder represents currently a very improved solution.

6. Conclusion

It can be praised that the manufacturing of the products from metal powder is advantageous and far-reaching, and represents a highly qualitative and profitable way for producing of the toothed gears.

References

[1]. Bostan I. *Precessional transmissions with multi-pair gearing.* Stiinta Publishing House, 1991, 356 s.
[2]. Iacobescu A., Urecheatu Gh., Homei D. *Materials study,* Academia Trupelor de Uscat Publishing House, Sibiu, 1998.
[3]. Günter Rau, Lorenz S. Sigl *P/M gear for a passenger car gear box,* International Conference on Gears, Munich, September

THE ANNALS OF "DUNAREA DE JOS" UNIVERSITY OF GALATI
FASCICLE IX METALLURGY AND MATERIALS SCIENCE, ISSN 1453 – 083X. N^0. 2 – 2006

HARDENED ALUMINUM WITH DISCONTINUOUS COPPER THREADS

Octavian POTECASU, Florentina POTECASU, Petrica ALEXANDRU
"Dunarea de Jos" University,
e-mail: fpotec@ugal.ro

ABSTRACT

The paper presents the influence of the quantity of discontinuous reinforced threads on the mechanical characteristics of some samples obtained through deformation from composite material with metallic matrix.

As a raw material for obtaining the matrix it was used aluminum powder and as a reinforcing phase, short and long copper threads with different volumetric percentages. The products have been plastically deformed at a final diameter of 3mm.

The presence of the copper threads dispersed in the aluminum matrix in quantities of up to 16% copper (volumetric percentages), determines the hardening of the composite material. Above this limit the increase in the quantity of copper is no longer justified as it begins fragilizing the aluminum matrix.

KEYWORDS: aluminum, matrix, reinforcement, copper, threads.

1. Introduction

The aluminum powder used for experimentations was obtained in laboratory on a spraying installation with air-jet. After granulometric rating it was chosen for pressing the powder with grain size (0.1 – 0.2) mm having an apparent density of 1.14 g/cm^3. After mixing and homogenization of the two components, six series of composite materials were made through compressing, armed with different volumetric contents of copper threads (table 1).

The reinforcing component was made of copper threads with the diameter of ϕ = 0.4 mm and length of l_1 = 7 mm.

Table 1

Composite material	Series I	Series II	Series III	Series IV	Series V	Series VI
Copper [%]	10	12	14	16	18	20

The influence of the discontinuous thread quantity of copper used for reinforcing the aluminum powder on the mechanical characteristics (mechanical resistance, elongation) of the composite material obtained through extrusion is shown in graphics.

As blank test it was used extruded aluminum (without addition of copper threads) from the same range of powder and under the same deformation conditions. The mechanical characteristics calculated for tensile breaking test had for the blank tests values of 7 daN/mm^2 for mechanical resistance and of 31 % for elongation.

2. Experimental conditions

The container used for obtaining the comprimats, had a diameter of ϕ = 20 mm and the height of 92 mm and it was executed in strapped structure of steel Cr 120 as well as the bottom die and the punches for compression. The average specific pressure necessary for compressing the tests was of p_m = 90 daN/mm^2.

Tests were obtained with dimensions of ϕ 20 x 30 mm. Out of these comprimats, samples of composite materials were obtained, through direct extrusion and then through drawing.

Extrusion was made at hot conditions, with a diameter reduction from ϕ 20 mm to ϕ 4 mm. The tests were heated at 400^{0}C. At extrusion the average specific pressure was of p_m = 95 daN/mm^2. After extrusion samples were obtained with the diameter of 4 mm and a length of approximately 600 mm.

After the extrusion operation, to cold-hardened tests a annealing thermal treatment of recrystallization was applied, in order to give them back the plasticity necessary for an afterwards deformation.

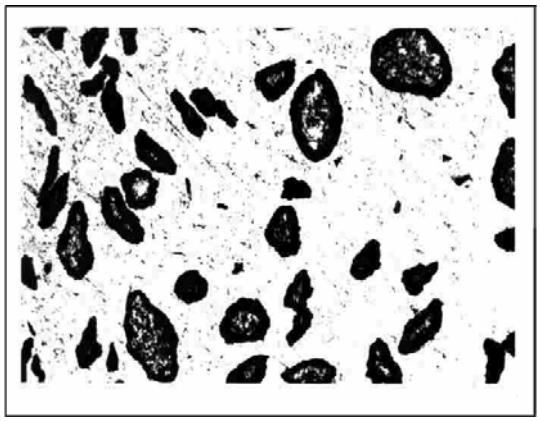

Fig. 1. *Distribution of copper threads dispersed in aluminum matrix; transversal section (200:1).*

The diameter reduction, from ϕ 4 mm to ϕ 3 mm, was realized by consecutive passes, using four auger dies in the following steps: ϕ 4 mm ↦ ϕ 3.9 mm ↦ϕ 3.5 mm ↦ ϕ 3.3 mm ↦ ϕ 3 mm. The last operation was the thermal treatment of recrystallization applied at 400^{0}C, with a period of 30 minutes.

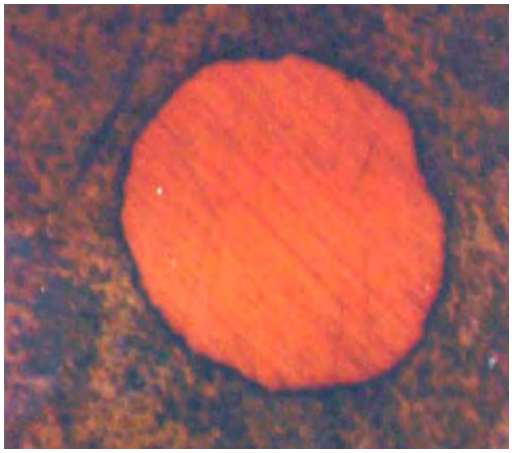

Fig.2. *The aspect of including a copper thread in the aluminum matrix in transversal section (1000 :1).*

Eventually, tests with ϕ=3 mm were obtained from Al-Cu composite material, having different volumetric percentages of copper: 10%, 12%, 14%, 16%, 18%, 20%.

The copper threads dispersed in the aluminum matrix and deformed along with this have different aspects (circular, oval) depending on the way they had been divided when making the assays (fig.1).

3. Experimental results

On samples, in annealed condition with length l = 160 mm made from the series of composite materials presented in table 1, it was determined at the tensile breaking test the resistance R_m [daN/mm^2] and the elongation A [%].

In figure 2 it is presented the graphic on the influence of the copper quantity on the mechanical resistance at the tensile breaking test for the series of composite materials presented in table 1.

In figure 3 it is presented the variation graphic of the mechanical resistance at the tensile breaking test for the series of composite materials presented in table 1 depending on the volumetric content of copper, when reinforcing with discontinuous copper threads. One can notice that the hardening effect through thread dispersions manifest itself up to a volumetric content of 16% copper.

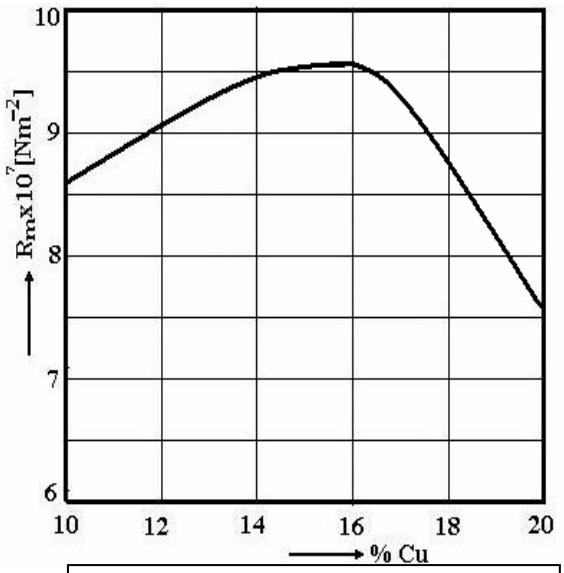

Fig. 3. *The influence of the quantity of copper threads on the mechanical resistance of the composite material.*

An enhanced quantity of reinforced phase in the aluminum matrix has no longer the desired effect, and therefore at over 16% copper, the values of mechanical resistance decrease, which suggests that the hardening effect is obtained up to around this quantity (16%), after which it begins appearing a fragilizing effect of the composite matrix. Apart from

the resistance, the plasticity characteristics (elongation) decrease continuously as the quantity of copper increases, the decrease being slower up to 16%, after which the fragilizing effect becomes more emphasized (fig. 4).

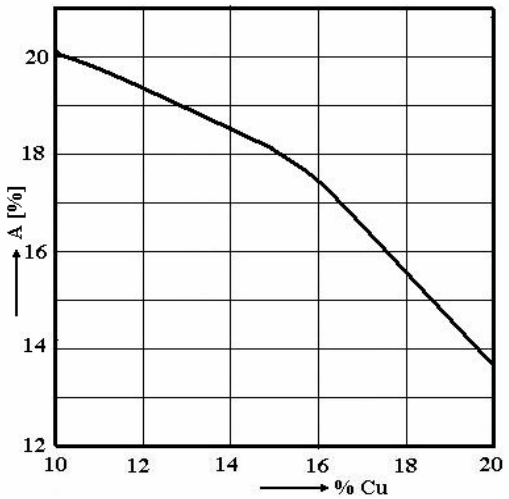

Fig.4. *The influence of the quantity of copper threads on the elongation of the extruded samples of composite material.*

4. Conclusions

The experiments realized confirmed the hardening role of the reinforcing phase up to a percentage of ~ 16% copper.

Over the quantity of ~ 16% copper used as reinforcing phase threaded-shape, one can notice that it begins appearing fragilizing of the metallic matrix.

References

[1]. S. Umekawa, C. H. Lee, J. Yamatomo and K. Wakashima: " *Effect of Coatings on Interfacial Reaction in Tungsten/Nickel and Tungsten/316L Composites* " in Recent Advances in Composites in the United States and Japan, J. R. Visison and M. Taya (eds.), ASTM STP 864, Philadelphia, pp. 619-31, 1985.

[2]. I. Ahmad and J. Barranco: " *W-2% ThO_2 Filament Reinforced Cobalt Base Alloy Composites for High Temperature Application* ", in Advanced Fibers and Composites for Elevated Temperatures, I. Ahmad and B. R. Noton (eds.), TMS-AIME, Warrendale, pp. 183-204, 1980.

[3]. **R. Warren, L. O. K. Larsson and T. Garvare**: " *Fibre-Matrix Interactions in a W-Wire Reinforced Stainless Steel Composite* ", Composites, 10, pp. 121-125, 1979.

[4]. W. S. Miller and F. J. Humphreys -*Strengthening Mechanisms in Metal Matrix Composites*- Fundamental Relationships Between Microstructure and Mechanical Properties of Metal-Matrix Composites, P.K. Liaw and M. N. Gungor (eds.), TMS, Warrendale, Pa., pp. 517-541, 1990

[5]. **D. J. Matthewman, P. J. Withers and J. Mason**: "*Particulate Reinforced Copper* ", in Metal Matrix Composites - Exploiting the Investment, London, Inst. of Metals, p. 25, 1991.

[6]. **T. W. Clyne, A. J. Phillipps, S. J. Howard and M. C. Watson**: *"Mechanical Characterisation of Metal/Ceramic Interfaces in Composites and Laminates* ", in Proc. 2 end European Colloquium on Designing Ceramic Interfaces, Petten, Netherlands, S. D. Peteves (ed.), 1992.

[7]. F.Oprea, O.Potecasu, E.Drugescu, F.Potecasu, O.Mitoseriu - *Interface Phenomena in Electroconducting Composites with Metallic Matrix* - International Journal Materials and Manufacturing Processes (USA),1999, vol.14, part 6, Publisher Marcel Dekker Jurnals, ISSN1042-6914, pages 809-820.

BEHAVIOR OF WELDED JOINTS FROM SOME STAINLESS AUSTENITE STEEL TYPES DURING NITRIDING PROCESS

Ovidiu DIMA
"Dunarea de Jos" University Galati
email: dima.ovidiu@ugal.ro

ABSTRACT

Researches made on welded and nitrided samples from stainless austenite steel types show that nitriding thermo chemical treatment can be applied also for welded joints. As a result of the treatment, a diffusion layer with austenite dendritic layer was obtained, max hardness of 500 HV_{005}- The layer's depth depends on the finishing degree of the structure. The finer the dendritic structure is the slower the diffusion process and smaller the layer depth.

KEYWORTS: welded joints, austenite stainless steel, nitriding process

1. Experimental conditions

For the analysis of welded joints behavior during nitriding process, some samples welded end to end by electric manual procedure EM, from steel types code 3, 4, 5, have been subjected to fluidized bed nitriding process in identical conditions as the analysed stainless austenite steel types.

The samples are from plates 3mm thick and they were welded with electrodes of 2.5 mm in diameter. The type of electrode is in accordance with the chemical composition of the steel. The type of electrodes and chemical composition of the material are presented in table 1.

Table 1

Steel type	Code	Electrode	%C	%Si	%Mn	%Cr	%Ni	%Mo
X2CrNil8.9	3	18/8 with low %C	<0.04	<1	<2.5	18-21	9-11	-
X2CrNiMo17.11.2 X6CrNiMoTil7.12.2	4 5	18/12/3Mo with low % C	0.04	<1	<1.5	18-19	11-12	2.5-3

The welding was made in direct current, reverse polarity c, and the electric parameters have the following values: U=24V, 1=55A. Taking into consideration the base coating of the electrodes, maybe they have been dried for two hours before using them, at a temperature of 250°C. The seam was thread-shaped, in one line, without oscillation, on a copper skid. Before welding the edges have been straightened. The analysis of the seam before the nitriding treatment shows that this presents a fine austenite dendritic structure for all steel types which is accompanied by a relative big ferrite (Fe_δ) quantity due to quick cooling and determined by welding on copper skid. The ferrite quantity in the seam was determined by means of a ferrite-meter and it is presented in table 2. The bigger quantity of ferrite Fe_δ in the steel types code 4 and 5 is determined by ferrite activity of molybdenum.

Figure 1 presents the welding seams microstructures made on steel types code 3, 4, and 5, at an increase of x200.

Table 2

Steel type	Code	% Fe_δ
X2CrNil8.9	3	4.5
X2CrNiMol7.11.2	4	6
X6CrNiMoTil7.12.2	5	9.5

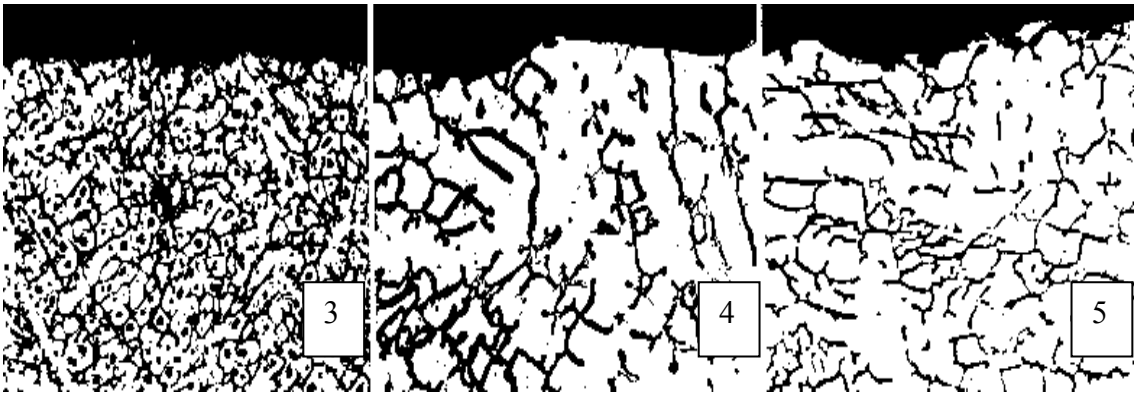

Fig. 1. *The welding seams microstructures made on steel types code 3, 4, and 5, at an increase of x200.*

The welded samples, like the steel nitrided samples, have been cut to the dimension of 20x60x3, and the seam arrangement is medial, frontal. The seam surface was polished and after that with granulated metallographic paper 280-320. Before being introduced in to nitriding installation, the samples have been washed, degreased with carbon tetrachloride and then dried with hot air.The fluidized bed nitriding process lasted for 3 hours.

2. Analysis of nitrided samples

Samples for metallographic analysis and for mechanical micro hardness tests have been taken from the welded and nitrided samples in order to point out the modifications inside the surface layer.

The metallographic analysis made by optical microscopy shows that nitrogen diffusion in the structure formed from austenite with ferrite separations Fe_δ , with dendritic aspect specific to welding seams has not produced visible changes in the aspect of the structure.

The nitrogen was diluted without producing complex nitrides separations, so without forming a composition layer with a distinct metallographic aspect. However it is possible for nitrogen diffusion to reduce very much the ferrite quantity Peg in the surface layer which will be transformed in austenite enriched with nitrogen.

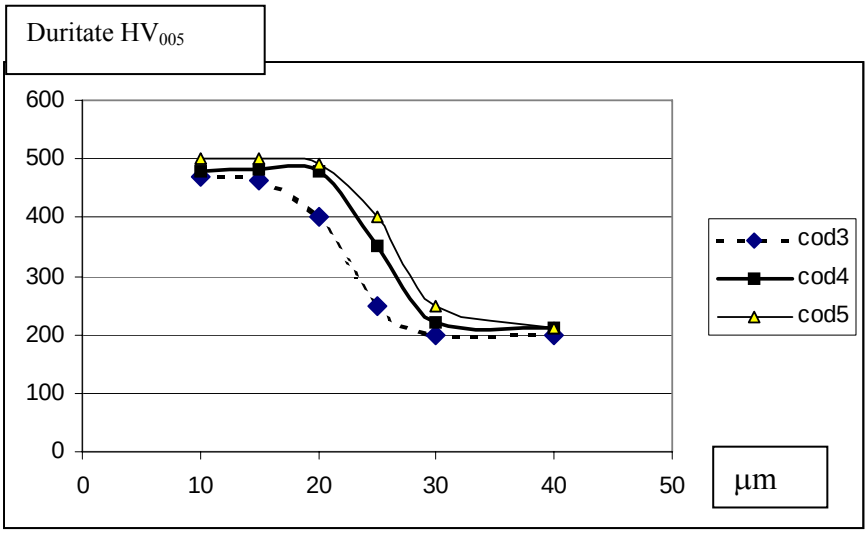

Fig.2*. Hardness variation in nitrided layer depth*

For the hardness test, Vickers trial with low loads was used and the pressure force was of 0,50N. The values of the three samples are presented in table 3. The analysis of hardness variation in the surface layer shows a two times bigger hardness, even bigger for molybdenum steel types and especially for the steel type which has a higher carbon content. Layer's depth is small enough 20-25µm because the dendritic structure is very thin and because the high density of grains limits suppresses the diffusion process.

Table 3

Code steel	Surface distance μm					
	10	15	20	25	30	40
	Hardness HV_{005}					
3	470	462	400	250	200	200
4	480	482	480	350	220	210
5	502	500	490	400	250	210

You may notice that layer's depth is smaller for steel type code 3 which has the higher structure finishing degree.

Fig. 2 presents the hardness variation in nitrided layer depth.

3. Conclusions

The researches made on welded and nitrided samples show that nitriding thermo-chemical treatment can be applied also to welded joints. After the treatment, a diffusion layer with austenite, dendritic structure having a hardness of max. 500 HV_{005} will be obtained. The layer's depth depends on finishing degree of the structure. More fine the dendritic structure is, more restrained the diffusion process and smaller the layer's depth are.

References

[1]. Dobrovici S. - *Cercetări privind tehnologia carbonitrurării în strat fluidizat aplicată oțelurilor*. Teză de doctorat Galați 1999.

[2]. Truşculescu M. - *Oțeluri inoxidabile şi refractare.* Ed. FACLA Timişoara 1983.

[3]. Berns H. - *Case hardening of stainless steel using nitrogen*. Ruhr University, Bochum, Germany 2002.

[4]. Berns H. - *Solution nitriding of stainless steel for process engineering,* Mat.-wisws. u. Werkstofftech. 31/2000.

[5]. Mocanu D. R. - *Încercarea materialelor*. Ed.Tehnică Buc. 1982.

[6]. Vellier M. - *Solution apportees aux problemes de la corosion-abrasion par certaines aciers inoxydables austenitiques et austenito-feritiques.* Conference internationale des arts chimiques Paris 1976.

[7]. Dima O. Mitoşeriu O. Levcovici S. - *Studiu asupra aspectelor de coroziune evidențiate pe table şi îmbinări sudate din instalațiile de fabricație a celulozei chimice prin procedeul sulfit din cadrul combinatelor CCH Zărneşti, CCH Letea Bacău, CCH Brăila*. Tehnologii Calitate Maşini şi Utilaje 36 Ed. Tehnică Buc.1999. Lucrările simpozionului Ecologie. Acoperiri metalice. Braşov 1999.

AIR QUALITY MONITORING IN GALAȚI. CASE STUDY

Lucica BALINT, Minodora RÎPĂ,
Simion Ioan BALINT, Petre Stelian NIȚĂ, Gina NASTASE
"Dunarea de Jos" University
e-mail: lbalint@ugal.ro

ABSTRACT

This paper presents information referring to the variation of aerosols concentration in a central area in Galati. For a period of time of november2005 to november 2006, there have been made correlations between aerosols concentrations and the predominant wind directions (E~W, N~NE~S-SW).

The results of the measurements are specific only for a point in time, being influenced by random variables (traffic intensity, temperature, pressure, wind speed, humidity etc.).

KEYWORDS: aerosol, pollution, particulate matter, air quality.

1. Introduction

The aerosols are systems of solid or liquid particles suspended in a gaseous medium, having a negligible falling velocity. Aerosols include a wide range of phenomena such as dust, fume, smoke, mist, fog, haze, and smog [1].

Aerosols may be produced either by ejection or emission into the atmosphere (primary aerosol production) or by physical and chemical processes within the atmosphere (secondary aerosol production) [3]. Particles in the atmosphere arise from natural sources as well as anthropogenic activities [1]. The former source includes wind blown dust, sea spray, volcanic activities and biomass burning, while emissions of particles attributable to the activities of humans primarily arise from four source categories: fuel combustion, industrial processes, nonindustrial fugitive sources (e.g. construction work) and transportation sources (e.g. automobiles) [1]. Atmospheric aerosols are generally considered to be particles that range in size from a few nanometres (nm) to several hundred micrometers (μm) in diameter. The particulate matter (PM) with a diameter, *d*, of 2.5 μm is referred as $PM_{2.5}$ and a diameter of 10 μm is referred as PM_{10} (EPA[1], 1997).

The smallest aerosols are small enough to get into the human respiratory system. British standards define the respirable fraction as those aerosols smaller than 5 μm, which is a significant proportion of the total [3]. The size of particles is directly linked to their potential for causing health problems. Small particles less than 10μm produce the greater problems, because they can get deep into the lungs, and some may even get into the bloodstream. Larger particles are of less concern, although they can irritate eyes, nose, and throat [2]. Particle mass concentrations are therefore regulated in the US and EU legislation. However, the ultrafine particles (UFP, i.e. having diameters less than 0.1 μm) are considered especially detrimental to human health, since these particles can be inhaled and deposited deep in the alveoli of human lungs.

Moreover, epidemiological studies suggest a connection between both UFP and PM concentration and mortality. Effects of PM were clearer in respiratory cases, whereas effects of UFP were clearer in cardiovascular cases. The largest particles are removed by settling and impaction in the head airways. Ultrafine particles less than 0.01 μm can also have significant deposition in this region due to their high diffusivity. In the tracheobronchial region, impaction and settling are important for particles larger than 0.5 μm although the overall deposition fraction in this size range is quite small.

2. Experimental research

2.1. Air quality monitoring location

Wind direction is a crucial parameter for the regional pollution as it indicates the origin of the air mass and the relative position of the measuring sites to the main pollution sources. The air quality has been monitored from autumn 2005 to autumn 2006 by "Environmental Engineering" laboratory of the Faculty of Metallurgy and Materials' Sciences, University "Dunărea de Jos" of Galati.

[1] EPA – Environment Protection Agency, USA.

The monitoring activity led to finding and accumulating information on the atmospheric aerosols charge in the neighborhood of Carnabel and Garii crossing (fig. 1).

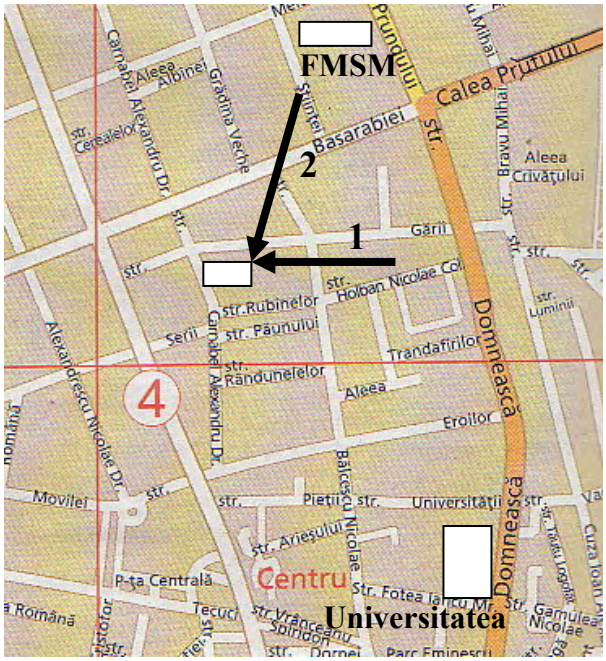

Fig. 1. *Location of the experimental research, marked on the map of Galati, wind direction: 1- E~W, 2 - N-NE~S-SW.*

In this area, due to the extremely intense traffic, supplementary pollutants were added to the pollutants occurring from industrial plants emissions. Information on aerosols concentration size ranges a = (0.4-0.5) µm, b= (0.5-0.6) µm, c = (0.4-6-0.7) µm, d = (0.7-0.8) µm, e = (0.8-0.9) µm, f = (0.9-1.0) µm, g = (1.0-1.5) µm, h = (1.0-1.5) µm, i = (1.5-2.0), , j = (2.0-4.0), and k = (4.0-10.0), µm was collected and processed. It was determined the level of air pollution with respect to wind direction in the area.

2.2. Experimental data

For the experimental research a particles' counter type AC-3 was used, which can determine up to 750,000 particles with size range of 0.4-10 µm in 1 dm^3 of ambient air. It is stated that atmosphere is considered polluted if there are more 450,000 particles/dm^3 of air.

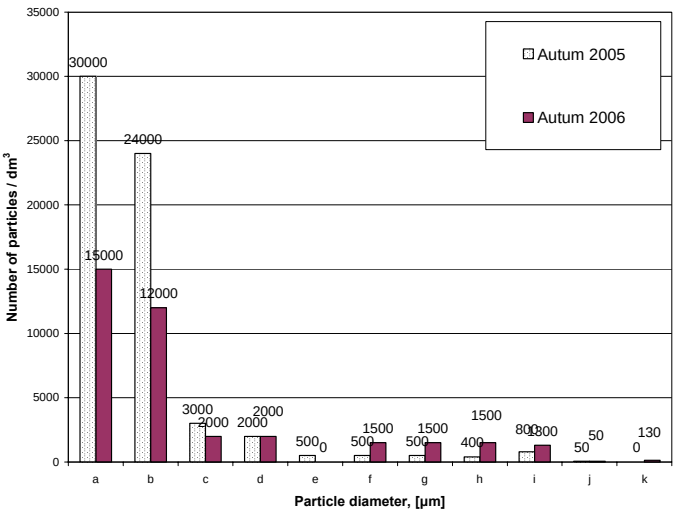

Fig. 2. *The variation of concentration in particles of 0.4-10.0 µm, when wind direction is E~W.*

The meteorological bulletins for Galati were added as supplementary data to the initial measurements, several factors being written down (temperature, humidity, atmospheric pressure, the point, the direction and the speed of the wind).

This paper analyses the most frequent wind direction dependence of the particle size distribution, as it was noticed that aerosols charge in atmospheric air varies significantly with wind direction.

The experimental data were grouped in four predominant wind directions, as it follows: E~W (fig.2) and N-NE~S-SW (fig.3). The graphics below present the particle size distribution (in 1dm^3 of air) for the period of autumn 2005 to autumn 2006.

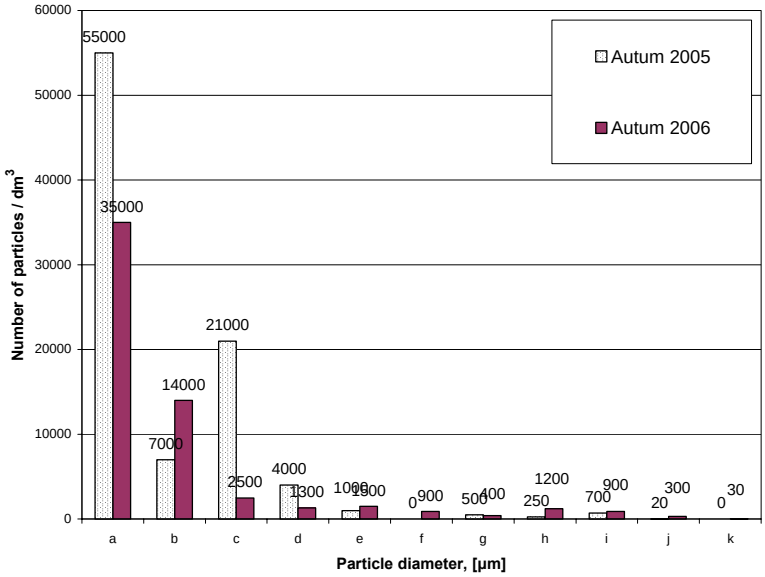

Fig. 3. *The variation of concentration in particles of 0.4-10.0 μm, when wind direction is N-NE~S-SW.*

4. Conclusions

- The monitoring activity led to finding and accumulating information on the atmospheric aerosols charge in the neighborhood of Carnabel and Garii crossing. In this site the concentration of particles is small 55 000 particles/dm^3;
- The predominant wind directions as it follows: E~W and N-NE~S-SW, in autumn 2005 and autumn 2006 period;
- The dates of diagrams were obtained by arithmetic's average at all experimental dates for each period;
- Winds from E~W direction (fig. 2), the concentration of particles are in larger quantities than the 0.4-0.6 μm, but they have a lower concentration than the 0.6-10.0 μm;
- Winds from E~W direction, the concentration of particles in autumn 2005 was twice more than autumn 2006;
- Winds from N-NE~S-SW direction (fig. 3), the concentration of particles are in larger quantities than the 0.4-0.7 μm, but they have a lower concentration than the 0.7-10.0 μm;
- Winds from N-NE~S-SW direction, the concentration of particles in autumn 2006 was lower than autumn 2005;
- Winds from N-NE~S-SW is associated with continental and therefore more polluted air masses.

References

[1]. Alfarra, M. R., "*Insights Into Atmospheric Organic Aerosols Using An Aerosol Mass Spectrometer*", Ph.D. Thesis, University of of Manchester, 2004.

[2]. Chang, H. Y., "*Principles of Air Pollution. Human Health II - Health effects from O3, NOX, SO2, PM, CO, Pb, HAPs*", available at www.envsci.rutgers.edu/~pap_ta/Health%20Effects %20II.ppt (15.03.05).

[3]. Dorsey, J., "*Introduction to Aerosols*", available at http://cloudbase.phy.umist.ac.uk/ people/dorsey/Aero.htm (10.03.2005).

STUDIES REGARDING THE COOLING OF THE ROLLED PIECES WITH ATOMIZING WATER

Aurel CIUREA, Marian BORDEI, Stefan DRAGOMIR
"Dunarea de Jos"University of Galati
email: aurelciurea@ugal.ro

ABSTRACT

The diversity of metallurgical materials and processes imposes a large scale of cooling speeds. The classical cooling mediums restrict the scale of the cooling speeds, reason for which nonconventional alternatives were necessary to be studied. In this respect, the atomizing mater ensures a large scale of cooling speeds which can cover the requirements in the metallurgical processes. In this article it is present the cooling speed of some rolled products in atomizing water in comparison with the classical conditions.

KEYWORDS: rolled, atomizing water, ultrasounds.

1. The water atomizing process with ultrasounds

The acoustic cavitation represents the main effect of the ultrasonic energy in liquids, which is the basis of the liquids atomization. The atomization process can be explained by means of the ultrasonic dispersion phenomenon, namely when the activated system is under the form of liquid-gas, then at the separation between the two mediums, a thick and thin fog is created. It is know that the capillary waves can be excited on the free surface of a low viscosity liquid by means of an ultrasonic transmitter placed exactly under the surface of the liquid.

If the amplitude of the oscillation beyond a certain limit value, the waves become instable and project thin particles of liquid to the gas, under the form of fog. According to R. Pohlmann and K. Stamm laws, in the case of a liquid with free surface in a gas or vacuum, the following relations that define the phenomenon can be taken into consideration:

$$\lambda = \frac{2\eta}{\rho}\left(\frac{\rho}{\pi\sigma f}\right)^{1/3} \qquad (1)$$

$$d_m = \frac{1}{2}\left(\frac{\sigma\pi}{\rho f^2}\right)^{1/3} \qquad (2)$$

Where: λ, f are the wave length and the ultrasonic wave frequency [m], [Hz]; ρ - liquid density [kg/m^3]; σ - surface stress [N/m]; η - liquid viscosity [Ns/m^2].

From here it results that the particles' size and fog density can be prestablished according to necessities.

The ultrasonic dispersion of the liquids in gases is produced when the intensity of the ultrasonic radiation gets sufficiently high values in order to the phenomena that generate the dispersion process.

2. The cooling process of some rolled products with atomizing water

Among the methods of liquids dispersion, it is worth mentioning the pneumatic pulverization by means of with a high speed liquid-gas can be obtained. In the pneumatic pulverization devices, the jet or liquid film is introduced in the gas flow and on the gas-liquid separation surface, instability waves appear which bring about the liquid jet dispersion (or the flow) in drops.

The gas, having the form of jet, can be brought under an angle at the liquid flow, fact that determines additional deformations of the separation surface.

The liquid flow dispersion represents a complex physical process which depends on many exterior and interior causes. Generally, the process is determined by aerodynamic forces which the superficial tension forces hinder the dispersion process.

The medium created, obtained through pneumatic pulverization of water (a combination gas-liquid) was named atomizing water and has applications in the laminated products cooling process.

From the speciality references [1,2] it results that the efficiency of rolled products cooling process in gas-liquid flow is obtained at a higher impact speed of the biphasic jet with the heated metal of 10 mm/s at water/air mass rate, in limits from ½ to 1/10.

Precise data are to be presented in this material concerning the behaviour during the cooling in atomizing water process, in comparison with classical mediums for three rolled products: plate, pipe and billet.

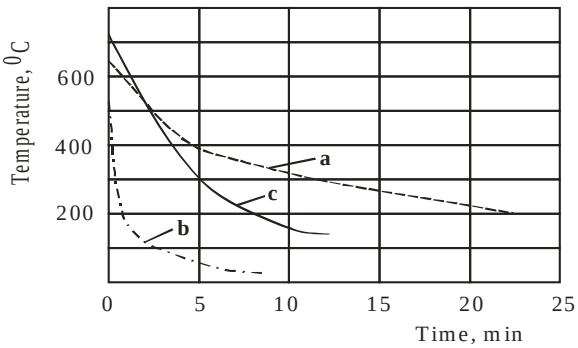

Fig.1. *The curves of the rolled tables cooling process: a. cooling with aerosols (v = 15 m/s); b. cooling with aerosols (v = 70 m/s); c. diving in water.*

In figure 1 data regarding the cooling speeds of the rolled table surface for different cooling methods.

The a and b curves characterises the intensity of the cooling process during the atomizing water blasting operation of the table surface in air current at speeds of 15 and 70 m/s. to make a comparison we are presenting the cooling speed of the tables during water diving process [1].

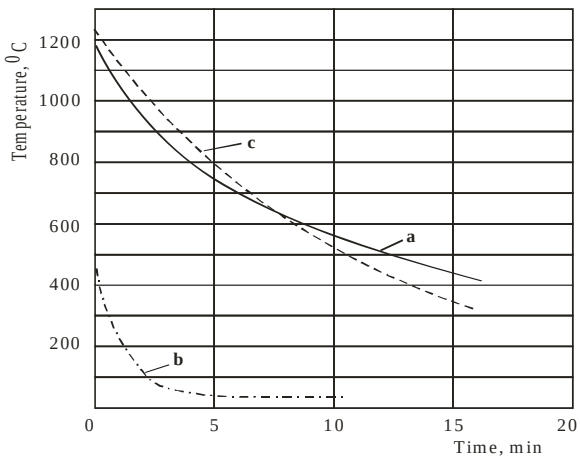

Fig.2. *The pipes cooling curves: a. cooling with aerosols (v = 15 m/s); b. cooling with aerosols (v = 70 m/s); c. diving in water.*

In figure 2 the cooling speeds of pipes surface with a diameter of 80 m are presented, during their blasting with water aerosols having speeds of 15 m/s (curve "a") and 70 m/s (curve "b") [1]. Curve "c" represents the cooling speed of the pipes during water diving.

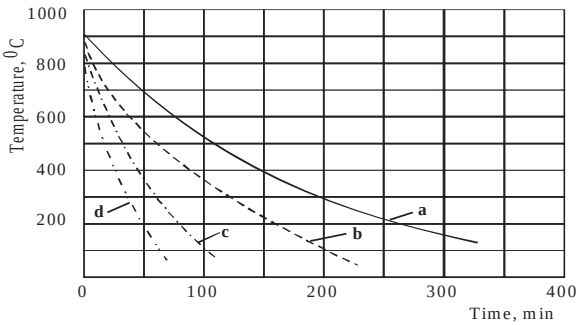

Fig.3. *The curves of semi finished Φ 127 mm cooling process: a. air cooling; b. cooling by pass through a cooling chamber; c. cooling by air blasting; d. cooling by aerosols blasting.*

In figure 3 the cooling speeds curves of the square semi finished products with section 127x127 mm [2] are presented, where "a" curve characterizes the cooling in still air, "b" curve the billets cooling transported with rotation through a cooling chamber, "c" curve the cooling through jet air blasting and semi finished rotation and curve "d" the cooling of the semi finished product with aerosols (air-water) and with the rotation of the semi finished products.

The graphics analysis from figures 1, 2, 3 shows that for different rolled product types, the cooling process with aerosol jet (water-air) reduces considerably the cooling time of the rolled product in comparison with the cooling process in conventional mediums (water-air).

The cooling water-air jets of great speed must have a great level of dispersion, this ensuring at small liquid volumes a maximum possible cooling speed.

The main factors that influence the cooling speed of the rolled products with an aerosol jet are the following:

- the mass ratio of liquid-gas volumes;
- the distribution in the transversal section of jet.
- the finesses degree (dimension) of the liquid particles in aerosol jet;
- the speed and impact angle of the aerosols jet with the cooling surface of the dispersed jet.

3. Theoretical aspects of the cooling speed

The cooling time is one of the main variables which characterize the cooling process [5].

For the cooling time calculus and that of the cooling curves at some pieces surfaces one can use the heat exchange equation:

$$t_r = \frac{m \cdot C_p}{\alpha \cdot A} \cdot \ln \frac{T_0 - T_m}{T_r - T_m} \qquad (3)$$

Where: T_0 is the initial temperature is equivalent with the final temperature of the heating process [K]; T_m – the temperature of the cooling mediums [K]; T_r – the temperature up to when the cooling process is done during t_r; m – the piece mass [kg]; α – the total superficial exchange coefficient of heating $[W/m^2K]$; A – the contact surface between the cooling medium and piece [m^2]; C_p – the medium specific heat of the metallic material from which the piece is made [J/kgK].

For the gas quenching of a piece from the initial temperature T_1 to the final temperature of the charge T_2, the relation becomes:

$$t_r = \frac{m \cdot c_p}{\alpha \cdot A_s} \cdot \ln \frac{T_1 - T_f}{T_2 - T_f} \qquad (4)$$

Where: T_f – the temperature of the recirculates gas; α – the total coefficient of heat exchange:

$$\alpha = \frac{1}{\frac{1}{h} + \frac{D}{2k_p}} \qquad [W/m^2K] \qquad (5)$$

A_s – area of charge surface[m^2]; m – the charge mass [kg]; c_p – the specific heat of the charge [J/kgK]; h – the heat exchange coefficient of the gaseous phase [W/m^{2}K]; D – the specific dimension of the piece; k_p – the thermal conductibility of the piece [W/mK].

Analysing the equations [4] and [5] we draw the conclusion that for a maximum cooling process we can act on the "U" variable and implicitly on "h" one.

For a turbulent flow parallel to the surface:

$$\frac{h \cdot D}{K} = 0.23 [Re]_{gas}^{0.8} \cdot [Pr]_{gas}^{0.3} \qquad (6)$$

and for a turbulent flow perpendicular to the surface:

$$\frac{h \cdot D}{K} = 0.3 + \frac{0.62 [Re]^{0.5} \div [Pr]^{0.333}}{\left[1 + \left(\frac{0.4}{Pr}\right)^{0.667}\right]^{0.75}} \cdot \left[1 + \left(\frac{Re}{282}\right)^{0.625}\right]^{0.8} \qquad (7)$$

Where: $Re = \frac{Dv \cdot \rho}{\eta}$; $Pr = \frac{c_p \cdot \eta}{k}$; h – the heat exchange coefficient of the gaseous phase at the ambient temperature [W/m^{2}K]; k – the thermal conductibility of the gas at the ambient temperature [W/mK]; v – the gas speed at the surface [m/s]; ρ – the gas density at the ambient surface temperature [kg/m^3]; η– the gas viscosity at the ambient temperature [Ns/m^2].

For the particular case of the nitrogen, at speeds of 60 cm/s over a roll with a diameter of 10 mm, h = 112 W/m^2 ^{0}K, in parallel current, and in perpendicular current, h = 350 W/m^2 ^{0}K.

The gas pressure is associated with the gas speed. Their combination shows the mass flow capacity, and its growth produces the increase of the heat exchange speed.

The combination among the physical features of the two phases: liquid, gas shows the value of the heat exchange coefficient at a certain temperature.

4. Conclusion

Obtaining some cooling mediums with controlled speeds but different from the conventional ones is a necessity for the metallurgical industry. The biphase air-water medium obtained through atomizing water with ultrasonic generators can solve a large range of cooling speeds with certain applications in metallurgy.

References

[1]. *Patent SUA nr. 3659428* – cl. 62-64.
[2]. *Stal und Eisen*, 2/1974, w2/1144
[3]. Harvey D.W. – *Drop size distribution from liquid jet injection across a supersonic streams*, AIVAA Journal, 1973, v11, p 1271-1280;
[4]. Diteakin Y.F, et al. – *Pulverizarea lichidelor*, Masinostroenie, Moscova, 1977;
[5]. Semenescu A., Oprescu I, et al., *Procese si echipamente de racire la tratamentul temic al pieselor*, Ed. Matrix Rom, Bucuresti, 2002.

THE ANNALS OF "DUNAREA DE JOS" UNIVERSITY OF GALATI
FASCICLE IX METALLURGY AND MATERIALS SCIENCE, ISSN 1453 – 083X. N^0. 2 – 2006

KINETIC OF MARTENSITE TRANSFORMATION IN A Cu-13wt. %Al-4 wt.%Ni SHAPE MEMORY ALLOY

Gheorghe GURAU, Carmela GURAU, N. ANDRONACHE
"Dunarea de Jos" University
email: gheorghe.gurau@ugal.ro

ABSTARCT

In this paper we present some results was obtained on the Cu-13wt. %Al-4 wt. %Ni shape memory alloy. This alloy was elaborated by a classic melting method starting at pure metals. A DSC analysis was made for quenched sample cut from 4 mm diameter hot extruded wires. The results confirm thermoelastic transformation and provide for further application the critical temperatures for martensitic transformation.

KEYWORDS: Cu-13wt. %Al-4 wt. %Ni shape memory alloy, differential scanning calorimetry, JMA model

1. Introduction

Shape memory alloys (SMA) constitute an important alloy system due they capacity to use both as sensor and actuators. At the present, polycrystalline Cu-Al-Ni SMA have been developed as an alternative to the classically used Cu-Zn-Al and Ni-Ti alloys [1].

The main interest of these alloys is their possible use at temperatures near 200 ^{0}C in advantage over Ti-Ni alloys whose maximum working temperature is around 100^{0}C.

On the other hand polycrystalline Cu-Al-Ni SMA obtained under classic technology benefit by a low price.

Shape memory effect is related to the thermoelastic martensitic transformation. It is implicit in the concept of the thermoelastic transformation that there is reversible behavior involved in the martensite-austenite transformations [2].

Therefore, reversible transformation occurs on heating an alloy, martensitic transformation advances with the transformation of the martensite plates and the earlier formed plates vanish later during the reverse transition on heating.

After an alloy which exhibits thermoelastic martensitic transition is deformed at a temperature below M_f where the transition completes, even if the deformation stress are removed, it remains at the deformed shape but recovers the original shape on heating over the austenite phase finish temperature-A_f and gains the deformed shape on re-cooling below M_f.

2. Experimental procedure

The polycrystalline Cu-13wt. %Al-4 wt. %Ni alloy used was elaborated by a classic melting in a tilting induction furnace from DJ University of Galati. The samples were extracted from hot extruded wires 4 mm diameter and 145 mm length. The samples were quenched comprised heat treatment using a vertical furnace (air environment) holding at 850^{0}C during 30 minutes for annealing and immediately in ice water quenched. For DSC measurement was used a small piece weighting less the 0.100 g. The differential calorimetric experiment were performed by means of SETARAM 92 instrument in air at a heating and cooling rate of 10^{0}C/min between -50 ^{0}C and 250 ^{0}C. The cooling treatment was acted by using liquid nitrogen. The sample weigh was 0.07 grams. Prior to the DSC experiment the sample were submitted to a chemical etched 1:1 HNO_3 in water for 13 minutes in order to remove the layer deformed by cutting operation as well as the oxide. Endothermic and exothermic peaks on DSC profiles were taken from two consecutive thermal cycles.

Nucleation and growth process in studied Cu-13wt. %Al-4 wt. %Ni alloy follow the Jhonson-Mehl-Avrami (JMA) model:

$$Y = 1 - e^{-kt^n}$$

where Y is fraction transformed, k is a time independent but temperature dependent rate constant, and n is referred to the as the mechanism constant.

The above equation can be rearranged into a linear equation:

$ln\ (1-Y)=-kt^n$ or $ln\ [-ln\ (1-Y)]=ln\ k+n\ lnt.$

From fraction transformed versus time data, the values of Y and t can be inserted into this function, to generate a straight line

3. Results and discussions

Figure 1 show the results for two thermal cycles DSC. Fist of all the base line was established and then the peaks value. After subtracted peak values four curves was obtained (Fig.2.)

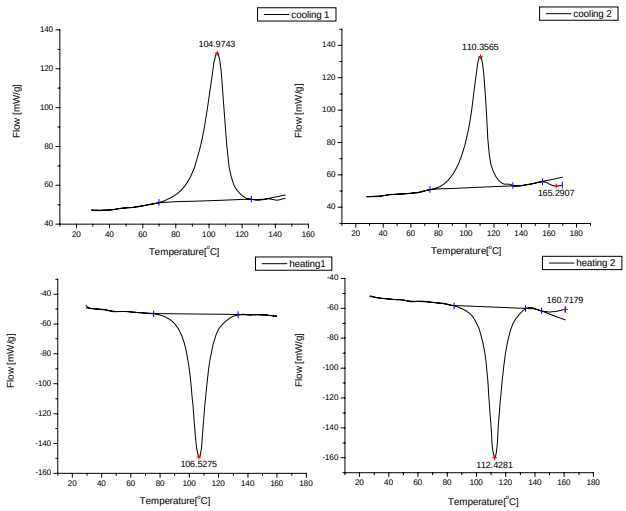

Fig.1. *DSC temperature peaks. Two thermal cycles between -50 ^{0}C and 250 ^{0}C*

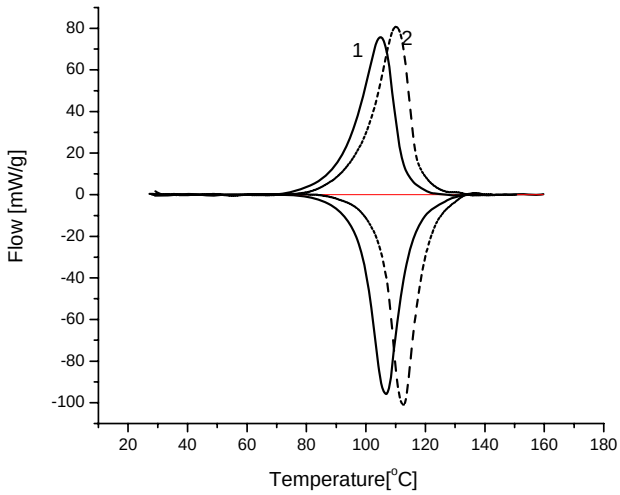

Fig.2. *DSC subtracted curves.*

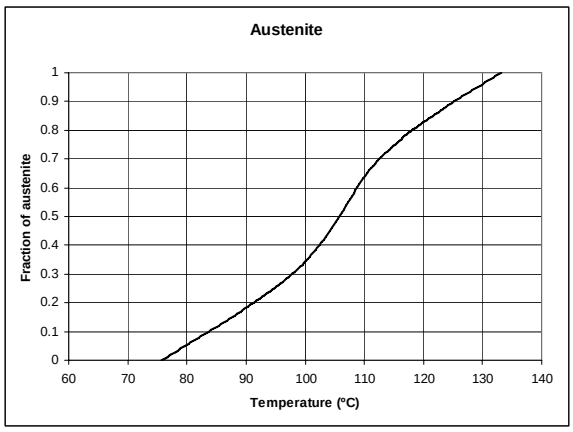

Fig.3. *Kinetic curve for inverse transformation on heating Cu-13wt. %Al-4 wt. %Ni sample.*

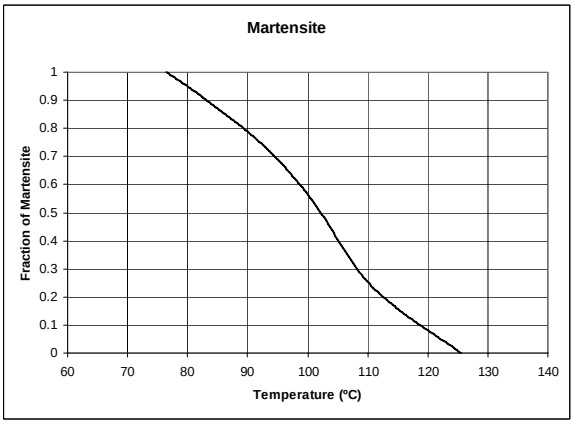

Fig.4. *Kinetic curve for direct transformation on cooling Cu-13wt. %Al-4 wt. %Ni sample.*

These curves allow carrying out a more detailed analysis of the thermoelastic transformation process (fig.3, fig.4).

Following JMA model the so obtained transformation temperatures M_s, M_f, A_s, A_f, is shown in table 1. The start transformation temperatures was considered for 1% transformed phase and the finish temperature for 99% transformed phase.

For Cu-13wt. %Al-4 wt. %Ni we obtain: M_s at 124.9 ^{0}C, M_f at 77.43 ^{0}C, A_s at 76.3 ^{0}Cand A_f 132.1 ^{0}C. Kinetic of transformation martensite to austenite on heating is shown in figure 5. Illustration of a transformation of fraction transformed plot to JMA plot for Cu-13wt. %Al-4 wt. %Ni alloy is presented in figure 6.

Table1.

Fraction of austenite [%]	Temperature of transformation [^{0}C]	Fraction of martensite [%]	Temperature of transformation [^{0}C]
0.1	75.6	0.1	125.5
1.0	76.3	1.0	124.9
5.0	79.6	5.0	122.3
10.0	83.7	10.0	118.7
50.0	105.5	50.0	102.4
90.0	125.2	90.0	83.3
95.0	128.8	95.0	80.05
99.0	132.1	99.0	77.4
99.9	132.8	99.9	76.7822

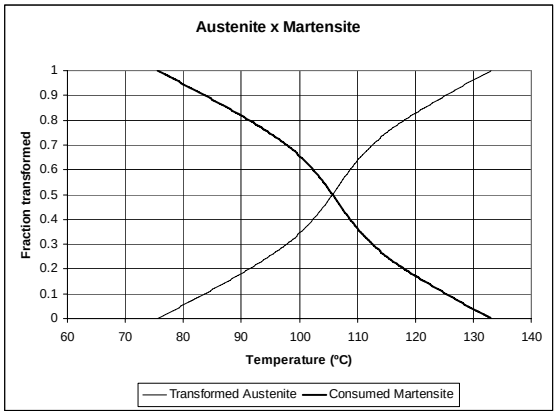

Fig.5. *Kinetic curves Martensite -Austenite Transformation on heating for Cu-13wt. %Al-4 wt. %Ni alloy.*

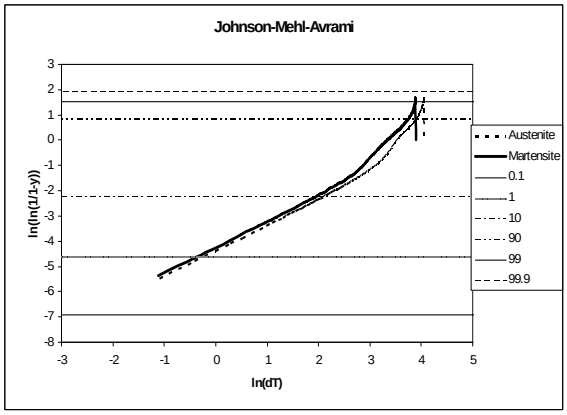

Fig.6. *JMA plot for Cu-13wt. %Al-4 wt. %Ni sample.*

4. Conclusions

a) Cu-13wt. %Al-4 wt. %Ni obtained by classic casting method is a thermoelastic alloy. The direct and inverse martensitic transformation is present. This alloy is reliable SMA alloy.
b) The samples in ice water quenched at the end of annealing treatment have the increasing transformation temperatures with thermal cycling because defects in the lattice are induced additional stress.
c) The kinetic curves for studied alloy are the normal plot for a SMA alloy.
d) The specific martensitic transformation for Cu-13wt. %Al-4 wt. %Ni alloy was precisely determined with JMA model.

Acknowledgements

The authors would like to acknowledge the support from CENIMAT FCT/UNL Caparica Portugal, specially Mister Professor F.M.Braz Fernandez and his team.

References

[1]. V. Recarte, J.I. Perez-Landazabal, A. Ibarra, M.L. No, J. San Juan, *High temperature β phase decomposition process in a Cu-Al-Ni shape memory alloy*, Mat.Sci.Eng. A378 (2004)
[2]. R. Zengin, S. Ozgen, M. Ceylan, *Oxidation behaviour and kinetic properties of shape memory $CuAl_xNi_4$ alloys*, Thermochimica Acta 414 (2004)
[3]. G Gurau, C Gurau, D Tanase, *P*rocessing Smart Wires Cu Al Ni System authors, Metal 2006, 15th International Metallurgical & Material Conference, TANGER Ltd., Ostrava, Czech Society for New Materials and Technologies, ASM International, Czech Chapter, Czech Metallurgical Society, VSB-Technical University, Ostrava
[4]. H. Morawiec, J. Lelatko, D, Stroz, . Gila, *Structure and properties of melt-spun Cu-Al-Ni shape memory alloys*, Met Sci Eng, A273- 275 (1999)
[5]. K.Otsuka and C.M. Wayman " *Shape memory materials*"-
[6]. R.Gastien, C.E.Corbellani, M.Sade Thermomechanical aspects of martensitic transformations in CuAlNi single crystals"
[7]. Paula, J.P.H.G. Canejo, R.M.S. Martins, F.M. Braz Fernandes " *Effect of thermal cycling on the transformation temperature ranges of Ni-Ti shape memory alloy*"- A.S., Mat.Sci. Eng., A378 (2004)

THE ANNALS OF "DUNAREA DE JOS" UNIVERSITY OF GALATI
FASCICLE IX METALLURGY AND MATERIALS SCIENCE, ISSN 1453 – 083X. N^0. 2 – 2006

BEHAVIOR OF 1%Cr STEELS AT FLUIDIZED BED NITROCARBURIZING

Sorin DOBROVICI[1], Nelu CAZACU[1], Adolf BÂCLEA[2], Elena DRUGESCU[1], Nelu PREDA[3]
[1]Universitatea "Dunărea de Jos" din Galaţi, [2]SOCOMAR SRL, Sorento Italia,
[3]Bristol International, Los Angeles, California, USA
e-mail: Sorin.Dobrovici@ugal.ro

ABSTRACT

Paper is based by nitrocarburizing experiments made on laboratory plant. For experiments were used different samples of steel at different nitrocarburizing regimes. Influence factors were: temperature and ammonia concentration. Treatment time had a constant value 2h30min. Influences of factors were investigated by: samples mass modifications, surface structure (micrograph), layer depth to all samples and hardness HV5 on the surface. The results confirm possibility to use fluidized bed like nitrocarburizing media and good behaviour of steel.

KEYWORDS: Nitrocarburizing, fluidized bed, steel

1. Introduction

After nitriding, nitrocarburizing becomes the most usual treatments for pieces at lower temperature. Nitrocarburizing and oxynitrocarburizing became alternative technologies for parts of car industries [1]. After this thermochemical treatment a surface layer with properties approaching at nitriding treatment is obtained, 0. Post oxidation is used to obtaining a Fe_3O_4 superficial layer, which increases corrosion resistance of parts. Porous layer offer a good adherence for different sealant that conduce to one order increasing for a corrosion resistance. The efficiency of nitrocarburizing treatment consists in shows tendencies for high quality and low costs. A complex processes are performed in fluidized bed. Gasses (ammonia and methane in different proportion) in active zone, near over separation plaque, are thermal decomposing in contact with hot solid granular.

The homogeneous reactions are possible to continue on the high of bed, but equilibrium is quickly established at higher uniform regime temperatures. A secondary stage is for heterogeneous reactions at surface samples, with adsorption of nitrogen and carbon atoms. As results of these two stages of reactions chemical compositions of gasses having major modifying hydrogen and nitrogen and rests of methane and ammonia. These gasses produced normal fluidizations in bed and that maintaining a normal and a constant gas dynamics for constant properties of fluidized bed. A fluidized bed technology (FBT) for heat and thermochemical treatments offers a low cost for investments and an acceptable quality 0. The most important characteristics of fluidized bed are influenced by: chemical compositions of fluidization gas through physical gas properties and the solid granular properties (physical characteristics, shape, dimension)

High values for heat and mass transfer coefficient conduce to shorter treatment time and this technology may have applications for small enterprises and for small series of pieces.

2. Experimental conditions

Nitrocarburizing was made on the pilot conditions (Fig.1.). The fluidised bed furnace has minimal conditions for nitrocarburizing. The furnace working up to 1000°C and a various gas mixtures is possible to use for different heat and thermochemical treatments. Fluidized beds are made from burned clay and a gas mixture by methane and ammonia, with different proportion of methane. Nitrocarburizing in fluidized bed is based by repeatability of process, 0. The nitrocarburizing media was made in fluidized bed. In this case the internal and external properties of fluidized bed are important for treatment, because a large exchange surface is formed between fluidized bed and parts (specimens). After fluidization, at outlet from furnace, gases were burned.

For nitrocarburizing experiments three steels with 1%medium contents of chrome were used: 21TiMnCr12, 18MnCr10 and 40Cr10 (Romanian

standards). Chemical compositions are showing in Tab.1. The critical points for transformation for all steels are showing in Tab.2. For all steels nitrocarburizing temperatures are below critical Ac1 temperature.

As a result these nitrocarburizing processes have not influence over core structure and properties.

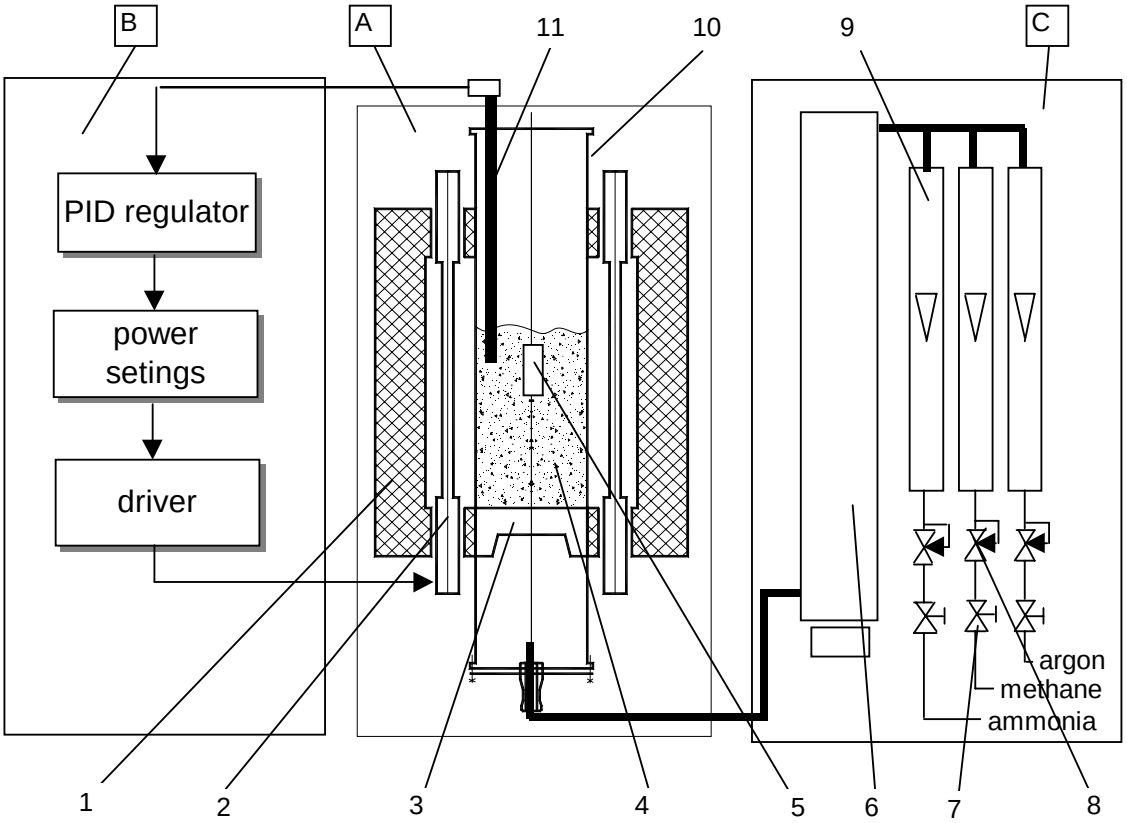

Fig. 1. *Schematic representation of fluidized bed furnace: B-automatization unit, A- furnace unit, C-gas unit, 1-isolation, 2-resistors, 3-fluidiszation plaque,4-fluidized bed, 5-samples, 6-silicogel column, 7-valves, 8-gas regulators, 9-rotameters, 10-fluidized bed furnace, 11-K thermocouple*

Tab. 1. *Chemical composition for steel used in experiments*

Steel	Chemical composition,%.							
	C	Mn	Si	P	S	Cu	Cr	Ti
21TiMnCr12	0,20	0,95	0,28	0,014	0,016	-	1,05	0,06
18MnCr10	0,18	1,05	0,22	0,035	0,035	-	1,05	-
40Cr10	0,40	0,65	0,27	-	-	-	1,00	-

Tab. 2. *Critical points for steels used in experiments*

No.	Steel	Ac1	Ac3
m.u.	-	°C	°C
1	21TiMnCr12	740	840
2	18MnCr10	765	838
3	40Cr10	743	782

Tab. 3. *Nitrocarburising in fluidized bed regimes*

No.	Temperature	Time	gas composition
	°C	h, min	%
1	550	2h30min	25% ammonia + 75% methane
2			15% ammonia + 85% methane
3			5% ammonia + 95% methane

Tab. 4. *Hardness measurements on the nitrocarburizing surface*

steel	ammonia contents (rest methane)	HV_5
m.u.	%	kgf/mm^2
21TiMnCr12	5	667
	15	752
	25	655
18MnCr10	5	524
	15	623
	25	549
40Cr10	5	655
	15	713
	25	677

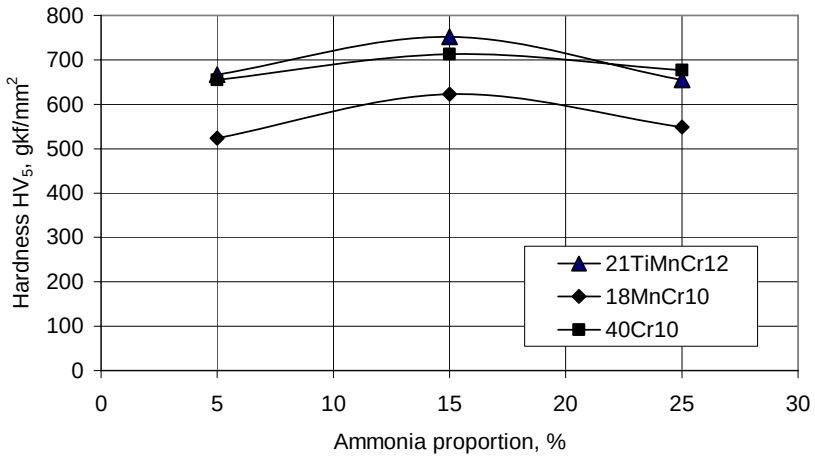

Fig. 2. *Hardness on the nitrocarburizing surface.*

Because ammonia is more expensive gas the proportion was varied between 5 and 25%, and the influence of ammonia proportion over experiments was studied (Tab.3).

3. Results

The hardness on the surfaces is the technological properties that are usual determined. All steels have in chemical compositions approximatively 1%Cr. This conduced to hard combinations at temperature and nitrogen presence in surface. As a normal result for all samples hardness (HV5) having higher values (Tab.4., Fig.2). For 15% ammonia contents in gas mixture for fluidization a maximum values were obtained for all samples. Measurements of layer thickness for all nitrocarburizing samples are showed in Fig.3. A normal increasing of layer depth by ammonia proportion is presence to all steel samples, but having different behaviour.

The structure and properties of nitrocarburizing layer is determined by chemical compositions that conduced to particular behaviour of each steel samples.

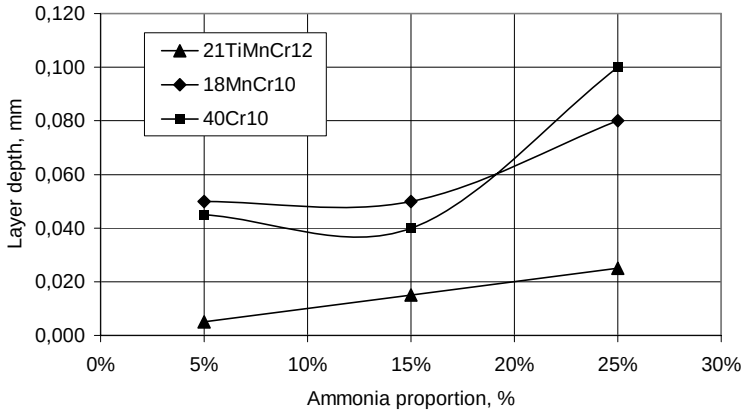

Fig. 3. *Nitrocarburizing layer variation with ammonia proportion*

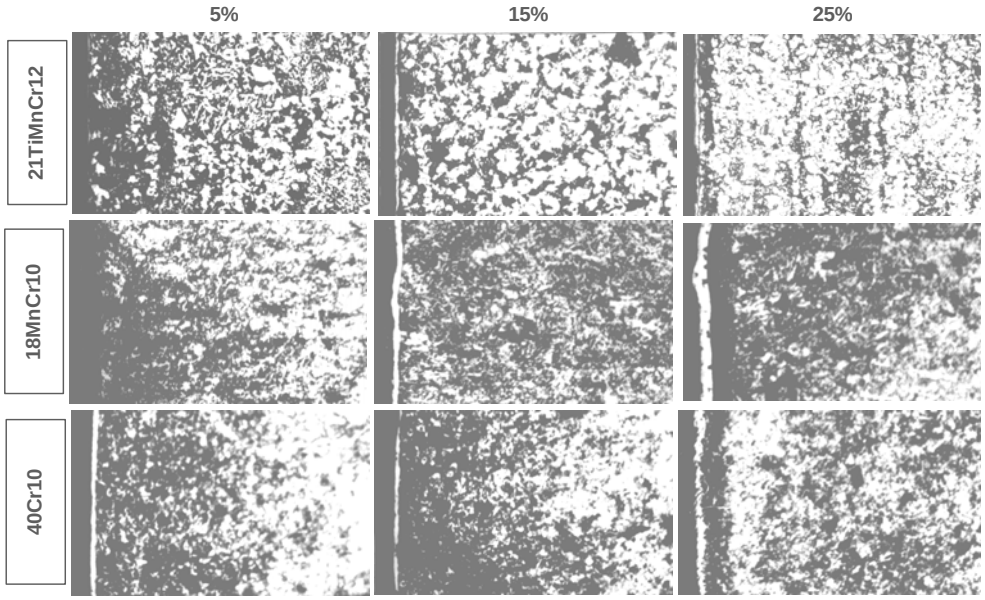

Fig. 4. *Representative microstructure for nitrocarburizing in fluidized bed layers*

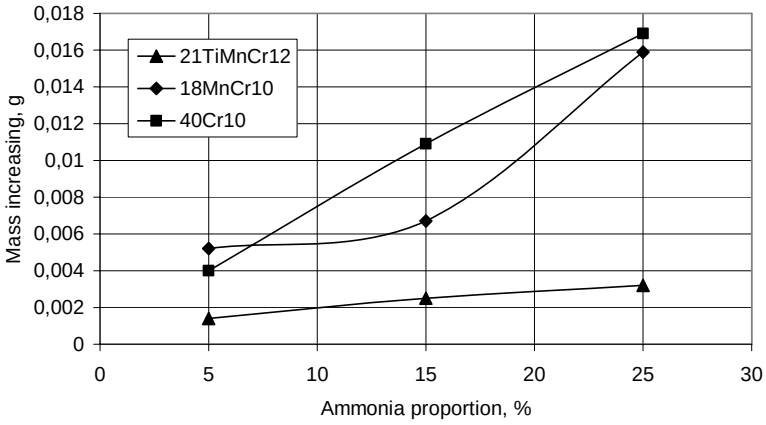

Fig. 5. *Mass increasing of nitrocarburizing samples*

For all steel specimens the representative microstructures are showed in Fig.4. The combination layer has a normal increasing with ammonia proportion. Mass increasing for all steel samples was calculated by difference between final mass an initial mass, when the specimens have identical shape and identical dimensions. The results are showed in Fig.5. Increasing of ammonia proportions in initial fluidization gas mixture conduced to mass increasing to all specimens.

4. Conclusions

Nitrocarburizing experiments made in fluidized bed over the samples from 1% Cr steels confirm fluidized bed capacity for mass transfer at higher temperature. Nitrocarburizing layer was formed for all regimes, and structures and properties of layer are depending by ammonia proportion in initial gas mixture. A maximum values for hardness is in 720-750daN/mm^2 interval, which is higher values for 150min nitrocarburizing time at 550°C temperature. A shorter treatment time is the most important characteristics of fluidized bed technology.

References

[1]. Dulcy M., Gantois M., *Principe de base de la cementation et de la carbo-nitruration*, Traitements termique No.289, 1996, p.46-54
[2]. Roland A, *Oxicad (R) NT en four a tapis, Nitrocarburation Oxidation Trempe*, Traitement thermique No.346/Avr 2003, pg.37
[3]. Willing R, Faulkner C, *Nouvelle facon d'utiliser le bain de sel en nitrocarburation*, Traitement thermique No.333/ Aou-Sep 2001, pg.33
[4]. Beguin Cl, Crevoiserat O, *Controle des processus de nitruration et de nitrocarburation gazeuses avec la sonde Datanit*, Traitement thermique No.352/Janv-Fevr 2004, pg.33

BEHAVIOR OF SOME STAINLESS NITRIDED AUSTENITE STEEL TYPES TO CORROSION AND ABRASION

Ovidiu DIMA, Olga MITOSERIU
"Dunarea de Jos" University Galati
email: dima.ovidiu@ugal.ro

ABSTRACT

By nitriding, stainless austenite steel types can become surface hardened. Hardness can be greater at more than 1000 HV_{005} when the composition layer made of complex nitrides is obtained and more reduced till 500 HV_{005} when a diffusion layer made of highly alloyed austenite including nitrogen is obtained. The tests in salt fog for resistance to corrosion show a decrease of this resistance to corrosion from Perfectly resistant materials (appreciation mark 1.1) to Very resistant materials (appreciation mark 2.1 or 2.2), for the nitrided steel types which form complex nitrides layers and which can keep the resistance to corrosion in the group of perfectly resistant materials or an insignificant decrease for the steel type that forms a diffusion layer. The tests for resistance to abrasion show a decrease of two or three times for mass losses this meaning a significant increase in resistance. This is as important as surface treatment and thickness of nitrided layer are bigger. The steel, the surface treatment, so the type of diffusion surface layer with austenite structure or the combinations with nitrides complex separations will be chosen depending on aggressive factors weight for corrosion and abrasion of the environment in which the product is working.

KEYWORTS :stainless steel, austenite, nitriding process, corrosion, abrasion.

1. Introduction

Stainless austenite steel types are very resistant to corrosion but less resistant to abrasion due to depressed hardness, below 200 daN/mm^2. An increase in surface hardness and implicitly in resistance to abrasion is possible through nitriding process. For this purpose some samples from plates of 60x20x3, from 6 characteristic stainless steel types with low carbon content, with higher carbon content stabilized or not by titanium, have been subjected to fluidized bed nitriding process. The identification marks and chemical composition of these steel types are presented in table 1.

Table 1

Steel code	Related mark	C	S	P	Mn	Si	Cu	Cr	Ni	Mo	Ti	V
		[%]										
1	X10CrNil8.8	0.12	0.028	0.055	1.24	1.64	0.06	23.2	9.8	0.11	0.01	0.02
2	X6CrNiTil8.10	0.06	0.008	0.036	1.55	0.65	0.08	17.1	9.3	0.05	0.60	
3	X2CrNil8.9	0.03	0.005	0.028	1.27	0.42	0.19	18.9	8.95	0.15	0.01	0.02
4	X2CrNiMol7.11.2	0.02	0.005	0.039	2.06	0.78	0.27	20.0	8.8	2.7	0.03	0.03
5	X6CrNiMoTil7.12.2	0.045	0.012	0.031	0.96	0.54	0.16	18.1	11.6	2.04	0.32	
6	X1CrNiMoCu20.18.7	0.02	0.008	0.027	1.12	0.41	0.70	20.1	18.1	6.1		0.2

2. Experiments and results

In order to estimate the resistance to corrosion, the accelerated corrosion test in salt fog STAS 9229 per 1995 was made. Estimation of behavior to corrosion was made by comparing the samples from initial materials and nitrided samples.

The test was carried out for 300 hours weighing the samples every 100 hours in order to point out the process dynamics.

The values of mass losses resulted after weighing as well as corrosion average speed are shown in table 2.

Table 2

Steel code	Mass loss after 100h	Mass loss after 200h	Mass loss after 300h	Corrosion average speed
	[g]			[g/m^{2}h]
Materials in initial form(quenching for adding in to solution)				
1	0.00053	0.00093	0.00133	0.0016
2	0.00070	0.00133	0.00183	0.0024
3	0.00063	0.00126	0.00186	0.0026
4	0.00043	0.00083	0.00123	0.0015
5	0.00046	0.00080	0.00120	0.0016
6	0.00021	0.00044	0.00072	0.0009
Fluidized bed nitrided materials				
1	0.00263	0.00467	0.00570	0.0075
2	0.00384	0.00648	0.00778	0.0105
3	0.00416	0.00796	0.00989	0.0128
4	0.00343	0.00601	0.00858	0.0114
5	0.00483	0.00904	0.01186	0.0152
6	0.00033	0.00064	0.00086	0.0012

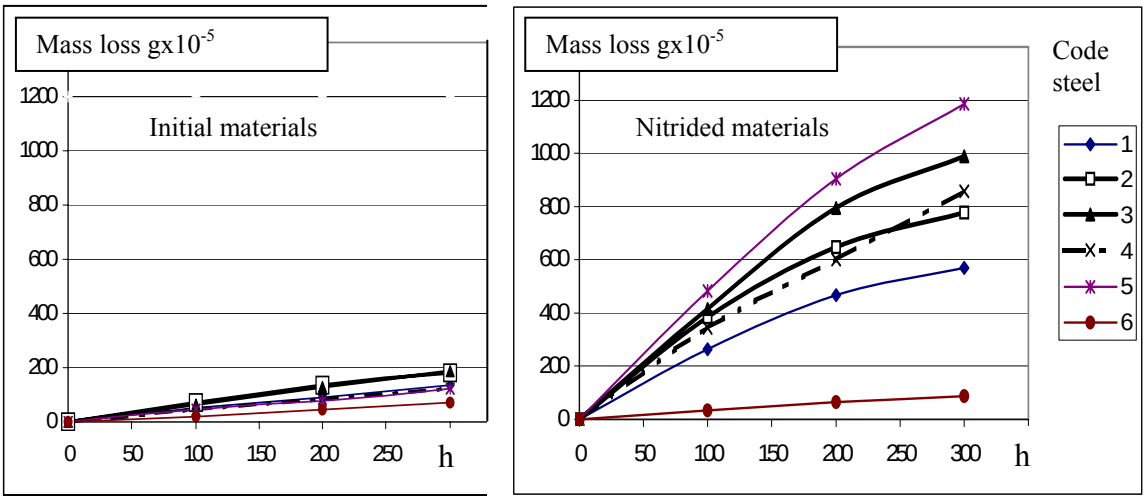

Fig.1. *Time variation of mass losses for initial and nitrided materials*

The diagrams in fig. 1 present the time variation of mass losses for all the 6 steel types which have been analyzed both for initial materials and for nitrided ones.

The analysis of these diagrams points out that the corrosion phenomenon is more acute for nitrided materials compared to initial materials. This can be explained by the fact that the single-phase austenite structure of initial materials is more stable than any other multi-phase structure. As a result of nitridind process, the hard layer which is formed presents important separations of iron nitrides and chrome from austenite.

The two types of phase have different corrosion potentials and form micro-piles that accelerate the general corrosion process.

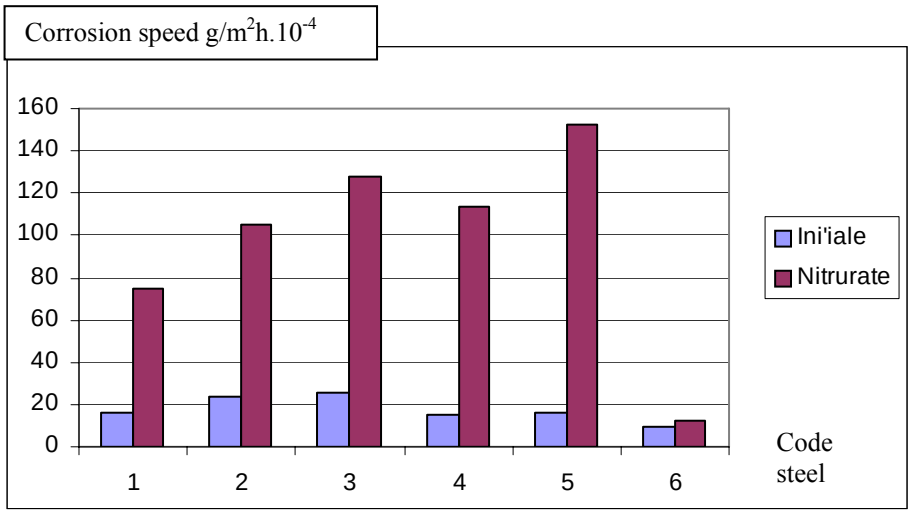

Fig.2. *Average corrosion speeds for initial and nitrided materials.*

Figure 2 presents the corrosion average speed for the 6 materials in initial and nitrided status that were calculated during the testing cycle of 300 hours.

In order to group the steel types which have been analyzed into classes adequate to general corrosion resistance, table 3 presents the provisions in STAS 6855 per 1978 regarding this subject.

Table 3

Class	Corrosion speed		Appreciation mark	
	[mm/year]	[g/m^{2}h]		
1	<0.001	<0.0009	1.1	Perfectly resistant
2	0.001-0.005	0.0009-0.0045	1.2	Perfectly resistant
3	0.005-0.01	0.0045-0.009	2.1	Very resistant
4	0.01-0.05	0.009-0.045	2.2	Very resistant
5	0.05-0.1	0.045-0.09	3.1	Resistant
6	0.1-0.5	0.09-0.45	3.2	Resistant
7	0.5-1.0	0.45-0.9	4.1	Decreased resistance
8	1.0-5.0	0.9-4.5	4.2	Decreased resistance
9	5.0-10	4.5-9	5	Low resistance
10	>10	>9	6	Non-resistant

Table 4

Steel code	Corrosion speed after l00 h	Corrosion speed after 200 h	Corrosion speed after 300 h
	[g/m^{2}h]		
Fluidized bed nitrided materials			
1	0.0104	0.0081	0.0040
2	0.0158	0.0107	0.0051
3	0.0167	0.0141	0.0078
4	0.0136	0.0102	0.0098
5	0.0187	0.0159	0.0109
6	0.0014	0.0012	0.0009

Comparing the data we obtained with the STAS ones, it is estimated that all samples from initial status steel types are included in the class of perfectly resistant materials respectively steel type code 6 in the 1st class (appreciation mark 1.1) and the other steel types code 1, 2, 3, 4, 5 in the 2nd class (appreciation mark 1.2).

The tests on nitrided samples indicate a decrease of the resistance to corrosion more clear for steel types code 1, 2, 3, 4, 5 which are enclosed in the class of very resistant materials respectively steel type code 1 in class 3 (appreciation mark 2.1) and the others in class 4 (appreciation mark 2.2) Steel type code 6 contains more than 50% alloying elements Cr, Ni, and Mo for which the nitrided layer was enriched with nitrogen without changing its austenite structure. Although it presents a slight reduction of resistance to corrosion it remains in the class of perfectly resistant materials but in class 2, having an appreciation mark of 1.2.

Also, from the analysis of data achieved after corrosion test resulted that corrosion speed for nitrided samples decreases in time. The data is given in table 4.Decreasing of corrosion speed is explained by depth variation of the layer, of nitrogen quantity separated from the base austenite mass. As a result of corrosion, the surface layer becomes thinner and deeper layers with less nitride separations are being exposed to corrosion effect till the layer is completely corroded. This way you can reach the base austenite material more or less sensitized by the heating process during nitriding.

Figure. 3 presents the speed variation to corrosion, in time.

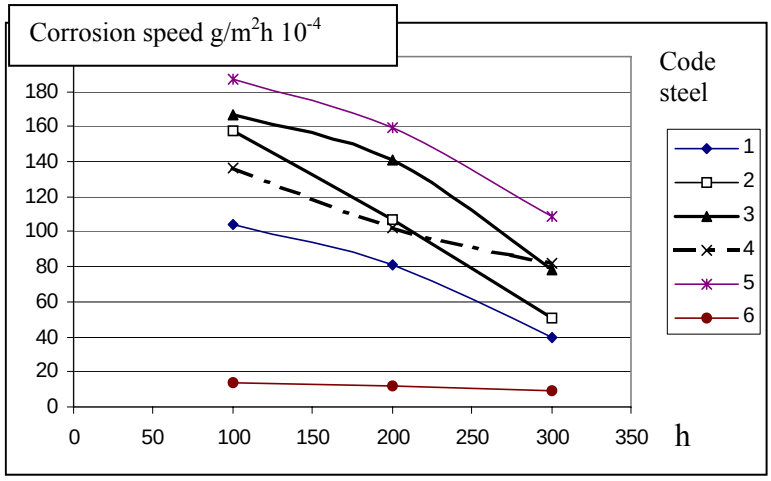

Fig.3. *Variation of corrosion speed in time.*

In order to point out the resistance to wear, samples from initial and from nitrided materials with the section of 50 mm^2 have been subjected to abrasive test STAS 9639 per 1981 using the abrasion coupling represented by the sample and a rotary disk with abrasive paper with a granulation point of 800.

The effective parameters of the test were: disk rotation 25 rot/min.; sample radial advance 0.5 mm/rot.; sample pressure 1 daN/cm^2 ; average sliding speed 10m/min.; distance length 25 m.

The results of abrasive test are shown in table 5.

Table 5

Steel code	S index	Initial materials		Nitrided materials		
		HV_{005} Hardness	Abrasive wear	Layer depth	HV_{005} Hardness	Abrasive wear
		[daN/mm^2]	[g]	[μm]	[daN/mm^2]	[g]
1	24	198	0.0066	21	1310-500	0.0027
2	19	202	0.0065	37	1180-500	0.0015
3	17.5	188	0.0065	38	1315-500	0.0015
4	21.6	180	0.0069	33	1320-500	0.0022
5	22.6	204	0.0064	32	1170-500	0.0023
6	29.8	182	0.0071	35^s	508-500	0.0036

The analysis of these results shows a decrease in mass losses through abrasion and consequently, an increase of 2 or 3 times at resistance to wear in the case of nitrided samples. The increase depends on hardness and it is bigger for steel types code 1, 2, 3, 4, 5 which, as a result of the treatment, has formed a hard nitrided layer of more than 1000 HV_{005} and smaller for steel type code 6 which is approx. 500 HV_{005} hard. Also, the increase depends on layer thickness and hardness variation in the nitrided, hard layer.

Thus, the resistance to wear of steel type code 1 is smaller than that of steel types code 2, 3, 4, 5. Also for steel type code l the layer is harder because the thickness is smaller and hardness decreases more abrupt.

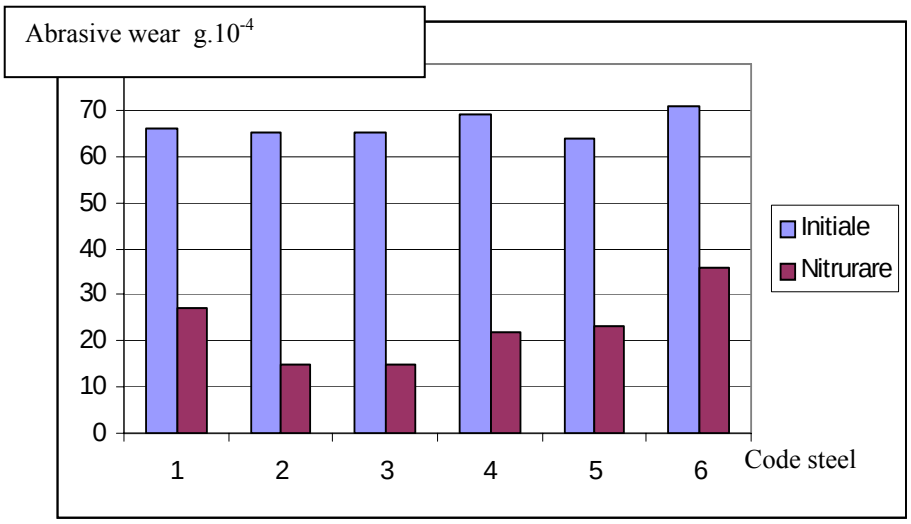

Fig. 4 presents a comparison between the abrasion wear in initial and nitrided status, pointing out the strict decrease of mass losses for nitrided samples against the initial ones.

3. Conclusions

Researches on nitrided samples indicate a decrease of resistance to corrosion, more clear for steel types code 1, 2, 3, 4, 5 which are enclosed in the class of very resistant materials respectively steel type code 1 in class 3 (appreciation mark 2.1) and the others in class 4 (appreciation mark 2.2) The steel type code 6 contains more than 50% alloying elements Cr, Ni, and Mo for which the nitrided layer was enriched with nitrogen without changing its austenite structure. Although it presents a slight decrease in resistance to corrosion, it remains in the class of perfectly resistant materials but in the 2nd class (appreciation mark 1.2). The results of tests for abrasive wear show a decrease of mass losses and, consequently, an increase of 2, 3 times in resistance to wear in the case of nitrided samples. The increase depends on hardness. It is bigger for steel types code 1, 2, 3, 4, 5 which after the treatment have a hard nitrided layer of more than l000 HV_{005} and smaller for steel type code 6 for which the hardness was approx. 500 HV_{005}- The increase depends also on the thickness of the layer and hardness variation in the nitrided layer. This way, the resistance to wear of steel type code 1 is smaller than of steel types code 2, 3, 4, 5. The layer hardness is bigger. This is explained by the fact that layer thickness is smaller and hardness decrease more abrupt. The steel type, the surface treatment and though the type of diffusion surface layer with austenite structure or the combinations with nitrides complex separations will be chosen depending on the weighing of corrosion aggressive factors, respectively on abrasion.

References

[1]. Dobrovici S. - *Cercetări privind tehnologia carbonitrurării în strat fluidizat aplicată oţelurilor.* Teză de doctorat Galaţi 1999.
[2]. Truşculescu M. - *Oţeluri inoxidabile şi refractare.* Ed. FACLA Timişoara 1983.
[3]. Berns H. - *Case hardening of stainless steel using nitrogen.* Ruhr University, Bochum, Germany 2002.
[4]. Berns H. - *Solution nitriding of stainless steel for process engineering,* Mat.-wisws. u. Werkstofftech. 31/2000.
[5]. Mocanu D. R. - *Încercarea materialelor.* Ed.Tehnică Buc. 1982.
[6]. Cornet A. - *Inginerie des surfaces* Ecole nationale superiieure des arts et industries de Strasbourg Ed.11-1993
[7]. Levcovici M. S. - *Ingineria suprafeţelor* EDP Buc.2003
[8]. Constantinescu A. - *Detectarea si masurarea coroziunii* Ed.Tehnica Buc. 1976
[9]. Vellier M. - *Solution apportees aux problemes de la corosion-abrasion par certaines aciers inoxydables austenitiques et austenito-feritiques.* Conference internationale des arts chimiques Paris 1976.

THE DECREASING OF THE ENERGETIC LOSSES AT A COKE DRY COOLING PLANT

Adrian VASILIU[1], Gina NĂSTASE[1], Natalia BEGLET[2], Vasile MIREA[3]
[1] Dunărea de Jos University of Galati,
[2] Technical University of Moldavia" Kishinew, Moldova Republic
[3] „POLITEHNICA" University of Bucuresti
e-mail: avasiliu@email.ro

ABSTRACT

The paper presents an energetic and technologic analysis of the metallurgic coke dry cooling plant (CDCPO) operating, and also the optimization of this process in the case of an industrial plant, existing in the Steel Works S.A. Galati. The drawn–up analysis is based on the thermal balance of the industrial plant, in order to establish some mathematical equations that characterize the technological process.

KEYWORDS: coke, thermal flux, recuperation boiler, mathematical model

1. Introduction

The efficiently of (ISUC – Cooke Dry Cooling Plant) from "MITTAL STEEL SA" is made by using the thermal balance of this installation.

This means, that proper establish a mathematical model that characterize a good functionary for (ISUC) based on entrance system parameters.

2. This installation is used on a coke cooling (I.S.U.C.)

This installation is used on a coke cooling by using inert gases and warm recuperation with recuperation boiler. This plant has five blocks. Each block have: an extinction recipient, a recuperation boiler, a principally exhausting and systems for powder elimination and too a system for measuring and automation of functionary parameters (fig. 1).

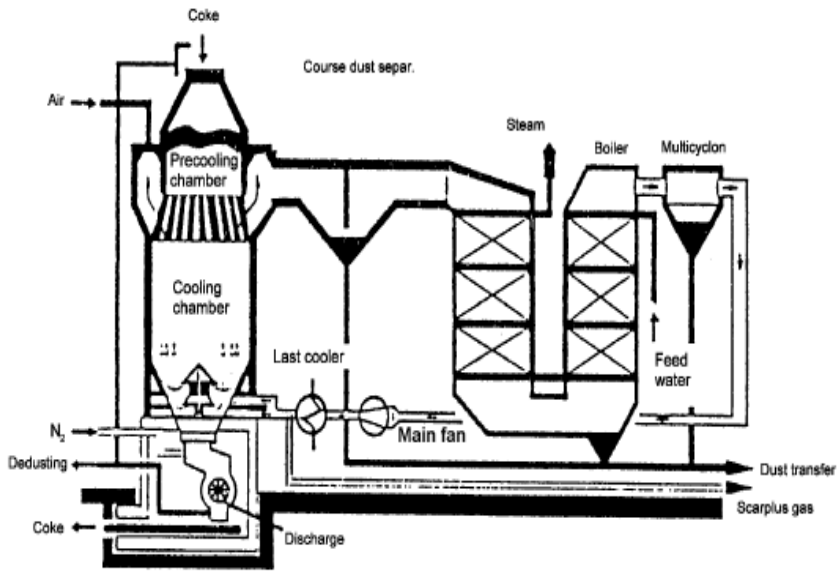

Fig 1. *Coke Dry Quenching Installation.*

The extinction recipient has two compartments (extinction recipient and a room for warming cocks accumulation) and at the bottom an installation for gases distribution and a hole for cooling coke evacuation. At the top there are channels for gasses accumulated finishing with a hole for inert gases evacuation. The charging of warning coke in a mechanized operation on the top of installation and than is mode an hydraulic entrance opening.

The inert gases are sender in continuous system throw inellary hole in layer of warning coke. At 800^{0}C this gases left the recipient and enter into recuperating boiler. The inert gases an evacuated continuously into atmosphere. The cokes get down from top to the shaft bottom and the "cold" coke at 250 – 280^{0}C.

The gases moving in installation, is made by an exhausting tip VH 160/850 with Q=160.000 m^3/h and a low pressure Δp=804x10^2 N/mm^2. The work temperature of the exhausting is 180 – 200^{0}C.

The parameters of (ISUC) installation are:

– warming coke temperature 1000 – 1050^{0}C;

– cooling coke temperature 250 – 280^{0}C;

– the temperature of moving gases before recuperation boiler: 750 – 800^{0}C;

– the temperature of moving gases before the entrance in the recipient 180 – 200^{0}C;

– the quantity of warming blow at one tone of coke 400 – 420 kg;

– the productivity of recuperating boiler is 85t/h of warning blow at the temperature of 430 – 440^{0}C.

The measuring installation has the next possibility:

– measuring the temperature of coke on the transported of installation;

– measuring the temperature of lining Y in the channels zone;

– measuring the temperature of inert gas at the entrance into the bottom of recipient;

– measuring the temperature of inert gas at the exit at the top shaft;

– measuring of the inert pressure at the entrance into the shaft (400 ÷450 · 10^2 N/mm^2);

– measuring of the coke level into the installation by radioactive sources.

3. The technology of I.S.U.C

The principally chemical reactions produced during the air moving into installation are:

a) completely oxidation of the carbon from the coke:

$$C + O_2 \rightarrow CO_2 + 409500\ kJ \quad (1)$$

$$q = (97853 - 0{,}469T + 0{,}000879T^2 + 0{,}62 \cdot 10^{-6} T^3) \cdot 4{,}1868 \quad (1.1)$$

b) incompletely oxidation of the carbon the coke:

$$2\ C + O_2 \rightarrow 2\ CO + 248700\ kJ \quad (2)$$

$$q = (60320 - 4{,}298T + 0{,}003594T^2 + 1{,}25 \cdot 10^{-6} T^3) \cdot 4{,}1868 \quad (2.1)$$

c) the reducing of water vapour from air with carbon (t≥900^{0}C) :

$$H_2O + C \rightarrow CO + H_2 - 118000\ kJ \quad (3)$$

$$q = (-26853 - 5{,}269T + 0{,}002719T^2 + 0{,}546 \cdot 10^{-6} T^3) \cdot 4{,}1868 \quad (3.1)$$

d) the reducing of water vapour with carbon (t≤900^{0}C) :

$$2\ H_2O + C \rightarrow CO_2 + 2H_2 - 74940\ kJ \quad (4)$$

$$q = (16162 - 6{,}709T + 0{,}002723T^2 + 0{,}462 \cdot 10^{-6} T^3) \cdot 4{,}1868 \quad (4.1)$$

The reaction with water vapour has been in generally at the start of installation on at the breaking of recuperating boiler, when water vapour penetration the gases circuit.

e) the methane is forming :

$$C + 2H_2 \rightarrow CH_4 + 77870\ kJ \quad (5)$$

$$q = (15713 + 11{,}351T - 0{,}00673T^2 + 2{,}182 \cdot 10^{-6} T^3) \cdot 4{,}1868 \quad (5.1)$$

f) the reducing of CO_2 at high temperature no oxygen:

$$CO_2 + C \rightarrow 2\ CO - 161000\ kJ \quad (6)$$

$$q = (-37533 - 3{,}829T + 0{,}002715T^2 + 0{,}63 \cdot 10^{-6} T^3) \cdot 4{,}1868 \quad (6.1)$$

With increasing of combustible elements has been a increase of diverse concentration whose combustible components into the moving gases are given in table 1.

Table 1 *Different functionary models of (ISUC)*

Functionary of (ISUC)	The composition of gases						Explosion boundaries		The admissible concentration
	CO	H_2	CH_4	C	CO_2	N_2	inf %	sup%	
No nitrogen	23,6	7,50	0,60	0,20	4,42	63,5	8,40	75,0	5,25
With added of nitrogen	12,6	3,84	0,60	0,20	6,04	76,8	8,30	65,0	7,35
With burned of combustible	4,92	6,06	2,62	0,36	16,0	76,2	8,20	31,0	14,10

4. Mathematical model

The analysis mode permit to appreciate the purpose of each thermal flux of (I.S.U.C.) for a energetically efficiently of this process.

The optimal regime for recuperating boiler of (ISUC) who keeping the warming blow parameters is the calculus regime for a production of 25 t/h and a productivity at 50 t/h cooling coke at gases debit of 82000 m^{3}N/h at a entrance temperature of gas into the recuperating boiler of 800^{0}C.

The primary thermal fluxes of I.S.U.C. are burning coke and sour–warm steam. The link between these two fluxes is making by flux of moving warm gas. If the energy of sour–warm steam is highly, the energy at the exit from dry cooling room is much highly and too is aspect a greatest energy at the exit of recuperation boiler and grow the efficiently of I.S.U.C. like energotechnology system.

The values of energetically losses are characteristics of coke dry cooling and can be considered like efficiently criterions.

For a optimally developing of coke dry cooling is necessary to study the efficiently criteria and to determine by measuring the total energetically looses and than to find the way increase the efficiently of I.S.U.C. The most important problem is to diminish the total energetically looses (equation 7).

It must to find the order variable of this process and than to drive in a optimal way the I.S.U.C.

$$Q_p = f(X_i) = \min \qquad (7)$$

were:

X_i – technological variable; (i=1, 2, 3, , k)

The most important energetically looses is generated by a badly change of warm into – the dry cooling room, the recuperation boiler, looses of moving gas throw the aspiration smoke pipes, the temperature of gas flux at the exit of recuperation boiler and the flux of dry coke.

All looses of coke dry cooling plant are describe in the next equation:

$$Q_p = -5{,}53 + 4{,}37\cdot10^{-4}X_1 + 0{,}96\cdot10^{-4}X_2 + 0{,}61\cdot10^{-4}X_3 + 4{,}22\cdot10^{-4}X_4 + 1{,}55X_5 + 1{,}38X_6 \qquad (8)$$

Equation is not valid at the boundary:

$$36000 \le X_1 \le 54000 \qquad (9)$$

$$X_2 \le 160000 \qquad (10)$$

$$1400 \le X_3 + X_4 \le 7000 \qquad (11)$$

$$0{,}0039\cdot(X_2 + X_3 + X_4) \le 630 \qquad (12)$$

$$1{,}2 \le X_5 + X_6 \le 5 \qquad (13)$$

$$0{,}0324\cdot X_1 - 0{,}0176X_2 + 111\cdot X_5 + 110\,X_6 - 120 \le 250 \qquad (14)$$

were:

– X_1 – the consumption of burning coke, [t/h];

– X_2 – consumption of moving cold gas, [m^3/h];

– X_3 – consumption of gas, [m^3/h];

– X_4 – consumption of gas throw aspiration smoke pipe, [m^3/h];

– X_5 – the increase of contents of CO_2 in moving gas, %;

– X_6 – the increase CO in moving gas, %.

For to know the minimal energetically looses is necessary to find the values of $X_1 \div X_6$ (technologically variables).

The efficiently criterions is a linear function and boundary equations (9) – (14) are binary, than for solving minimized problem is used the SIMPLEX method of linear programming.

The transforming of boundary equation at the canonized tip throw nearly transformation in corresponding with (9)–(14) is very complicated. For a really solving of this system of equation is used a performed computers and same algorithm for left and right zone by making 5 iteration (left) and 6 iteration (right). In table no. 2 is shown the results of this calculus.

Table 2

The tehnological variables	Left zone		Right zone	
	Optimum values	Real values	Optimum values	Real values
X_1	54	–	42	22
X_2	86243	69323	54750	107045
X_3	6989	–	1400	5400
X_4	1,3	3,8	–	–
X_5	–	–	1,4	4,2
X_6	27,98	–	18,23	–

5. Conclusion

The productivity of coke plant is dependent of consumption of the coke. The temperature of dry coke order variable and can be mention between two borders.

Another component of energetically looses is moving flux gas. The decrease of this component is possible by reducing the temperature of gas flux often recuperating boiler. The consumption of cold gas is conditioning by charging of coke and the asked for temperature of dry coke.

If the energy in recuperating boiler is much, the temperature of gas is low and the functionary of plant is good (efficiently). The decrease of morning gas temperature make possible reduce of energetically looses and can be assured a good transmission of alimentation water into the boiler. The looses in pipes rooms and smoke aspiration is not too much.

For to reduce the energetically looses by pipes is necessary to decrease or to close completely the room pipe and to eliminate the surplus of cold moving gas and in the same time is grow up the ecological security.

The looses resulting by the burning of coke can be reduced by diminish of oxygen aspiration from air in the channel of moving gas. The value of oxygen aspiration is dependent of: the degrees of opening of smoke aspiration pipes and the guide apparatus of smoke aspiration. The two factors are considered for regulation actions in channel.

Thus, for the effective progress of coke dry quenching process, i.e. for the reduction of the energy losses in the installation, as it results from the analysis, the following must be provided: minimum possible temperature of quenched coke, required value of the discharges in the circulation system (so as aspirations to be minimum), the minimum temperature of the circulation gas at the entry in the quenching chamber, the optimum feeding water quantity in agreement with the level of the boiler.

References

[1]. Constantinescu I. şa - „*Prelucrarea datelor cu calculatoare numerice*" Ed. Teh., Bucureşti 1990.
[2]. Taloi D., Florian E. - „*Optimizarea proceselor metalurgice*", Ed. Did. şi Ped. Bucureşti 1983
[3]. Hilbert M., Sundman B. şa – Metall. *Trans.* A, 1990, vol. 21, p2759 - 2776.
[4]. Ienciu M. , Berca F. sa –„*Produse cărbunoase*" Bucureşti, Litografia I.P.B. 1989
[5]. Stefanescu D., Marinescu M., şa – „*Transferul de căldură in tehnică*", Ed. Teh., Bucureşti 1982

THE ANNALS OF "DUNAREA DE JOS" UNIVERSITY OF GALATI
FASCICLE IX METALLURGY AND MATERIALS SCIENCE, ISSN 1453 – 083X. N^0. 2 – 2006

POSSIBILITIES TO EVALUATE THE VALUE OF THE MARANGONI EFFECT AND OF THE MARANGONI NUMBER IN REFINING STEEL-SLAG/INCLUSION SYSTEMS

Petre Stelian NITA
"Dunarea de Jos"University of Galati
email: pnita@ugal.ro

ABSTRACT

Starting from the impressive progress in studying the instabilities induced by capillary effects in systems of two immiscible fluids in chemistry, an analysis of factors in solutal Marangoni effect and Marangoni number is performed, regarding the liquid steel surface as a part of the interface in systems steel-slag/inclusion. Low alloyed, microalloyed and carbon steel are taken into consideration because of their closed behavior to liquid iron solutions. Computing relations of surface tension of solutions Fe-O-S and interface tension between the same solutions and Al_2O_3 inclusion, also of the diffusion coefficients of the solutes are proposed to be used in computind the contribution of solutal effects in Marangoni effect and Marangoni number.

KEYWORDS: Marangoni effect, Marangoni number, surface tension, oxygen, sulphur.

1. Introduction

"The mechanical properties of the interface layer between two fluids, including the equilibrium shape of the surface, may be calculated by applying the standard mathematics techniques of mechanics to the forces associated with the surface tension" is formulated in the IUPAC as definition of the subject of capillarity [1].

In the recent decades of years this definition was enriched by a hudge amount of scientific research concerning the intimated aspects of capillarity and its implication in clarifying mechanisms of processes involved in current and advanced technologies, at industrial scales and at micro and nanoscale. Many achievements, obtained in the research at micro and nanoscale are of a full utility in explaining many processes at industrial scale in steel refining, serving as a good base for developing new ways of improving the performance and in developing new intelligent devices to control some specific working parameters.

The following survey of adequate found published papers helps in understanding of the achieved knowledge in similar systems in chemistry engineering, used after in bringing a contribution in the attempt to promote a similar treatment, in steel refing metallurgy, based on treatments using slag.

The systems liquid steel-slag and more generally, liquid metals (or alloys)-slag, are systems of two immiscible fluids, because of the differences as physical and chemical nature of the component fluids, but their evolutions, during the industrial processes, take place mainly by reactions and mass exchange between them, at interface. Thermal flux and the exotermicity of some reactions, taking place during refining treatments of steels using slag, are also to be taken into consideration in a more quantitative manner. Binary liquid–liquid and gas–liquid systems, where an interfacial chemical reaction take place, have been intensively and broadly studied and investigated, especially in chemical engineering, to clarify the interaction between reaction-diffusion phenomena and pure hydrodynamic instabilities.

Liquid steels and the refining slag are not at all simply liquids, they are complex liquid solution of totally different nature as bonding between component species, these also themselves different in the two solutions. This reality, of nature to produce many complications in analyzing the proposed aspects, without any doubt is an argument to sustain once more, if it would be necessary, that in systems steel –slag, the role of the capillary effects is of outmost importance and they merit more than to be simply declared. The difficulty to observe in situ how the phenomena proceed, due to the high temperature around of 1873K, obliges to a careful analysis of other chemical systems of immiscible solutions but direct accessible as observation and measurements, due to their near room temperature or not too different to these values.

2. Aspects of hydrodynamics and capillarity at interface between immiscible fluids

Hydrodynamic instability of the fluid interface may induce local convective fluxes and by these, it affects, in an important manner, the reaction, the interface heat and mass transfers. In these cases, self organization processes may lead to a specific dissipation pattern formation of chemo-hydrodynamic nature [2].

Experimental evidence in liquid–liquid systems of interfacial convection exhibiting a high degree of ordering or interfacial turbulence, when mass transfer is accompanied by chemical reaction, has been reported in the literature for reactions of different types. Among the first descriptions such phenomena is that in the paper [3] where was reported a spontaneous emulsification at the contact between solution of lauric acid in oil and an aqueous solution of NaOH. A spontaneous turbulence and acceleration of the interfacial reaction by convection was observed during the extraction of acetic acid from an organic solvent into an alkaline solution [3.].The interfacial turbulence was reported as taking place when a reaction take place at an oil–aqueous interface [4]-[6][9]. Many data, concerning the spontaneous turbulence, also are reported in a wide range of other activities, such as in nuclear fuel reprocessing activities [7] or at liquid–gas interfaces driven by photochemical reactions [8]. Aspects of interfacial interfacial instabilities were observed during the extraction of uranyl nitrate from its nitric acid solution. Another example was given in paper [8], where was studied the pattern formation. In [9] are presented the dynamics of chemically driven nonlinear waves and oscillations at an oil–water interface.

Phenomena attributed to heat and solutal effects due to an exothermic neutralization reaction interplaying with a liquid–liquid interface and convection, observed experimentally, are reported in the paper [10] and are characterized by the authors as a novel instability, occurring when an organic solution, containing an acid, is in contact with an aqueous solution in which NaOH is dissolved. It was suggested that the self-sustained dynamics and pattern formation, in the form of plumes and fingers are produced because of the coupling between different hydrodynamic instabilities; boundary layer and double diffusion instabilities are mainly involved. When in the same system NaOH was replaced by an organic base it was observed a regular structure, in the form of long self-growing cells, with one side keeping contact with the interface and the other side propagating in the direction out of the interface [11].According to these cited papers, several mechanisms of instability, like surface tension driven or buoyancy driven, may compete. Replacement of NaOH anorganic base by an organic base has produced the increase of the influence of the Marangoni effects probably because of increasing of the chain length of the new resulting salt. Similar aspects to those before mentioned are presented also in papers [12][13][14] at different moments sustaining the importance and the permanent actuality of the subject.

3. Marangoni effect and instabilities induced in some refining steel systems

In the system of two immiscible fluids, separated on the vertical direction according to the difference of density, there are several kinds of gradients of the superficial tension upon the factors affecting this quantity and this is expressed in the global relation (1) for the 1-D case:

$$\tau_S = \frac{d\gamma}{dx} = \frac{\partial\gamma}{\partial c}\frac{dc}{dx} + \frac{\partial\gamma}{\partial T}\frac{\partial T}{\partial x} + \frac{\partial\gamma}{\partial\psi}\frac{d\psi}{dx} \quad (1)$$

where: γ is superficial tension of the fluid taken into consideration; c – concentration of the superficial active element; T – temperature; Ψ – electric potential, when is applied as external action; x – direction on which is estimated or computed the respective gradient of the superficial tension, or the surface tension gradient is acting.

The systems are not usually under the influence of an external electric field and in this case the third term is missing.

The total variation of the superficial tension, due to all factors, as shown in the relation (1), at interface or on the liquid surface, on the direction x , represent a surface tension τ_S.

Systems steel-slag and steel – inclusion are of outmost importance for steel refining to obtain high levels of purity in non-desired elements, like oxygen and sulphur, also non-metallic inclusions. In an earlier paper [16], an extend qualitative analysis of the Marangoni effect in steel was presented.

When the Marangoni effect is the result of the concentration gradients, it is nominated as solutal Marangoni effect and is a direct result of mass transfer between liquid phases or can be an indirect result of buoyancy or of another kind of convection as they are forced flow, heat transfer, temperature gradients. The Marangoni effect is called also as effect of thermocapillarity, or shortly thermocapillarity when it appears as a consequence of the temperature gradients, these last being the results of the heat transfer processes, as well as mass transfer processes, involving enthalpy changes, or also other kinds of natural or forced flow.

Taking into account the existence of large spaces at interface liquid steel-slag strongly stirred by inert gas bubbling, where either the temperature

gradient is nil, in a thin surface layer, or is of a limited small magnitude, it remains of a major importance the solutal Marangoni effect and the associated convection to be analyzed. To evaluate the possibilities of interfacial instability producing usually are used criteria as Marangoni number Ma, frequently presented in the form:

$$\text{Ma}=\frac{(-\frac{\partial\gamma}{\partial c})c_0 H}{\mu D} \qquad (2)$$

Where: $\partial\gamma/\partial c$ is the variation of the surface tension upon concentration of the chemical element affecting the surface tension; in other cases the variation of the interfacial tension is taken into consideration; c_0 is the characteristic concentration; H – is characteristic length; D – is the diffusion coefficient of the solute in the phase taken into account; μ – is the dynamic viscosity.

4. Possibilities to compute some factors of the solutal Marangoni effect Marangoni number

Until now, according to a wide range of scientific publications, there is not a stable value of the superficial tension of pure iron at temperatures around 1873K. Also, derived from the above reason, there are different relations of the superficial tension dependence of Fe-O and Fe-S solutions on the solute concentration, separately and in the same time. The relevance of the numerical data, regarding different factors of magnitude of the Marangoni effect, computed when active refining processes take place, also the evaluation of instabilities and dynamic effects at the steel-slag and steel inclusion interfaces are of outmost importance, but also are very sensitive to the representatively of the relations used in these calculations.

The quantitative aspects regarding the magnitude of the surface stress τ_S and Ma number can be obtained from obtained data and relations showing the dependence of the surface tension on concentration and temperature.

A such relation is the following:

$$\gamma = 1.936 - 0.00051(T-1808) - 0.28\ln(1-170[\%O]) - \\ - 0.2\ln(1-330[\%S]) \qquad (3)$$

obtained in paper [15], based on compilation data from many papers and accepted because is valid in the range of T=1800-1900K.The contents of oxygen and sulphur are in mass%.

At the temperature 1811K, values of the surface tension γ=1.931N/m and of the coefficient of temperature $\frac{\partial\gamma}{\partial T}$=0.000455 N/m • K were established in the paper [17] based on the configurationally energy model and this is the reason of taking into account of the nominated relation (3) despite the fact that there are other several relations of the same acceptance in the specific literature. A special reason of the acceptance of this data is that they are established using the method of the levitated drop which is a dynamic one, being closer as conditions to the practice of steel refining, where there is a permanent flow of the liquid phases.

Of a particular importance is also the interfacial tension liquid steel –nonmetallic inclusion and liquid steel-slag. For interfacial tension iron (liquid)- Al_2O_3 inclusion is proposed the relation [15]:

$$\gamma_{Fe-Al2O3} = 1.128 - 10^{-4}T - [1.936 - 0.00051(T-1808) - \\ - 0.28\ln(1+170[\%O]) - 0.2\ln(1+330[\%S])]\cdot \\ \cdot\cos[132 - 6.3\ln(1+400[\%O]) - 0.63\ln(1+640[\%S])] \qquad (4)$$

Based on the selected relations some quantitative surface and interfacial effects can be established in the deoxidization and the desulphurization of the steel under refining slag.

The values of Ma number in the solutal Marangoni effect can be computed using the before mentioned relations to which is necessary to add also values or form of dependence for the solute element. The problem is very delicate but, at least roughly, could be used relation (5), proposed by the authors[18] to compute the solute diffusivity of gases oxygen and nitrogen in liquid metals:

$$D_{i-Fe} = (0.2BRd_{Fe}^3/d_i)[(T/V)(V-V_0)/V_0] \qquad (5)$$

where: D_{i-Fe} is diffusion coefficient of the solute *i* in liquid solvent *Fe*; d_{Fe} – Goldschmidt diameter of the solvent *Fe*; d_i –atomic diameter of the solute *i* (gas);

V_0 – atomic volume of the solvent *Fe* corresponding to the state of zero Fluidity (equivalent to the state of infinite viscosity);

$V_{0,Fe}=7.05\text{x}10^{-6}m^3mol^{-1}$; V - atomic volume of the liquid solvent *Fe*; *T*- absolute temperature; *B* - characteristic constant of the liquid metal solvent introduced in the fluidity equation by Hidegrand [19] and for *Fe* the value is *B=2.04*.

From the same paper [19] for consistency of data used in computation of the value of viscosity, we have $\mu_{Fe}=4.9\text{x}10^{-3}Nm^{-2}s$ and it is given for a temperature when $V/V_0=1.1$.

From international tables of fundamental values of elements $d_{Fe}=2.8\text{x}10^{-10}m$, $d_O=1.2\text{x}10^{-10}m$, $d_S=2\text{x}10^{-10}m$.

4. Conclusions

The combined efforts made in different fields of research and their published results are of nature to allow numeric computations and to get quantitative information about the magnitude of solutal Marangoni effect, Marangoni number, also to evaluate some aspects of the dynamics of the surface processes during refining under slag as deoxidization and desulphurization, including growing and removal of the non metallic inclusions of alumina.

These quantitative data are necessary to clarify better some fine aspects regarding touching and keeping of the high levels of purity and cleanness, necessary to obtain the maximum of performance in low alloyed, HSLA and other steel grades, acting to control and to minimize adverse effects, exerted by those before mentioned factors, in different stages of their processing in liquid state. For ultra fine grain steels and nano-scale driven formation structures in steels, the control of liquid steel dynamics on active surfaces, especially in the final stage of refining treatments, is definitory.

The selected relations, combined with others, regarding similar aspects in refing slag will permit a more complete estimation of the control and benefic aspects at industrial plant scale.

References

[1]. IUPAC, *Manual of Symbols and Terminology for Physicochemical Quantities and Units*, App.II, reprinted Pure Appl. Chem.,31, 577(1972)

[2]. Nepomnyashchy, A.A, Velarde, M.G., Colinet,P. *"Interfacial Phenomena and Convection* " Chapman and Hall/CRC, Boca Raton, 2002.

[3]. Sherwood, T.S., Wei, J.C., "*Interfacial phenomena in liquid extraction*"Ind.Eng. Chem. 49(1957), 1030.

[**4]. Dupeyrat, M., Nakache, E**. ''*Direct conversion of chemical energy into mechanical energy at an oil–water interface*'' Bioelectrochem.Bioenerg. 5 (1978), 134.

[5]. Nakache, E., Dupeyrat, M., Vignes-Adler, M. "*Experimental and theoretical study of an interfacial instability at some oil–water interfaces involving a surface-active agent*" J. Colloid Interface Sci. 94(1983), 187.

[6]. Nakache, E., Dupeyrat, M. "*The contribution of chemistry to new Marangoni mass transfer instabilities at the oil/water interface*"Faraday Discuss.Chem.Soc.,77(1984), 189.

[7]. Science and Practice of Liquid–Liquid Extraction, edited J. D. Thornton, Clarendon, Oxford, 1992.

8. Avnir, D., Kagan, L.M. "*The evolution of chemical patterns in reactive liquids driven by hydrodynamic instabilities*."Chaos, 5 (1995), 589.

[**9]. Kai,S., Muller,S.C., Mori, T., Miki,M.** "*Chemically driven nonlinear waves and oscillations at an oil–water interface*." Physica D, 50(1991), 412.

[10]. Eckert, K., Grahn, A. "*Plume and finger regimes driven by a exothermic interfacial reaction.*" Phys. Rev. Lett. 82(1999), 4436.

[**11]. Eckert, K., Acker, M., Shi, Y**.''*Chemical pattern formation driven by a neutralization reaction. I. Mechanism and basic features,*'' Phys. Fluids 16(2004), 385.

[12]. Ermakov, S.A., Ermakov, A.A., Chupakhin, O.N., Vaissov, D.V. "*Mass transfer with chemical reaction in conditions of spontaneous interfacial convection in processes of liquid extraction,*'' Chem. Eng. J. 84(2001), 321.

[13]. Ruckenstein, E., Berbente, C., "*The occurrence of interfacial turbulence in the case of diffusion accompanied by chemical reaction,*'' Chem. Eng. Sci. 19(1964), 329.

[14] Sternling, C.V., Scriven, L.E., "*Interfacial turbulence: Hydrodynamic instability and the Marangoni effect.*" AIChE J. 5(1959), 514 .

[15] Chung, Y., Cramb, A.W. "*Dynamic and Equilibrium Interfacial Phenomena in Liquid Steel-Slag Systems*" Metallurgical and Materials Transactions,vol.31B(2000), 957-971.

[16]. Nita, P.S. "*Influence of Marangoni effect on steel refining processes, in ladle-type reactor treatment*" Metalurgia 54(2002), 17-20.

[17]. Nita, P.S., Goarza, A.C., "*An improved model of the surface energy for iron group transition metals"*, The Annals of "Dunarea de Jos" University of Galati,volII-2003,107-115.

[18].Chabra Rajendra, P., Roy, A.K., "*Z. Metallkunde*", 64(1988), 79.

[19]. Hildegrand, J.H., Lamoreaux, R.H. "*Viscosity of liquid metals: an interpretation (fluidity of liquid metals/ /solubility parameters)*" Proc. Nat. Acad. Sci. USA, 73(1976), 988-989.

MANUSCRISELE, CĂRȚILE ŞI REVISTELE PENTRU SCHIMB, PRECUM ŞI ORICE CORESPONDENȚE SE VOR TRIMITE PE ADRESA:

MANUSCRIPTS, REVIEWS AND BOOKS FOR EXCHANGE COOPERATION, AS WELL AS ANY CORRESPONDANCE WILL BE MAILED TO:

LES MANUSCRIPTS, LES REVUES ET LES LIVRES POUR L'ECHANGE, TOUT AUSSI QUE LA CORRESPONDANCE SERONT ENVOYES A L'ADRESSE:

MANUSCKRIPTEN, ZIETSCHRITFTEN UND BUCHER FUR AUSTAUCH SOWIE DIE KORRESPONDENZ SID AN FOLGENDE ANSCHRIFT ZU SEDEN:

UNIVERSITATEA "DUNĂREA DE JOS" DIN GALAȚI
REDACȚIA ANALELOR
Str. Domnească nr. 47 – 800036 Galați, ROMÂNIA
E-mail: marian.bordei@ugal.ro

Adresa site:
http://www.fmet.ugal.ro

Revistă bianuală acreditată CNCSIS

Editată sub egida
Facultății de
METALURGIE ŞI ŞTIINȚA MATERIALELOR
şi a Centrului de Cercetare
CALITATEA MATERIALELOR ŞI A MEDIULUI

Annual subscription (2 issues per year) accredited CNCSIS

Edited under the care of
Faculty of
METALLURGY AND MATERIALS SCIENCE
and Research Center
QUALITY OF MATERIALS AND ENVIRONMENT

Data editării: 15.11.2006
Tiraj: 200 exemplare
Tiparul executat la
Fundația "Universității Dunărea de Jos"
din Galați, editură acreditată CNCSIS
Str. Domnească nr. 47. Galati 800036 Romania

Edited date: 15.11.2006
Issues number: 200
Printed by
"Dunărea de Jos" University Fundation
accredited CNCSIS
47 Domnească Street, 800036 Galati, Romania